# CONTROL OF HISTONE H3 LYSINE 27 TRIMETHYLATION IN *NEUROSPORA CRASSA*

by

KIRSTY SARAH FIONA JAMIESON

A DISSERTATION

Presented to the Department of Biology
and the Graduate School of the University of Oregon
in partial fulfillment of the requirements
for the degree of
Doctor of Philosophy

December 2014

DISSERTATION APPROVAL PAGE

Student: Kirsty Sarah Fiona Jamieson

Title: Control of Histone H3 Lysine 27 Trimethylation in *Neurospora crassa*

This dissertation has been accepted and approved in partial fulfillment of the requirements for the Doctor of Philosophy degree in the Department of Biology by:

| | |
|---|---|
| Dr. Bruce A. Bowerman | Chairperson |
| Dr. Eric U. Selker | Advisor |
| Dr. Karen Guillemin | Core Member |
| Dr. Kryn Stankunas | Core Member |
| Dr. J. Andrew Berglund | Institutional Representative |

and

| | |
|---|---|
| J. Andrew Berglund | Dean of the Graduate School |

Original approval signatures are on file with the University of Oregon Graduate School.

Degree awarded December 2014

DISSERTATION ABSTRACT

Kirsty Sarah Fiona Jamieson

Doctor of Philosophy

Department of Biology

December 2014

Title: Control of Histone H3 Lysine 27 Trimethylation in *Neurospora crassa*

Trimethylation of histone H3 lysine 27 (H3K27me3) marks facultative heterochromatin, containing silent genes. My research investigated factors that influence the distribution of H3K27me3 in the filamentous fungus *Neurospora crassa*. The H3K27 methyltransferase complex, PRC2, is well conserved in eukaryotes and consists of four core members: E(Z), EED, SUZ12 and P55. I showed that three of the PRC2 subunits (SET-7, the homolog of E(Z), EED and SUZ12) are required for H3K27me3 in *Neurospora*, while NPF, the homolog of P55, is only required for a subset of H3K27me3 domains.

H3K27me3 is organized into large, gene-rich domains in *Neurospora* and normally does not overlap with constitutive heterochromatin, which is marked by both H3K9me3 and DNA methylation and bound by heterochromatin protein 1 (HP1). I discovered that loss of HP1 binding results in a genome-wide relocalization of H3K27me3. Specifically, it is lost from many of its normal domains while it becomes associated with much of the genome that is constitutive heterochromatin. This contrasts plant and mouse studies in which the loss of DNA methylation relocalizes H3K27me3.

The DCDC complex is the H3K9-specific methyltransferase consisting of DIM-5, DIM-7, DIM-9, CUL4 and DIM-8. Separate deletions of DCDC subunits, with the

exception of *dim-7*, relocalized H3K27me3 to constitutive heterochromatin, presumably due to the loss of HP1 binding. The deletion of *dim-7* resulted in the loss of all H3K27me3, suggesting a novel role for *dim-7*.

To look for a recruitment signal for PRC2, I moved large fragments contained within an H3K27me3 domain to loci devoid of H3K27me3, *his-3* and *csr-1*. None of the fragments induced H3K27me3, demonstrating that a recruitment signal is not present within every fragment of H3K27me3-marked DNA. Large chromosomal rearrangements had profound effects on H3K27me3 domains, resulting in the loss of some H3K27me3 domains and the formation of others.

In *Drosophila* and mammals, a subset of PRC2 complexes contains the histone deacetylase, Rpd3. A close homolog of Rpd3 in *Neurospora*, HDA-3, did not appear to be a member of PRC2 in *Neurospora*.

This dissertation includes both previously published and unpublished co-authored material.

CURRICULUM VITAE

NAME OF AUTHOR: Kirsty Sarah Fiona Jamieson

GRADUATE AND UNDERGRADUATE SCHOOLS ATTENDED:

University of Oregon, Eugene
Boston University, Boston, Massachusetts

DEGREES AWARDED:

Doctor of Philosophy, Biology, 2014, University of Oregon
Bachelor of Arts, Chemistry, 2005, Boston University

AREAS OF SPECIAL INTEREST:

Epigenetics
Chromatin
Genomics

PROFESSIONAL EXPERIENCE:

Graduate Student, Eric Selker, University of Oregon, 2008-2014

Teaching Assistant, Department of Biology, University of Oregon, 2007-2009

Research Assistant, Bioformulations Development, Genzyme Corporation, Framingham, MA, 2005-2007

GRANTS, AWARDS, AND HONORS:

National Institutes of Health Training Grant, Genetics, 2009-2012

PUBLICATIONS:

Jamieson K, Leggett N, Rountree MR and Selker EU. HP1 binding prevents H3K27me3 deposition at constitutive heterochromatin of *Neurospora crassa*. *In preparation*

Jamieson K, Rountree MR, Lewis ZA, Stajich JE, Selker EU (2013) Regional control of histone H3 lysine 27 methylation in *Neurospora*. *Proceedings of the National Academy of Sciences* 110:6027–6032.

ACKNOWLEDGMENTS

I thank Eric Selker for all of the helpful discussions and guidance during my time in his lab. Keyur Adhvaryu, Shinji Honda and Zachary Lewis provided valuable advice at the beginning of this project. I thank Kevin McNaught and Tish Wiles for their helpful discussions. I also thank Doug Turnbull for running the high-throughput sequencing facility, Larry David for his expertise in mass-spectrometry and the Fungal Genetics Stock Center for providing me with strains. This investigation was supported in part by the National Institutes of Health Genetics Training grant.

I dedicate this dissertation to my parents, Hazel and Nigel Jamieson,
and to my brother, Kyle Jamieson. Thank you for all of your love and support.

TABLE OF CONTENTS

Chapter Page

Chapter Page

LIST OF FIGURES

LIST OF TABLES

# CHAPTER I

# INTRODUCTION

All histone proteins (H1, H2A, H2B, H3 and H4) are subject to post-translational modifications (PTMs), which include, but are not limited to methylation, acetylation, phosphorylation and ubiquitylation. The majority of histone PTMs occurs on the protruding amino-terminal tails, although several PTMs are located within globular domains. Histone methylation is restricted to lysine and arginine residues; lysines can be mono-, di- or trimethylated. While the addition of methyl groups does not alter the charge of the histone, mono-, di- and trimethylated residues often have separate biological roles and mutually exclusive distributions. In mammals, monomethylated histone H3 lysine 27 (H3K27me1) accumulates within transcribed regions and promotes transcription, dimethylated H3K27 (H3K27me2) plays a global role in preventing the acetylation of H3K27 (H3K27ac) and trimethylated H3K27 (H3K27me3) marks repressed developmental genes (1).

This dissertation investigates H3K27me3 using the filamentous fungus, *Neurospora crassa* (*N. crassa*), as a model organism (2, 3). *N. crassa* has a compact genome of approximately forty megabase pairs (Mb) with approximately ten thousand genes, many of which are present in single copies. Unlike in higher organisms (4), H3K27me3 is not essential in *N. crassa*. Furthermore yeasts such as *Saccharomyces cerevisiae* (*S. cerevisiae*) and *Schizosaccharomyces pombe* (*S. pombe*) lack methylated H3K27.

In higher organisms, H3K27me3 is central to important biological processes, such as X-chromosome inactivation. X-chromosome inactivation is the silencing of one of the two X chromosomes in XX females for the purpose of dosage compensation (5). A major event in X-chromosome inactivation is H3K27me3 spreading along large portions of the inactivated X while simultaneously being excluded from the active X, thereby managing the double dose of X-linked genes in females (6).

Elevated levels of EZH2, the H3K27-specific methyltransferase, is a hallmark of many cancers and is often observed in patients with poor prognoses (7). In fact, fourteen abnormally repressed, H3K27me3-marked genes serve as a reliable indicator of clinical outcome in both prostate and breast cancer patients (8). Decreased H3K27me3 is also thought to promote cancer; a methionine substitution at H3K27 (H3K27M) globally reduces H3K27me3 by inhibiting the enzymatic activity of the H3K27 methyltransferase complex, Polycomb Repressive Complex 2 (PRC2). A significant percentage of pediatric diffuse intrinsic pontine gliomas (DIPGs) show H3K27M; one study reported that 78% percent DIPGs (9) have the H3K27M substitution, while two other studies observed H3K27M in about a third of DIPGs (10, 11).

First identified in *Drosophila melanogaster* (*D. melanogaster*), Polycomb group (PcG) complexes catalyze or bind to the H3K27me3 mark, leading to transcriptional silencing through an unknown mechanism (12). PRC2 is the most conserved and the only PcG complex with obvious homology in *N. crassa*. To date, four additional PcG complexes have been identified in *D. melanogaster*: Polycomb Repressive Complex 1 (PRC1) is thought to be responsible for polynucleosome compaction, dRing associated factors complex (dRAF) is involved in histone H2A lysine 118 ubiquitylation, Polycomb

repressive deubiquitinase (PR-DUB) facilitates H2AK118 deubiquitylation and Pho Repressive Complex (PhoRC) binds DNA directly (12).

The work described in this dissertation contains both published and unpublished co-authored material. Chapter II was published with co-authors Michael Rountree, Zachary Lewis, Jason Stajich and Eric Selker. Chapter II describes the function of H3K27me3 and its global distribution, as well as the complex that catalyzes H3K27me3 in *N. crassa* and the conservation of genes marked by H3K27me3 in three *Neurospora* species. Chapter III contains unpublished co-authored work with Neena Leggett, Michael Rountree and Eric Selker that explores the control of H3K27me3 and describes the redistribution of H3K27me3 in the absence of HP1 binding to H3K9me3. A variant of the PRC2 in *D. melanogaster* and mammals contain the histone deacetylase, Rpd3 (13-15). *N. crassa* contains a close homolog to Rpd3, HDA-3, and Chapter IV discusses unpublished work co-authored by Dani Keahi, Shane Van der Zwan, Heejeung Yoo and Eric Selker to characterize two *N. crassa* HDA-3-containing complexes.

# CHAPTER II

# REGIONAL CONTROL OF HISTONE H3 LYSINE 27 METHYLATION IN *NEUROSPORA*

This work was published in volume 110 of the journal *Proceedings of the National Academy of Sciences of the United States of America* on April 9, 2013. I performed quantitative chromatin immunoprecipitation (qChIP) experiments, purified and characterized EED-associated proteins and measured the linear growth rate of PRC2 mutants. Michael Rountree performed the ChIP-sequencing (ChIP-seq) and RNA-sequencing (RNA-seq), Zachary Lewis (currently at the University of Georgia) performed ChIP-microarray experiments and Jason E. Stajich (University of California, Riverside) performed bioinformatics analysis. Eric Selker was the principle investigator for this work. Additional credit goes to Larry David (Oregon Health and Science University), who carried out proteomic analysis on EED-associated proteins and Douglas Turnbull who assisted in high-throughput sequencing.

## Introduction

Polycomb group proteins form multimeric complexes to establish, maintain, and recognize the trimethylation of histone H3K27 (H3K27me3) (16, 17). Polycomb repressive complex 2 (PRC2), which was first described in *Drosophila* and consists of four core proteins: enhancer of zeste [E(Z)], extra sex combs (ESC), suppressor of zeste12 [SU(Z)12], and p55, is directly responsible for methylation of H3K27 (16, 17).

The SET [Su(var)3–9; E(z); Trithorax] domain protein E(Z) is the catalytic subunit of the complex (18). SU(Z)12 and p55 each appear to facilitate nucleosome binding, whereas ESC apparently boosts the enzymatic activity of E(Z) and modestly contributes to nucleosome binding (19). Embryonic ectoderm development (EED), the mammalian homolog of ESC, was found to bind to H3K27me3, raising the possibility that it plays a role in the propagation of this histone mark (20). PRC2 has been conserved throughout evolution, with core subunits present in metazoans, plants, and even protists (21, 22).

In both animals and plants, H3K27me3 is commonly associated with transcriptionally silenced genes involved in development (23). Deletion of a PRC2 subunit increases the expression of some H3K27me3 genes (24-30), but the mechanism for gene repression by H3K27me3 is largely unknown (31, 32). The distribution of H3K27me3 varies among organisms; both *Drosophila* and mammals typically exhibit broad H3K27me3 domains of up to several hundred kilobases (kb), including both transcribed and regulatory regions (33, 34). In contrast, H3K27me3 regions are rather short in *Arabidopsis*, with most less than 1 kb, and are largely restricted to the transcribed regions of single genes (35). This difference in H3K27me3 distribution suggests the possibility of distinct mechanisms for the control of this modification in metazoans and plants.

H3K27me3, like H3K9me3, appears to be absent from some simple model organisms, such as *Saccharomyces cerevisiae*. Fission yeast *Schizosaccharomyces pombe* sports H3K9 methylation but lacks H3K27 methylation (36). In *Neurospora crassa*, H3K9me3 directs DNA methylation and marks centromeric and interstitial segments of heterochromatin, which largely comprise inactivated transposons (37, 38).

While studying gene silencing at the telomeres (39), we discovered that *N. crassa* also sports H3K27me3, allowing us to exploit this organism to study the control and function of this histone modification.

Considering the lack of information on H3K27me3 in fungi, we analyzed the distribution and function of H3K27me3 in *N. crassa* and two other species of *Neurospora*. Sizable H3K27me3 domains were found concentrated near the telomeres on all seven linkage groups (LGs) of *N. crassa*, and the distribution has been partially conserved in the genus. H3K27me3 covers a substantial number of specialized silent genes. The PRC2 complex, but not the PRC1 complex, is conserved in *N. crassa*. We found that three members of the PRC2 complex are required for H3K27me3 [SET-7, EED and SU(Z)12]; the fourth, *Neurospora* protein 55 (NPF; a homolog of p55), is required for H3K27me3 on just a subset of targets.

## Results

### Distribution of H3K27me3 in *Neurospora*

We used ChIP-sequencing (seq) to generate a high-resolution map of H3K27me3 distribution throughout the genome of *N. crassa* (Fig. 1A, see Appendix A for all figures) and identified 223 H3K27me3 domains, ranging from 0.5 to 107 kb (average 12.5 kb), together occupying 2.8 Mb of the 41 Mb genome (Table 1, see Appendix B for all data tables; Dataset S1, http://www.pnas.org/content/110/15/6027.full?tab=ds). This fraction of the genome (6.8%) is similar to the H3K27me3 occupancy found in *Arabidopsis*, *Drosophila*, and mammals (40-42). Interestingly, the H3K27me3 domains of *N. crassa*

are found predominantly near telomeres (Fig. 1A). We identified 774 predicted genes that are completely included within these domains and an additional 165 predicted genes partially covered by H3K27me3 ("border genes") (Dataset S2, http://www.pnas.org/content/110/15/6027.full?tab=ds). The multigene domain arrangement of H3K27me3 in *N. crassa* is reminiscent of animal systems (34, 43) and contrasts the situation observed in *Arabidopsis*, in which this mark is associated with individual genes (35).

We verified the H3K27me3 distribution determined by ChIP-seq in three ways. First, we carried out ChIP-microarray experiments for LG VII. Equivalent results were obtained with ChIP-seq and ChIP-microarray methods (Fig. 2A). Second, we used ChIP-seq to assess the distribution of H3K27me3 in different *Neurospora* culture media [Vogel's (44) and Bird media (45)]; virtually identical distributions of H3K27me3 (Fig. 2B; Datasets S1 and S3, http://www.pnas.org/content/110/15/6027.full?tab=ds) were observed. Third, we used ChIP followed by real-time quantitative PCR to verify H3K27me3 enrichment at LG I telomeres and at two genes on LG VII (qChIP; Fig. 1C).

Our study on telomere silencing in *N. crassa* provided early evidence of both H3K9me3 and H3K27me3 in several telomeric regions (39). The conventional ChIP experiments did not provide information on whether these two marks truly colocalize in *N. crassa*, however. To address this possibility, we performed ChIP-seq for H3K9me3 and compared the distributions of these two marks (Fig. 3). Interestingly, we found that H3K27me3 often neighbors H3K9me3, but each mark forms distinct domains with little or no overlap (Fig. 1B; Fig. 3). As found in more limited surveys (37, 38), H3K9me3, which mirrors the distribution of DNA methylation in *N. crassa* (38), was almost

exclusively associated with gene-depleted, A:T-rich sequences altered by repeat-induced point mutation (RIP). In contrast, H3K27me3 domains include numerous predicted genes and the base composition of these regions is not skewed in any obvious way.

### *Neurospora* H3K27me3-Marked Genes Are Distinctive

As a first step to explore the possible function of the H3K27me3 mark in *Neurospora*, we surveyed the underlying genes for their evolutionary conservation and predicted functions. It became obvious that the H3K27me3-marked genes are not representative of the overall genome. The average predicted size of proteins encoded by H3K27me3 genes is smaller than that of genes not marked by H3K27me3 (373 vs. 513 amino acids; Fig. 4). Furthermore, an unusually high fraction of the 774 H3K27me3-marked genes have no predicted function (71.4%; compared with 38.2% of genes in the genome overall; Fig. 5). Although most of the H3K27me3-marked genes are unannotated, the annotated set does contain representatives of a full spectrum of categories (e.g., metabolism, cellular transport; Fig. 5).

The high level of novelty among genes marked by H3K27me3 prompted us to investigate their relative conservation. We found that H3K27me3-marked genes are substantially less conserved than genes not marked by this modification. Seventy-nine percent of *N. crassa* H3K27me3-marked genes have orthologs found only in fungi, compared with 49% for non–H3K27me3-marked genes (Fig. 6A). Moreover, unlike *N. crassa* genes generally, a high proportion of H3K27me3-marked genes are limited to the *Neurospora* genus or to closely related genera in the *Sordariomycetes* class; 30% are *Neurospora*-specific (compared with 9% for non– H3K27me3-marked genes) and an

additional 26% are limited to the *Sordariomycetes* (compared with 8% for non–H3K27me3-marked genes) (Fig. 6A).

**Conservation of H3K27me3 in *Neurospora* Species**

Our observation that *N. crassa* H3K27me3-marked genes show a strong fungal-specific bias raised two potentially related questions: (i) How conserved are H3K27me3-marked genes within the *Neurospora* genus? and (ii) To what extent is the mark itself conserved? To address these questions, we determined the distribution of H3K27me3 in two other *Neurospora* species, *N. tetrasperma* and *N. discreta*. Our ChIP-seq analyses demonstrated that H3K27me3 covers a similar fraction of each of the three genomes and that all three species have a similar number of H3K27me3 domains (Table 2; Datasets S4 and S5, http://www.pnas.org/content/110/15/6027.full?tab=ds). The *N. tetrasperma* and *N. discreta* genomes are not yet fully assembled, so it is not certain that the H3K27me3 domains are preferentially near the ends of chromosomes as in *N. crassa*.

Although all three species show comparable fractions of their genomes associated with this mark, we found striking evidence of dynamics. Among *N. crassa* H3K27me3-marked genes, only ~35% are marked in both *N. tetrasperma* and *N. discreta*, ~12% are unmethylated in both comparative species, and nearly 25% are methylated in one comparative species but not the other (Fig. 6B; Table 3). Conversely, homologs of 2.5% of unmethylated *N. crassa* genes are marked with H3K27me3 in *N. tetrasperma* and/or *N. discreta* (Fig. 6B; Table 3). Moreover, compared with non-H3K27me3-marked genes, a high fraction of *N. crassa* genes associated with the H3K27me3 mark are absent in one or both of the comparative species (~14% and ~9%, respectively, compared with ~6% and

~3% for unmethylated *N. crassa* genes; Fig. 6B). Thus, *N. crassa* genes that are not found in one or both of the sister species are marked by H3K27me3 more frequently than those found in all three species (Fig. 6B; Table 3). In sum, we found partial conservation of the H3K27me3 mark among three closely related species of *Neurospora*.

**PRC2 Complex Is Conserved in *N. crassa***

Pioneering work in *Drosophila* demonstrated that the PRC2 complex is responsible for methylation of H3K27. This complex consists of four core subunits in *Drosophila*—E(Z), ESC, SU(Z)12, and p55 —which are highly conserved in plants and animals, although some subunits are duplicated in higher eukaryotes (21). The genome of *N. crassa* contains one homolog for each of the PRC2 subunits, with their predicted functional domains largely intact (Figs. 7 and 8). The *N. crassa* homolog of the gene for the catalytic subunit, E(Z), is *set-7* (46); the homolog of the p55 gene, which we named *npf*, was previously named chromatin assembly complex 3 (*cac-3*) because it was potentially a component of the putative *Neurospora* chromatin assembly factor 1 (CAF-1) complex (46).

To determine whether the four putative PRC2 subunits form a complex in *N. crassa*, we fused a 3xFLAG epitope tag to the amino terminus of the EED homolog expressed under the control of the *qa-2* promoter. We purified tagged EED using an anti-FLAG affinity gel and identified EED and associated proteins by mass spectrometry. In addition to EED, we found strong coverage for the other three putative PRC2 subunits, SET-7, SU(Z) 12, and NPF, implying that, indeed, a PRC2-like complex forms in *N. crassa* (Table 4).

To explore the function of the *N. crassa* PRC2 complex, we obtained knockout strains for the corresponding genes (47). In contrast to their essential role in developmental processes of higher eukaryotes (21), we found that none of the four PRC2 homologs is essential in *N. crassa*. Indeed, strains with knock-outs of *set-7*, *eed*, or *su(z)12* displayed no growth defects under standard growth conditions (Fig. 9A). However, deletion of *npf* resulted in a slow-growth phenotype; its linear extension rate is ~84% of that of WT (Fig. 9A and B). In other systems, besides its role in PRC2, NPF (called RbAp46/RbAp48 in mouse) has been shown to be a histone-binding protein and a component of ATP-dependent nuclear remodeling complexes (48). Considering that growth was not retarded in knockouts for the other three PRC2 subunits, it seems likely the slow-growth of the *npf* strain is due to a role of this protein in complexes other than PRC2. We also found that crosses homozygous for a deletion of *set*-7 were fruitful, indicating that H3K27me3 is not essential for the sexual cycle.

**NPF Is Differentially Required for H3K27me3**

We initially used both immunoblotting and ChIP to test mutants lacking components of the *N. crassa* PRC2 complex for H3K27me3, but found that available antibodies were most reliable for ChIP experiments. We used qChIP to access the level of H3K27me3 enrichment near both telomeres on LG I and at two genic regions on LG VII in each of the PRC2 knockout strains (Fig. 1C). H3K27me3 enrichment was completely lost from the LG I telomeres in all four PRC2 mutants. Similarly, H3K27me3 was eliminated at the two genic regions in the Δ*set-7*, Δ*eed*, and Δ*su(z)12* strains. Surprisingly, there was only a partial reduction of H3K27me3 at these genic regions in

the Δ*npf* strain. To explore this further, we analyzed the distribution of H3K27me3 across the whole genome by ChIP-seq in Δ*set-7* and Δ*npf* strains. Consistent with the qChIP results, we did not observe enrichment for H3K27me3 in the Δ*set-7* strain, implying that the histone methyltransferase catalytic subunit of the PRC2 complex is absolutely required (Fig. 1). Consistent with the initial qChIP results, we found a differential loss of H3K27me3 in the Δ*npf* strain (Fig. 1). Both the size and number of H3K27me3 domains was reduced in the Δ*npf* strain compared with WT (Table 1; Datasets S6 and S7, http://www.pnas.org/content/110/15/6027.full?tab=ds). Although H3K27me3 enrichment was reduced across most areas of the genome, the mark was specifically absent near the telomeres of all of the chromosomes. We conclude that SET-7, EED, and SU(Z)12, but not NFP, are absolutely required for H3K27me3 in *N. crassa*.

**H3K27me3 Domains Are Transcriptionally Quiescent**

To determine whether H3K27me3 represents a repressive mark in *N. crassa*, we analyzed gene expression in a WT strain by RNA-seq (Fig. 10A). As in other model systems, we found few or no transcripts produced from the H3K27me3-marked genes. To illustrate the negative correlation between H3K27me3-marked genes and expression, we plotted transcript abundance versus H3K27me3 level across the genome (Fig. 10C). The H3K27me3-marked genes (blue) and the genes falling on the domain borders (black) showed extremely low transcript levels; the vast majority of transcripts were produced by non-H3K27me3 genes (green).

We next asked whether the absence of H3K27me3 in a Δ*set-7* strain is sufficient to increase expression of H3K27me3-marked genes. Using a stringent threshold for the

change of expression (~7.5-fold), we found 130 genes with increased expression in the Δ*set-7* strain relative to the WT strain (Dataset S8, http://www.pnas.org/content/110/15/6027.full?tab=ds). Derepression of four H3K27me3-marked genes was confirmed by Northern blot analyses of total RNA (Fig. 10A and B; Fig. 11). In addition, five genes showed lower transcript levels in a Δ*set-7* strain (Dataset S9, http://www.pnas.org/content/110/15/6027.full?tab=ds). Overall, the functional classification of the up-regulated genes is similar to that of the total H3K27me3-marked genes, consisting of primarily unannotated genes (Figs. 5 and 12). Interestingly, of the 130 de-repressed genes, only 21 fell completely within the H3K27me3 domains identified in the WT strain. This result is similar to what has been observed in *Arabidopsis* (24). Thus, although loss of H3K27me3 may be necessary, it is not sufficient to increase expression of the majority of H3K27me3-marked genes under the conditions of our experiment.

## Discussion

Elements of the Polycomb repression system, originally uncovered in *Drosophila*, have been found in a variety of higher animals and plants, but not in yeast species that have been examined (*S. cerevisiae* and *S. pombe*). Previously we found that H3K27me3, a hallmark of the Polycomb system, is represented in the model filamentous fungus *N. crassa* (39, 49). Here, we present a genome-wide analysis of the distribution of this chromatin mark, characterize the underlying machinery, and start to explore its function and evolutionary dynamics. A sizable fraction of the *N. crassa* genome (6.8%) is marked

by H3K27me3, covering 774 genes in 223 domains. These domains, some of which are hundreds of kilobases long, are found preferentially near the ends of the chromosomes (Fig. 1). Unlike the case in *Arabidopsis*, in which H3K27me3 covers single genes in domains of less than 1 kb (35), the broad domains in *N. crassa* (12.5 kb average) are reminiscent of *Drosophila* and mammals, which average 70 and 43 kb, respectively (33, 50).

H3K27me3 and H3K9me3 are both regarded as repressive marks (16, 23, 30, 31, 51) but are distributed differently. In *N. crassa*, as in higher eukaryotes, H3K9me3 is a feature of constitutive heterochromatin and is found principally associated with centromeric heterochromatin, which is characterized by H3K9me3, DNA methylation, a paucity of genes, and an abundance of repeats that show evidence of RIP (38, 52). H3K9me3 is also found in *N. crassa* associated with numerous small islands of sequences mutated by RIP and near telomeres (39), adjacent to where we found H3K27me3. Unlike H3K9me3, we show that H3K27me3 is in gene-rich regions. Notably, the H3K27me3 and H3K9me3 regions do not appear to overlap (Fig. 1 and Fig. 3). This is consistent with reports from plant and animal systems that describe mostly mutually exclusive H3K27me3 and H3K9me3 distributions (33, 41-43, 53-55). It will be interesting to learn whether the machinery responsible for methylating H3K9 and H3K27 are inherently incompatible.

As a step to investigate the mechanism of H3K27me3 in *N. crassa*, we identified and tested homologs of PRC2 components identified in other organisms (Fig. 7). We found that H3K27me3 absolutely depends on three of the PRC2 components: SET-7 (equivalent to EZH2), EED, and SU(Z)12. Thus, unlike the situation in *Drosophila* and

other animals, H3K27me3 is not essential in *N. crassa*. Interestingly, we found that the fourth component of the presumptive *N. crassa* PRC2 complex, NPF (*Neurospora* homolog of *Drosophila* P55 and mammalian P48), is not required for all H3K27me3. In particular, NPF is only required for H3K27me3 domains near telomeres; domains farther from telomeres are somewhat affected, shrinking in the absence of NPF. We conclude that NPF is not required for the methyltransferase activity of PRC2, unlike SET-7, EED, and SUZ12. Perhaps NPF and its homologs in other organisms, which have been reported to bind histone H4 (56, 57), help tether the PRC2 complex to nucleosomes via its six WD40 domains. This is consistent with the observation that a trimeric Esc-E (z)-Su(z)12 complex trimethylates H3K27 *in vitro*, but is unable to bind nucleosomes (19). It is interesting that various genomic regions are differentially dependent on NPF. Perhaps regions that do not lose H3K27me3 in the Δ*npf* strain rely on another WD40 domain-containing protein. We are unaware of direct evidence from other organisms of a comparable, genome-wide influence of NPF homologs on H3K27me3 or other histone modifications, but there are clues that the effect is not limited to *N. crassa*; the combined findings of two studies with *Arabidopsis* revealed that H3K27me3 marks approximately half of the genes that become de-repressed in a mutant for the NPF homolog (35, 58). Although *Arabidopsis* does not contain the broad H3K27me3 domains observed in *N. crassa*, *Drosophila*, and mammals, selective reduction of H3K27me3 resulting from loss of *msi1* could be responsible for the de-repression of a subset of H3K27me3-marked genes and their presumptive indirect targets (35, 58).

As in other organisms, we found that *N. crassa* genes marked by H3K27me3 produce little or no transcripts. The silence of these genes is not a simple consequence of

this mark, however, because elimination of H3K27me3 by mutation of *set-7* did not de-repress the bulk of the genes. The Δ*set-7* strain showed up- regulation of 130 genes, but only 21 of these fell within H3K27me3 domains, representing 2.7% of the 774 genes marked by H3K27me3 in the WT strain. The 109 genes that showed increased expression but are located outside of H3K27me3 domains represent 1.1% of the total genes not marked by H3K27me3. Thus, the increased gene expression observed in the *set-7* mutant is modestly skewed toward H3K27me3-marked genes. That only a small subset of genes within H3K27me3 domains was up-regulated suggests that, in addition to loss of the repressive mark, activating signals may be required to express genes in H3K27me3 domains. There are also indications in human, *Drosophila*, and *Arabidopsis* that depletion of Polycomb group genes is only sufficient to activate a subset of H3K27me3- marked genes, leading researchers to postulate a secondary layer of regulation (24, 26, 29, 30, 59-61). In *Arabidopsis*, the up-regulation of genes not marked by H3K27me3 in an H3K27me3-deficient background is thought to result from induction of transcriptional regulators (24). Because the majority of H3K27me3-marked genes in *N. crassa* are unannotated, it is not yet clear if this is the case in *Neurospora*; it will be interesting to learn whether the up-regulated non–H3K27me3-marked genes are controlled by any of the up- regulated H3K27me3-marked genes.

Although H3K27me3 preferentially marks developmental genes in animals, it is not yet clear if this is the case in *N. crassa*, because the vast majority of the marked genes have not been characterized. Similarly, although some developmental genes are marked by H3K27me3 in *Arabidopsis*, a high proportion of H3K27me3-marked genes are also functionally unknown genes in this organism (35). Lack of gene annotation often reflects

a lack of characterized orthologs in other species. Indeed, we found that *N. crassa* H3K27me3-marked genes show a striking lack of conservation; most are confined to the fungal kingdom, with the largest fractions confined to the class *Sordariomycete* and genus *Neurospora* (Fig. 6A). Thus, H3K27me3 seems to preferentially mark poorly conserved or "new" genes. Conceivably, as new genes are incorporated into a genome, H3K27me3 could serve as a "safety" mechanism by silencing them.

To investigate the evolutionary dynamics of H3K27me3 and of the associated genes, we analyzed the distribution of H3K27me3 in two closely related *Neurospora* species. We found that H3K27me3 is present in both *N. tetrasperma* and *N. discreta* and that the number and size of the H3K27me3 domains in both species is similar to *N. crassa*. Although these closely related species predominantly share a common set of genes, we found that those that were not shared (i.e., those that are unique to *N. crassa* genes, or those only found in only one of the other *Neurospora* species examined) are approximately threefold more frequently marked with H3K27me3 than are genes in the overall genome (Fig. 13). Interestingly, among orthologs common to the three species, 35% of the *N. crassa* H3K27me3-marked genes are also marked by H3K27me3 in both *N. tetrasperma* and *N. discreta*. A sizable number of genes that are H3K27me3-marked in *N. crassa* are not marked in at least one of the other species (24.6% "MU" in Fig. 6B) or do not currently have the gene in one (14.1% "M–" in Fig. 6B) or both (9.0% "–" in Fig. 6B) other species. Thus, although the fraction of the genome that is marked by H3K27me3 in the three genomes is equivalent, the distribution of the mark and the associated genes are not highly conserved (Fig. 6B).

The presence of H3K27me3 and PRC2 components in *N. crassa* and some other

lower eukaryotes (e.g., *Chlamydomonas reinhardtii* (22)) and absence of this mark and the associated machinery from some other lower eukaryotes [e.g., *S. cerevisiae* and *S. pombe* (36, 39)] suggests that this system has not been retained throughout evolution (22), and is consistent with its nonessential role in *N. crassa*. Previous studies suggested PRC2 arose before PRC1 and showed that it is the more conserved of the two Polycomb complexes (17). *N. crassa* appears to lack PRC1 homologs, raising the question of how the H3K27me3 mark is "read" in this organism.

## Materials and Methods

### *Neurospora* Strains and Methods

*Neurospora* strains used in this study (see Appendix C for all strains) were grown and crossed following standard procedures (62). The Δ*set-7*, Δ*eed*, Δ*suz12*, and Δ*npf* strains were generated by the *Neurospora* gene knockout project (47) and obtained from the Fungal Genetic Stock Center (FGSC; www.fgsc.net). RNA isolation and Northern blotting was done as described (63), except the mycelium, grown 16 h at 32 °C, was disrupted using a minibead beater (Biospec).

### Chromatin Immunoprecipitation (ChIP)

ChIP was performed as previously described (52) using anti-H3K27me3 (Active Motif 39535; ChIP-seq and qChIP), anti-H3K27me3 (Upstate 07-449; ChIP-chip), anti-H3K9me3 (Active Motif 39161; ChIP-seq), and anti-H3K4me2 (Active Motif 39141; qChIP). ChIP-chip procedures, including microarray design, sample labeling, microarray

hybridization, and data analysis, were conducted as described (38). For qChIP, real-time PCR experiments were performed three times using FAST SYBR Green master mix (KAPA) and analyzed using a Step One Plus Real Time PCR System (Life Technologies). Relative enrichment of H3K27me3 at representative telomeres and genic regions was determined versus input and then standardized to relative enrichment of H3K4me2 at hH4 (see Appendix D for all primers).

**Sequencing**

*Neurospora* strains used for ChIP-seq and RNA-seq were grown in liquid media as described in the figures. Sequencing reads can be downloaded from NCBI (accession no. SRA0688854). ChIP-seq reads and ChIP-chip data were mapped to the *N. crassa* OR74A reference genome (64) (www.broadinstitute.org/ annotation/genome/neurospora/MultiDownloads.html), *N. crassa* OR74A v10 genome assembly, *N. tetrasperma* FGSC 2508 mat A v2.0 reference genome (65), or the *N. discreta* FGSC 8579 mat A (US Department of Energy Joint Genome Institute).

**Bioinformatic Analysis**

Orthologs were identified by aligning the three *Neurospora* genomes with Mercator (66) and identifying orthologs as genes found in the same position between the genomes. Phylogenetic clades were identified by clustering genes into orthologous groups using OrthoMCL (67), which first links genes by similarity with the BLASTP program followed by the MCL graph algorithm, which identifies groups through a Markov Clustering procedure (68). Comparison of orthology relationships and

H3K27me3-marked and -unmarked genes was completed with custom Perl scripts (https://github.com/hyphaltip/H3K27) written with BioPerl (69). Functional classification of genes/proteins was conducted using MIPS FunCat (http://mips.helmholtz-muenchen.de/genre/proj/ncrassa/Search/Catalogs/searchCatfirstFun.html). Domain prediction used RSEG software (http:// smithlab.usc.edu/histone/rseg/) with a bin-size of 500 bp. The RSEG difference program was run to determine domain differences between H3K27me3 domains predicted from independent ChIP-seq experiments.

**cDNA Preparation**

mRNA was purified from 100 μg of DNase-treated total RNA using the Oligotex mRNA Mini Kit (Qiagen, 70022). First and second strand cDNA synthesis was then conducted on 100 ng of mRNA with random primers using the SuperScript® Double-Stranded cDNA Synthesis Kit (Invitrogen Cat. # 11917-010). The cDNA was fragmented by sonication with a Branson Sonifier 450 on output 1.2, duty cycle 80, for 80 pulses. The fragmented cDNA was purified on Qiagen MinElute columns (Qiagen, #28206).

**Preparation of ChIP-Enriched DNA and Double-Stranded cDNA for Sequencing**

ChIP-enriched DNA and double-stranded cDNA were prepared for sequencing by first blunting the ends of the fragments using the Quick Blunting Kit (New England Biolabs, E1201L) followed by purification of the DNA on a Qiagen MinElute column using the PCR purification protocol. Adenosines (A's) were then added to the blunted

ends using Klenow fragment (3' to 5' exo-) (New England Biolabs, M0212S) followed by purification of the DNA on a Qiagen MinElute column using the reaction cleanup protocol. Paired-end adapters containing 6 bp barcodes, to allow for multiplexing, were ligated to the DNA fragments with Quick DNA Ligase (New England Biolabs, M2200S). The DNA was size-fractionated on a 2% agarose gel. "Invisible" fragments between 250-400 bp were excised and purified with the MinElute Qiagen Gel Purification system (Qiagen, 28604). Purified DNA was then amplified by PCR using the PfuTurbo Cx Hotstart DNA polymerase (Agilent Technologies Cat. #600410) using a limited number of cycles. Amplified DNA was size-fractionated on a 2% agarose gel in 1xTAE buffer. The "smear" of amplified DNA between 300-450 bp was excised from the gel and purified as before with the Qiagen MinElute Gel Purification kit. Purified DNA was quantitated using a Qubit fluorometer (Life Technologies), multiplexed with other samples containing different barcodes, and sequenced on either the Illumina Genome Analyzer II (40-nt read length) or HiSeq 2000 (50-nt read length) next-generation sequencers (Genomics Core Facility, University of Oregon).

**Sequence Analysis**

Sequence alignments were performed using Bowtie with default settings (70) and output in SAM format (71). The SAMTools tool kit was utilized to convert from the SAM format to the BAM format and to remove PCR artifacts (rmdup tool) that appeared as large spikes in the data (71). RNA-seq reads were mapped to the *N. crassa* OR74A reference genome using the default settings on TopHat (72). The mapped RNA-seq reads were then used to estimate transcript abundance (FPKM - fragments per kilobase of exon

per million fragments mapped) using the Cufflinks program (72). The Cuffdiff program was used to compare the relative abundance of transcripts between different RNA-seq samples (72). For display purposes, ChIP-seq and RNA-seq reads were processed using the "count" function of IGVtools (http://www.broadinstitute.org/igv/igvtools) to generate a tiled data file (.tdf) representing read densities over 300 bp windows across the genome. These .tdf files were displayed using the Integrative Genomics Viewer (IGV:http://www.broadinstitute.org/igv) (73).

## Bridge to Chapter III

After demonstrating that PRC2 was both structurally and functionally conserved in *N. crassa*, my next goal was to explore the control of H3K27me3 distribution. By ChIP-seq we made two major observations, which I will address in Chapter III; (1) H3K27me3 domains are not randomly positioned, but preferably localize close to telomeres and (2) the distribution of H3K27me3 and H3K9me3 domains is mutually exclusive. To address the first observation, we investigated whether the H3K27me3 mark is controlled by *cis*-acting signals. To address the second observation, we dissected the pathway of constitutive heterochromatin formation and assessed its effects on global H3K27me3 distribution. We discovered that HP1, a chromodomain protein that binds to H3K9me3, either directly or indirectly prevents H3K27me3 relocalization to constitutive heterochromatin.

# CHAPTER III

# THE ABSENCE OF HP1 BINDING RELOCALIZES H3K27ME3

This chapter contains unpublished work exploring the control of H3K27me3 distribution. This work was performed in collaboration with Neena Leggett, Kevin McNaught, Michael Rountree and Eric Selker. I performed all ChIP experiments described in this chapter with the exception of those performed by Michael Rountree, specified below. Neena Leggett analyzed most of the ChIP-seq high-throughput sequencing. Michael Rountree contributed wild-type distributions of H3K4me3, H3K9me3 and H3K27me3 and mapped the distribution of H3K27me3 in a Δ*dim-5* strain. I thank Kevin McNaught for assistance with the *csr-1* targeting strains. I also thank Douglas Turnbull for performing all high-throughput sequencing.

## Introduction

Constitutive heterochromatin remains permanently condensed and is typically associated with repetitive DNA, most notably at the centromeres and telomeres (74, 75). *N. crassa* constitutive heterochromatin contains relics of repeat-induced point (RIP) mutation, a genome defense system that produces C to T mutations, thereby leaving the DNA A:T-rich. This DNA recruits DCDC (the DIM-5/-7/-9, CUL4/DDB1 Complex) to catalyze the trimethylation of histone H3 lysine 9 (H3K9me3) (38, 76). The chromodomain protein HP1, which binds H3K9me3, is a member of several known complexes in *Neurospora*. First, it partners with Defective In DNA Methylation-2

(DIM-2), a DNA cytosine methyltransferase (77), resulting in the correlation of H3K9me3 and DNA methylation at A:T-rich DNA (38). HP1 is also a member of the HP1, Chromodomain Protein-2 (CDP-2), histone deacetylase-1 (HDA-1) and chromatin associated protein (CHAP) (HCHC) complex, a silencing complex that operates independent of 5mC (78). Finally, HP1 is part of the DMM DNA Methylation Modulator (DMM) complex, which prevents the inappropriate spreading of constitutive heterochromatin into nearby genes (79). Finally, *Neurospora* HP1 co-purifies with a close homolog of Mi-2, a member of the nucleosome remodeling and deacetylase (NuRD) complex (80).

Unlike constitutive heterochromatin, facultative heterochromatin has the potential to become transcriptionally active euchromatin, influenced by temporal, spatial or heritable factors (81). A hallmark of facultative heterochromatin is trimethylated histone H3 lysine 27 (H3K27me3), which is catalyzed by the Polycomb Repressive Complex 2 (PRC2), described in Chapter II. H3K27me3 preferentially marks developmental and species-specific genes in animals, plants and fungi (27, 35, 82). H3K27me3 covers domains of up to hundreds of kilobase pairs in animals and fungi (34, 43, 82, 83). This contrasts H3K27me3 distribution in plants, where H3K27me3 typically covers single genes (35).

*N. crassa* H3K27me3 domains generally do not overlap with constitutive heterochromatin, which are marked by both 5mC and H3K9me3 (82). The mutually exclusive distribution of H3K27me3 and DNA methylation has also been reported in other organisms (33, 41-43, 53-55). 5mC directly inhibits PRC2 from binding to nucleosomes in HeLa cells, *in vitro* (84). In plants and mammals, H3K27me3 domains

are mostly DNA hypomethylated (35, 85). However, H3K27me3 and DNA methylation overlap in human immune cells at regions of low CG density (86) and in cancer cells (85, 87, 88). Studies in other systems report that the disruption of DNA methylation globally redistributes H3K27me3 to constitutive heterochromatin, suggesting crosstalk between constitutive and facultative heterochromatin; several notable reports are summarized below.

In *A. thaliana*, three DNA methyltransferases catalyze DNA methylation in three sequence contexts, CG, CHG and CHH (where H is any base except G): MET-1 (DNA METHYLTRANSFERASE 1), which maintains CG methylation; CMT3 (CHROMOMETHYLASE 3), which catalyzes most CHG methylation and DRM2 (DOMAINS REARRANGED METHYLTRANSFERASE 2), which is recruited to chromatin by siRNAs through the RNA-directed DNA methylation (RdDM) pathway and establishes DNA methylation in all sequence contexts (89). In *met1* plants, three major events occur (1) H3K27me3 is elevated at H3K9me2 hypomethylated genes, such as transposons and other highly repetitive sequences, reactivating most transposons (90). (2) H3K27me3 is simultaneously reduced at Polycomb group targets, a subset of which gains ectopic H3K9me2, maintaining their repression. (3) Some genes that are pre-marked with low levels of either H3K9me2 or H3K27me3 in wild-type become H3K9me2 hypermethyated in *met1*. The increase in H3K9me2 then stimulates the RdDM pathway and subsequent CHG methylation, resulting in a gain of CHG methylation at genes normally marked by CG methylation (90).

In mammals, DNA methylation occurs predominantly in the CG context and *Dnmt1* is responsible for the maintenance DNA methylation. In mouse somatic cells

homozygous for a hypomorphic allele of *Dnmt1* (*Dnmt1*$^{-/-}$), 5mC is reduced by over eighty percent. In *Dnmt1*$^{-/-}$ cells, H3K27me3 is redistributed in a pattern similar to *met1* plants; typical targets of Polycomb group proteins lost H3K27me3 and regions of high 5mC gained H3K27me3 (91). H3K27me3 was similarly redistributed in wild-type cells upon treatment with 5-aza-2'-deoxycytidine, which eliminates over half of the 5mC in the genome. Two studies in mouse embryonic stem cells also describe global H3K27me3 redistribution using cells with a triple knockout of *Dnmt3a*, *Dnmt3b* and *Dnmt1* (*Dnmt*$^{TKO}$), which reduces global 5mC levels by ninety-nine percent (85, 92). Notably, while the altered patterns of H3K27me3 do not massively up-regulate genes normally marked by DNA methylation in either mouse study, the loss of H3K27me3 from Polycomb targets is sufficient for their upregulation (85, 92).

The signals that recruit PRC2 are not well defined. Recruitment of H3K27me3 in *D. melanogaster* appears to rely on Polycomb group Response Elements (PREs), which are *cis*-acting sequences containing multiple motifs that recruit DNA-binding proteins to heritably silence genes (93). Computational methods using experimentally-defined motifs to predict PREs have had some limited success (94-96). PREs have been difficult to define partly because the DNA-binding proteins corresponding to the binding sites in the PREs are poorly conserved outside of *D. melanogaster* (12). Isolated candidate PREs have been identified in mammals and *A. thaliana* (97-99), and most recently, a 220 nucleotide PRE was defined in mouse embryonic stem cells (100). Distinct mechanisms for recruiting H3K27me3 may exist in separate organisms; for example, mammals and plants may rely on unmethylated CpG-rich dinucleotides to recruit PRC2 (35, 101-103).

## Results

### H3K27me3 Is Globally Redistributed in the Absence of HP1 Binding

The mutually exclusive distributions of facultative heterochromatin and constitutive heterochromatin in *Neurospora* (82) prompted us to test whether there was crosstalk between the two forms of heterochromatin. We first investigated how the absence of DCDC subunits, which leads to loss of H3K9me3 (76), affects H3K27me3 distribution. We compared the distribution of H3K27me3 genome-wide, as assessed by ChIP-seq in wild-type *Neurospora* with the distribution of this mark in strains bearing deletions of the genes encoding the members of DCDC (82). Strikingly, we observed a global redistribution of H3K27me3 in each of the DCDC deletion strains, with the exception of Δ*dim-7*, which appeared to lose essentially all H3K27me3 (Figs. 14, 21, 22). H3K27me3 domains observed in a wild-type strain were lost or became significantly smaller in the *dim-5*, *dim-9*, *dim-8* and *cul4* deletion strains (Fig. 14A-D). In contrast, most regions of constitutive heterochromatin, including the centromeres, gained H3K27me3 (Figs. 14A, 15). Representative ChIP-seq results were validated by qChIP; specifically we tested two sub-telomere domains on LG I to observe the significant reduction of H3K27me3 and two genes on LG VII, NCU06955 and NCU09590, to observe the loss of H3K27me3 (Fig. 14D).

We observed minor differences in H3K27me3 relocalization among the *dim-5*, *dim-9*, *dim-8* and *cul4* strains (Fig. 14, 15). For example, in the Δ*dim-8* strain, H3K27me3 was not found entirely across many centromeres, unlike the case at many centromeres in the Δ*dim-5* strain, and H3K27me3 was more significantly enriched

toward the "left" side of the centromeres while mostly absent from the "right" side. It is curious that the same side of the centromere consistently lost H3K27me3, since "right" and "left" have been arbitrarily defined. To explore whether H3K27me3 relocalization was stochastic, we performed biological replicates of ChIP-seq experiments in both the Δ*dim-5* and Δ*dim-8* strains and observed apparently identical H3K27me3 distributions (Fig. 15).

We hypothesized that relocalized H3K27me3 maintains chromatin compaction at constitutive heterochromatin that is essential for viability and that the absence of both marks would be a lethal combination. To address whether the relocalization of H3K27me3 is necessary for viability, we created a Δ*set-7*;Δ*dim-5* strain; not only is this strain viable, but it does not show an obvious defect in morphology.

Lack of DCDC subunits abolish both 5mC and HP1 binding (76). To resolve whether H3K27me3 redistribution resulted from loss of H3K9me3, HP1 binding or 5mC, we performed ChIP-seq and qChIP for H3K27me3 in Δ*dim-2* strains and a Δ*hpo* strain (*hpo* is the gene that encodes HP1) (Figs. 16, 21, 22). Deletion of the *dim-2* gene abolishes DNA methylation but does not appreciably affect the genomic distributions of H3K9me3 and HP1 (38). Using two independent Δ*dim-2* strains, we observed that the distribution of H3K27me3 was essentially identical to that observed in the wild-type strain, suggesting that 5mC does not influence H3K27me3 (Fig. 17). However, we did observe an exception on LG VI, where three novel H3K27me3 domains were present in both Δ*dim-2* strains (Fig. 17). Notably one of these novel domains overlaps an H3K9me3 domain found in wild-type. It will be interesting to determine whether this H3K9me3 domain is both present in Δ*dim-2* and bound by HP1.

Previous work demonstrated that an *hpo* mutant created by RIP [N2556, see (104)] shows a complete loss of 5mC distribution and has largely unchanged H3K9me3 on LG VII and a few previously identified methylated sequences on other linkage groups (38). The few genomic regions that show loss of H3K9me3 in the $hpo^{RIP2}$ strain are shorter and more CG-rich than regions that retained H3K9me3 (38).

Since the $hpo^{RIP2}$ strain was not a null allele, we mapped H3K9me3 in an *hpo* deletion strain (Figs. 16, 21). As had been previously observed, a significant portion of H3K9me3 is retained in the absence of HP1. However, we observed slightly lower H3K9me3 across the centromere compared to wild-type and quite a few regions of constitutive heterochromatin lost H3K9me3 enrichment; we validated these results by qChIP.

To explore the possibility that loss of HP1-binding was responsible for the H3K27me3 redistribution observed in DCDC mutants, we performed H3K27me3 ChIP-seq on a strain bearing the *hpo* null allele and found that H3K27me3 was redistributed in the *hpo* mutant as in the DCDC mutants, suggesting that HP1 binding may normally prevent occurrence of H3K27me3 at constitutive heterochromatin.

**Substitutions Surrounding H3K9 Influence H3K27me3 and H3K9me3 Distributions**

Amino acid substitutions in histone H3 surrounding the K9 residue disrupt constitutive heterochromatin (49). Both the R8A and S10A substitutions significantly reduced the activity of DIM-5, resulting in major loss of H3K9me3 and HP1 binding as well as a semi-dominant or recessive loss of 5mC (49, 105). To assess whether the loss of H3K9me3 is uniform in these mutants, we determined the distribution of the mark by

ChIP-seq. In both mutants, we observed a marked loss of H3K9me3 at relatively small regions of constitutive heterochromatin, such as 8:A6, while this modification was retained at large heterochromatin regions, such as the centromere. Given the widespread loss of H3K9me3, we next assessed H3K27me3 in strains bearing the R8A and S10A substitutions by ChIP-seq. As with the DCDC mutants, with the exception of Δ*dim-7*, we observed global H3K27me3 relocalization (Figs. 18 and 21).

The A7M substitution does not greatly reduce H3K9me3 or influence HP1 binding, although it does significantly reduce 5mC (49). In order to investigate H3K27me3 distribution in the A7M strain, we performed ChIP-seq and qChIP. Considering that this mutant shows an apparently normal distribution of HP1, we did not expect H3K27me3 relocalization. Instead, we observed an almost complete loss of H3K27me3 in an A7M strain (Figs 19 and 21). H3K27me3 domains were only retained very close to most of the telomeres and were completely lost from distal regions that normally show H3K27me3.

Although H3R2 is not located within the region of the histone that DIM-5 recognizes (106), mutating this residue to a leucine led to a nearly complete loss of 5mC (49). H3K9me3 and HP1 binding appeared normal by western blot and immunofluorescence, respectively, suggesting a role for R2 downstream of H3K9 methylation and HP1 binding (49). To explore the effect of R2L on H3K27me3, we performed ChIP-seq for this modification. We found that H3K27me3 was abolished across the genome, except at H3K27me3 domains very close to the telomeres. While this finding is similar to our observations in the A7M substitution, the detailed H3K27me3

distribution in strain showed some differences; specifically we observed slightly larger H3K27me3 domains proximal to the telomeres in the R2L strain.

We also performed qChIP with H3A15M, P16A, R17L, K18R and K23R substitution strains, as well as with the "heterozygous" K4L substitution strain, which contains one wild-type copy of *hH3* at the endogenous locus and one ectopic copy of *hH3* that had been mutated. In each of these strains, both DIM-5 activity and 5mC were unaffected, with the exception of P16A and R17L, in which minor reductions in 5mC were observed (49). None of these substitutions had a noticeable effect on H3K27me3 enrichment, assessed by qChIP, indicating that only select substitutions of histone tail residues affect H3K27me3.

**H3K9me3 Distribution Is Unaffected in PRC2 Mutants**

Given the redistribution of H3K27me3 upon loss of HP1 binding, we wanted to further explore the relationship between facultative and constitutive heterochromatin. We asked whether disruption of facultative heterochromatin disrupts constitutive heterochromatin, so we tested if the loss of H3K27me3 alters H3K9me3. The PRC2 complex is responsible for all H3K27me3 (82). Deletion of any of the three core PRC2 members (*set-7*, *eed* or *suz12*) is sufficient to abolish H3K27me3 (Chapter I). We mapped H3K9me3 distribution in strains bearing deletions of the PRC2 catalytic subunit, *set-7*, and the non-catalytic subunit *eed*. Both ChIP-seq, and qChIP experiments did not reveal a difference in the distribution of H3K9me3 in either of the PRC2 deletion strains relative to wild-type (Figs. 20, 21), suggesting a unidirectional relationship between constitutive and facultative heterochromatin. This leads us to conclude that while the loss

of H3K9me3 leads to changes in the distribution of H3K27me3, the reverse does not appear to be the case in *Neurospora*.

**Segments of an H3K27me3 Domain Are Unable to Trigger *de novo* H3K27me3 at *his-3* and *csr-1***

H3K27me3 is organized into large domains, averaging 12.5 kb in *N. crassa.* We wished to explore the possibility that *cis*-acting signals recruit H3K27me3, perhaps comparable to PRE elements in *Drosophila*. As a first step, we tested whether segments of an H3K27me3 domain would gain H3K27me3 when moved to an ectopic site. We tested eight three kb segments, each located within a large 45 kb H3K27me3 domain, when moved to the *his-3* locus, which is not normally marked by H3K27me3 (Fig. 23A, B).

To ensure that our qChIP primers only detected the ectopic segment, we created a host strain (N4933) with a deletion of the endogenous H3K27me3 domain. We did not detect enrichment at each of the eight segments at *his-3* by qChIP, using two primers pairs specific to each three kb segment. It was possible that *his-3* is refractory to H3K27me3, so we also tested each of the eight segments at a second locus, *csr-1*, and evaluated H3K27me3 enrichment in a similar manner. None of the eight segments were sufficient to recruit H3K27me3 either locus (Fig. 23C,D).

**H3K27me3 Enrichment at Randomly Integrated Regions**

Since H3K27me3 could not be recruited to either *his-3* or *csr-1*, we randomly integrated H3K27me3 segments. We used several of the same three kb segments (labeled

1, 2 and 3 in Fig. 23B) that we tested at *his-3* and *csr-1* and also tested 10 and 12 kb fragments (labeled 9 and 10, respectively, in Fig. 23B), in case H3K27me3 signals require a larger "genomic context" to initiate H3K27me3. Each of the H3K27me3 segments was separately co-transformed, along with the *bar* gene, which confers resistance to the antifungal agent basta, into a host strain (N4933), containing a 47.4 kb deletion which removes the entire H3K27me3 domain. Basta-resistant transformants were screened by Southern hybridization to assess approximate copy number of the transforming DNA and qChIP, using two primers located within each H3K27me3 segment, was used to determine H3K27me3 enrichment.

We created eight strains in total: five strains randomly integrated 1, 2 and 3, two strains randomly integrated 9 and one strain randomly integrated 10. Seven of the eight randomly integrations were insufficient to recruit H3K27me3. However, one strain, containing ectopically integrated 9, showed *de novo* H3K27me3 (Fig. 23E). Since the other fragments were insufficient to recruit H3K27me3 when targeted to *his-3*, *csr-1* or at random locations, one possibility is that the fragment integrated into an existing H3K27me3 domain and that surrounding H3K27me3 spread into the fragment. Unfortunately, our attempt to determine the location of the integration site of the H3K27me3 regions to test this hypothesis was unsuccessful.

**Investigating the Effect of Partial Deletions on H3K27me3**

To define a minimal DNA sequence that is required to recruit H3K27me3, we constructed fifteen deletions within an H3K27me3 domain that contains fourteen predicted genes, containing *hph* at each of the deleted regions (Fig. 24). The deletions

range from 0.9 to 16.8 kb. We tested H3K27me3 enrichment proximal to *hph* by qChIP to determine if critical H3K27me3 signals had been deleted (Fig. 24).

Many deletions significantly reduced H3K27me3, suggesting that recruitment signal(s) were disrupted, either by the deletion or by the introduction of the *hph* sequences (Fig. 24). Several deletions did not show a significant effect on the level of H3K27me3, suggesting that portions of the domain are dispensable for H3K27me3.

Two strains showed particularly perplexing results. N4724 contains a deletion of 1.8 kb, while N4937 contains a smaller deletion of 0.9 kb, which overlaps the 1.8 kb deletion. It is curious that the 1.8 kb deletion strain showed minor H3K27me3 reduction while the 0.9 kb deletion strain significantly reduced H3K27me3. It is possible that three-dimensional contacts are responsible for this result.

To test if the introduction of *hph* is sufficient to disrupt H3K27me3 within the domain, we inserted *hph* into the center of the H3K27me3 domain (N4727 in Fig. 24). We did not observe a reduction of H3K27me3 in the *hph* insertion strain compared to wild-type, suggesting that the insertion of *hph* is not sufficient to perturb H3K27me3 enrichment, at least at the site tested.

**Chromosomal Translocations Alter the Distribution of H3K27me3**

The absence of H3K27me3 induction by ectopically targeting DNA that is normally H3K27me3-marked suggests that the signal for H3K27me3 is not contained within all DNA that is normally H3K27me3-marked. As described in Chapter I, H3K27me3 is organized into large domains preferentially located proximal to telomeres. We hypothesized that proximity to the telomere influences the locations of H3K27me3

domains, so we explored whether translocations resulting in rearrangement of the sub-telomeres relative to the centromere affected H3K27me3 domains. We took advantage of two translocation strains, AR16 and OY329, each generated by ultra-violet mutagenesis (107), obtained from the FGSC (www.fgsc.org), and performed H3K27me3 ChIP-seq with each of these strains.

AR16 is a pericentric inversion affecting LG I, in which a segment of the left telomere, containing approximately 1.9 Mb, interchanged with the right telomere, containing approximately 510 kb [Fig. 25 and (108)]. By ChIP-seq we find a novel H3K27me3 domain on LG IL in the AR16 strain relative to wild-type. Since the region affected by the translocation on IR is shorter than that of IL, it is possible that this novel H3K27me3 domain results from a closer proximity to the telomere in the translocation strain compared to the wild-type strain. We also observe the loss of an H3K27me3 domain on LG IR that is typically fairly close to the telomere and we are currently unable to explain the loss of H3K27me3 at this region.

Perplexingly, we found an H3K27me3 domain on LG III in the AR16 strain that was absent in the wild-type strain. The novel H3K27me3 domain could be a consequence of a disruption to chromatin on LG III that has not been characterized. It is also possible that the novel domain is due to the alteration of three-dimensional contacts within AR16 relative to a wild-type strain. The whole-genome sequencing of this strain will distinguish between these possibilities.

OY329 is an insertional translocation in which a segment of LG VIR, approximately 560 kb, is inserted into LG III at a region very distant from either telomere [Fig. 26, (108) and D. P. Kasbekar and Sonamit Crassa, personal communication]. By

ChIP-seq, H3K27me3 enrichment located downstream from the proximal breakpoint (relative to the centromere) is similar to a wild-type strain. Several H3K27me3 domains proximal to the telomere in a wild-type strain are absent in the OY329 strain. Importantly, novel H3K27me3 domains located upstream of the proximal breakpoint at the new sub-telomere.

Our ChIP-seq analysis of H3K27me3 in the AR16 and OY329 translocation strains suggest a critical role for proximity to the telomeres in the placement of H3K27me3 domains. However, since large domains of H3K27me3 are conserved in the translocation strains, the telomere does not solely control H3K27me3 distribution. Further analysis of H3K27me3 in other translocation strains will hopefully aid in our understanding of H3K27me3 distribution.

**Occasional Spreading of H3K27me3 Into *hph***

The 45 kb H3K27me3 domain on LG VI that we investigated in our deletions, *his-3* and *csr-1* targeting contains fourteen predicted genes. While H3K27me3 genes generally show low expression by RNA-seq (Chapter II), eight of the fourteen genes have corresponding expressed sequence tags (ESTs), annotated by the Broad Institute. To determine whether H3K27me3 is capable of spreading into "foreign" sequences, such as *hph*, we used strains from the *Neurospora* knockout project, in which eight genes within the 45 kb domain had been separately replaced with *hph*. Of the eight strains, five have associated ESTs (deletions of NCU07082, NCU07083, NCU07091, NCU07092 and NCU07094) while three do not (deletion of NCU07085, NCU07086 and NCU07087).

We monitored H3K27me3 spreading by qChIP using primers specific to *hph* (primers listed in Appendix D).

We observed spreading of H3K27me3 into *hph* in the ΔNCU07085, ΔNCU07086, ΔNCU07087, ΔNCU07091, ΔNCU07092 and ΔNCU07094 strains, but did not observe significant spreading within either the ΔNCU07082 or ΔNCU07083 strains (Fig 27A). It is noteworthy that these strains were grown on medium containing hygromycin. To determine whether the selection for *hph* transcription affected H3K27me3, we passaged four of the strains that showed spreading on hygromycin medium (ΔNCU07087, ΔNCU07091, ΔNCU07091 and ΔNCU07094) three times on slants containing hygromycin-free minimal medium and again performed qChIP experiments. Unexpectedly, we observed significant depletions of H3K27me3 among all strains (Fig 27B). It is possible that growing these strains on hygromycin medium forced the transcription of *hph*, which recruited H3K27me3 machinery and that when the strains were grown on minimal medium, the lack of *hph* transcript failed to recruit the H3K27me3 mark. These experiments should be repeated to confirm these preliminary results.

**Chromosomal Sites of PRC2 Binding**

In an attempt to determine sites of PRC2 binding and perhaps putative PREs, we constructed 3xFLAG tagged EED and NPF strains (N4879 and N4880, respectively) to map EED and NPF binding sites by ChIP-seq. However, we did not detect sufficient enrichment of either 3xFLAG-EED or 3xFLAG-NPF. It is possible is that these proteins weakly or only transiently interact with chromatin, therefore necessitating the use of

cross-linking agents other than formaldehyde.

We next turned to an alternative method, namely DNA adenine methyltransferase identification (DamID) to assess PRC2-subunit localization. We constructed C-terminus Dam-tagged strains with the chimeric genes at the endogenous loci of *eed*, *suz12* and *npf* (N5267, N5268, N5269, respectively; attempts to tag *set-7* were unsuccessful). Unfortunately, we were unable to detect digestion by DpnI at several H3K27me3 regions using the Dam-EED and Dam-SUZ12-tagged strains, suggesting poor expression of the Dam epitope in both strains. In contrast, the Dam-NPF strain appeared to localize to both facultative heterochromatin as well as euchromatin, suggesting nonspecific binding. The binding locations of PRC2 subunits in *N. crassa* are therefore currently unknown.

**A Variety of Mutants Have No Obvious Effect on H3K27me3**

The unexpected relationship between H3K27me3 and constitutive heterochromatin prompted a search for additional novel connections between H3K27me3 and a variety of mutants. We tested mutants of three histone deacetylases: NST-1 (*Neurospora* Sir Two-1; a nicotinamide adenine dinucleotide ($NAD^+$)-dependent deacetylase that is thought to specifically act on histone H4 (39); HDA-1, a homolog of the yeast histone deacetylase Rpd3, which acts on deacetylates histones H3 and H4 and is a subunit of the *Neurospora* HCHC (HP1, CDP-2, HDA-1 and CHAP) complex (78, 109); HDA-3, an essential type II histone deacetylase that is part of the two distinct complexes [(109) and Chapter IV]. We performed qChIP with deletions of *cdp-2*, *hda-1*, *chap* and *hda-3* and found that none of these histone deacetylase mutants or associated members of HCHC had an observable effect on H3K27me3.

SET-7 is the enzymatic subunit of PRC2 that catalyzes the trimethylation of H3K27 (Chapter I). We tested other SET domain mutants to evaluate their effect on H3K27me3: *set-1*, *set-2* and *set-3*, as well as the non-SET domain histone methyltransferase, *dot-1* (Disruptor of Telomeric Silencing-1). None of these SET mutants altered H3K27me3 enrichment. Lastly, DMM-1 (DNA Methylation Modulator-1) is a JmjC domain protein that prevents the inappropriate spreading of H3K9me3 and 5mC into nearby genes (79). We did not detect altered H3K27me3 enrichment by qChIP in a strain containing the deletion of *dmm-1*.

JARID2 is a JmjC containing protein that is present in a subset of PRC2 complexes (110). Unlike other proteins that contain the JmjC domain, JARID2 does not exhibit demethylase activity (111). In *Neurospora*, a gene annotated as NCU01238 contains a putative JmjC domain. Since we did not detect this protein in our purification of EED (Chapter I), we speculated that it was a good candidate H3K27 demethylase. Since the H3K27me3 antibody exhibits with poor specificity by western blot, we turned to H3K27me3 ChIP-seq in a strain containing the deletion of NCU01238. By ChIP-seq, we observed a distribution of H3K27me3 comparable to that of a wild-type strain.

## Discussion

*Neurospora* contains mutually exclusive distributions of facultative heterochromatin, marked by H3K27me3, and constitutive heterochromatin, containing HP1-bound H3K9me3 and DNA methylation. Facultative and constitutive heterochromatin does not overlap in several other organisms (33, 41-43, 53-55). Studies

in both mouse and plants find that DNA methylation inhibits H3K27me3 and that the removal of DNA methylation is sufficient to relocalize H3K27me3 to constitutive heterochromatin (85, 90, 92). Here, we investigated what might be responsible for the incompatibility between facultative and constitutive heterochromatin in *Neurospora*.

We made two major observations (1) H3K27me3 is mostly lost from its normal locations and (2) H3K27me3 is retargeted to constitutive heterochromatin, in strains containing the deletion of *hpo*, the deletion of DCDC subunits with the exception of *dim-7*, and hH3 substitutions at R8 and S10. It is intriguing that H3K27me3 was mostly eliminated from regions where it was found in the wild-type strain; one possibility is that PRC2 is limiting and could favor constitutive heterochromatin over facultative chromatin, therefore diluting PRC2 from wild-type targets. Overexpression of all four PRC2 subunits in any of the aforementioned strains would address this hypothesis. If overexpression leads to H3K27me3 on both the standard H3K27me3 regions and constitutive heterochromatin would support this hypothesis. With regard to the second observation, the H3K27me3 redistribution in each of these strains coincides with the loss of HP1 binding. In wild-type, DCDC is either directly or indirectly targeted to A:T-rich DNA through an unknown mechanism. An open question is, in the absence of HP1 binding, does PRC2 rely on the same recruitment signal(s) as DCDC to target A:T-rich DNA?

The chromodomain of HP1 binds to H3K9me3, allowing DIM-2 to catalyze 5mC (52, 104). H3K9me3 is not lost in a Δ*dim-2* strain, suggesting a unidirectional pathway in which the establishment of H3K9me3 precedes DNA methylation (38). Importantly, two Δ*dim-2* strains, which are progeny from the same cross, showed nearly normal

H3K27me3 distribution, demonstrating that removal of 5mC does not affect H3K27me3 distribution.

HP1 is also part of the HCHC complex, which contains the chromodomain protein, CDP-2, as well as HDA-1 and CHAP (78). A previous study reported that CDP-2 stability depends on HP1, so it was conceivable that the H3K27me3 relocalization observed in the Δ*hpo* strain was indirectly due to the loss of CDP-2 (78). However, a Δ*cdp-2* strain contained H3K27me3 enrichment similar to wild-type, eliminating the possibility that the HCHC complex was responsible for H3K27me3 redistribution (Fig. 16G). We also tested strains containing deletions of the remaining HCHC subunits, *hda-1* and *chap*, and observed H3K27me3 enrichment similar to a wild-type strain (Fig. 16G). HP1 is also a member of the DMM complex, however it only acts at the edges of constitutive heterochromatin and is insufficient to explain H3K27me3 blanketing large regions of constitutive heterochromatin (79).

Our observation that HP1 prevents H3K27me3 at constitutive heterochromatin in *N. crassa* is complementary to findings that regions marked by 5mC are refractory to H3K27me3 in plants (upon the disruption of *met1*) and mice (upon disruption of or *Dnmt1*). *Arabidopsis* does not contain a close homolog to HP1, but there is strong evidence in plants that a different mechanism controls the relocalization of H3K27me3 (90). A triple mutant of *Arabidopsis*, with defective *suvh4*, *suvh5* and *suvh6* (*suvh456*) genes abolished both H3K9me2 and CHG methylation and retained CG methylation; while the *met1* mutant retained H3K9me2 and CHG methylation but CG methylation was lost (90). The authors observed much stronger ectopic H3K27me3 at two transposable

elements, *ROMANIAT5* and *AtCOPIA28*, in *met1* plants compared to *suvh456*, suggesting that loss of CG methylation is responsible for H3K27me3 relocalization.

We considered the possibility that H3K27me3 compensates for silencing at normally 5mC domains and transcriptional inactivation at constitutive heterochromatin is important for viability. Our finding that a Δ*set-7*;Δ*dim-5* double mutant is viable and has no significant growth defects argues against this possibility. It will be interesting to learn whether genes within constitutive heterochromatin that gain H3K27me3 remain inactive. If so, this would be consistent with mouse studies, in which the relocalization of H3K27me3 due to loss of H3K9me3 or DNA methylation does not significantly alter transcription (85, 92). In contrast, the coupled absence of CG methylation and gain of ectopic H3K27me3 in plants is sufficient to activate transposable elements, indicating that H3K27me3 cannot functionally replace CG-mediated silencing in at least one species (90).

Although H3K27me3 and H3K9me3 normally occupy distinct chromosomal regions in *Neurospora*, we observed that these marks spatially overlap at most constitutive heterochromatin in an *hpo* mutant. This is consistent with evidence that PRC2 weakly bound H3K9me3-containing nucleosomes (84). To better understand the coincidence of H3K27me3 and H3K9me3 in the *hpo* mutant, future studies will address whether both marks are physically located on the same H3 tail, on different H3 molecules within a common nucleosome or simply within nearby nucleosomes. It has been reported that H3K27me3 marks chromosomes both on the tail of one histone (asymmetric) and on the tails of both sister histones within the same nucleosome (symmetric) (112). There is precedence for H3K27me3 overlapping with another histone mark. In mammals,

bivalent domains form when the repressive H3K27me3 mark and the active mark H3K4me3 coexist at the same loci, although these marks rarely coexist on the same histone tails (112).

DCDC is the H3K9-specific methyltransferase in *Neurospora* and consists of five members: DIM-5, DIM-7, DIM-9, CUL4 and DDB1 (encoded by *dim-8*) (76). In *N. crassa* DIM-7 interacts directly with DIM-5 to catalyze H3K9me3 at A:T-rich DNA (113). In the absence of *dim-7*, there is no H3K9me3, HP1 binding or 5mC. Clear DIM-7 homologs do not exist outside of fungi and among fungi they have rapidly diverged. Here we found that unlike deletions of *dim-5*, *dim-9*, c*ul4* and *dim-8*, a deletion of *dim-7* results in the global loss of H3K27me3 instead of the H3K27me3 relocalization. We did not detect DIM-7 in our purification of the PRC2 complex, suggesting it is not a member of PRC2 [Table 4 and (82)]. Despite its absence from PRC2, DIM-7 may play a role in targeting or activity of PRC2. However, there was no evidence of DIM-7 being targeted to either an H3K27me3-marked sub-telomere IL or interstitial genic region on LG VII using DIM-7-Dam (personal communication, Andrew Klocko). Perhaps additional H3K27me3-marked regions should be tested to confirm this result.

We found that the disruption of constitutive heterochromatin, by loss of HP1 binding to H3K9me3, leads to the relocalization of H3K27me3. The interplay between constitutive and facultative heterochromatin appears to be unidirectional in *Neurospora* since we did not observe altered H3K9me3 in deletions of two PRC2 subunits required for H3K27me3, *set-7* and *eed*. Reports on whether there exist reciprocal interactions between the two forms of heterochromatin have been mixed, namely involving whether the loss of facultative heterochromatin alters constitutive heterochromatin. In one study,

*Eed*$^{-/-}$ null, undifferentiated mouse ES cells show both increases and decreases in 5mC at developmental genes (92). However, a second study using both undifferentiated and differentiated mouse ES cells found that the knockdown of *Suz12* results in loss of H3K9me3 only in differentiated but not undifferentiated cells (114).

We next asked whether residues along the histone tail, other than K27, affect H3K27me3. HP1 binds trimethylated H3K9, although nearby residues are important for proper *in vivo* DIM-5 activity and HP1 binding (49). The R8A and S10 mutations disrupt the activity of DIM-5, which significantly reduces global levels of H3K9me3 in both R8A and S10A strains by western blot (49). We explored the reduction in H3K9me3 in more detail in R8A and S10A strains. By ChIP-seq, we observed either the absence or significant reduction of H3K9me3 at constitutive heterochromatin relative to a wild-type strain (Fig. 18). Given the relocalization of H3K27me3 in deletions of *dim-5*, *dim-9*, *cul4* and *dim-8*, which all lack H3K9me3, we were not surprised to observe the relocalization of H3K27me3 in both the R8A and S10A strains (Fig. 18).

Fluorescence microscopy in R8A and S10A strains also containing HP1-GFP shows diffuse HP1, suggesting the loss of HP1 binding in the R8A and S10A strains (49). Given the reduction of H3K9me3 at many domains by ChIP-seq, it appears that H3K27me3 relocation is due to the loss of HP1 binding resulting from severe reduction of H3K9me3. We will perform ChIP-seq on HP1-GFP in R8A and S10A strains and predict the loss of HP1 binding in both strains, consistent with the fluorescence microscopy results.

To continue our investigation regarding the residues along the histone H3 tail that influence trimethylation at H3K27, we focused on two substitutions that did not

significantly affect DIM-5 activity *in vitro*, A7M and R2L (49, 115). Substitutions at R2 do not have a pronounced effect on DIM-5 activity or H3K9me3 but show loss of DNA methylation (49, 115). Presumably this is due to a disruption downstream of H3K9me3 and HP1 binding but upstream of DNA methylation. *In vitro*, the A7M mutation leads to a steric clash with residue V26 within the chromodomain of HP1, resulting in a twenty-five fold reduction in binding (116). However, fluorescence microscopy shows normal HP1-GPF binding in *Neurospora* A7M and R2L strains (49), leading us to predict that H3K27me3 would not relocalize in either strain.

We observed nearly a complete loss of H3K27me3, except in close proximity to the telomere, where H3K27me3 was partially retained, in both the R2L and A7M strains (Fig. 19). This suggests that both the R2 and A7 residues on histone H3 have critical roles in H3K27me3 that are separate from HP1 binding to H3K9me3. It is possible that residues other than K27, such as R2 and A7, can influence PRC2 activity. Additional experiments should address the mechanism by which H3K27me3 was disrupted in these strains.

Our group has previously shown that 5mC can be triggered ectopically by transplanting any sequence of A:T-rich DNA (117, 118). To investigate whether we could induce *de novo* H3K27me3 at ectopic sites, we targeted eight normally H3K27me3-marked regions of three kb in length to two loci normally devoid of H3K27me3, *his-3* and *csr-1*. None of the eight H3K27me3 segments transplanted to either *his-3* or *csr-1* were sufficient to induce H3K27me3. While this does eliminate the possibility of a PRE-like element in *N. crassa*, it does suggest that the signal for H3K27me3 induction is not located within every segment of DNA marked by

H3K27me3. This implies a very different mechanism of H3K27me3 recruitment compared to that for 5mC.

How PRC2 is targeted to specific regions of the genome and what rules govern the location of H3K27me3 domains is still unknown. Although multiple PREs have been defined in *Drosophila*, it has been difficult to define PREs in other organisms given that many of the DNA-binding proteins that are recruited to PREs are poorly conserved outside of *Drosophila*, with the exception of mammalian Ying-yang 1 (YY1), the homolog of *Drosophila* Pleiohomeotic (PHO). It is unlikely that YY1 globally determines the locations of H3K27me3 domains in mammals, given their poor spatial correlation (43). It is also possible that CpG islands and long non-coding RNAs may have global roles in the control of H3K27me3 domains (119, 120).

By creating a series of deletions within a 45 kb H3K27me3 domain, we observed that certain strains significantly depleted surrounding H3K27me3. This result is consistent with *cis*-acting signals capable of recruiting PRC2 located within deleted region. We observed some results that are difficult to interpret, in which smaller deletions more significantly decreased H3K27me3 compared to larger deletions covering an overlapping area. The characterization of three-dimensional chromatin contacts in these strains might help to explain these observations.

H3K27me3 is organized into large domains that are preferentially found close to the telomeres. To investigate how proximity to telomeres affected H3K27me3 distribution, we took advantage of two translocation strains. One of the translocations, AR16, interchanged the telomere on LG IL with that of IR (Fig. 25). The segment from IR that moves to IL is shorter (512 kb) than the segment from IL that moves to IR (1.860

Mb). This results in a shortening of sub-telomere IL and a lengthening of sub-telomere IR. By H3K27me3 ChIP-seq, we observed a novel H3K27me3 on IL, just upstream of the breakpoint, in the AR16 translocation strain relative to the wild-type strain. It is possible that H3K27me3 spread from the telomere into more interior regions, due to the shortening of IL in the translocation strain. We also observed a loss of H3K27me3 on the sub-telomere of IL in the translocation strain, which we cannot explain by proximity to the telomere.

In the second translocation strain, OY329, a region that is normally proximal to telomeres is moved to a new location on LG III that is situated away from either telomere (Fig. 26). By ChIP-seq we found that the majority of H3K27me3 within the affected area was retained, although several H3K27me3 domains that were normally proximal to the telomere were lost in the translocation strain relative to a wild-type strain. In addition, novel H3K27me3 formed just upstream of the breakpoint.

Taken together, our H3K27me3 ChIP-seq experiments in both translocation strains suggest that proximity to the telomere is a contributing factor but not the sole determinant of H3K27me3 distribution.

## Materials and Methods

### *Neurospora* Strains and Methods

*Neurospora* strains were grown according to standard procedures (62). Strains used in this chapter are listed in Appendix C. *Neurospora* transformations were performed as in (121).

**Construction of Deletion and Insertion Strains**

Our strategy was based on the gene knockout method described by (47). PCR primers were designed for each deletion and insertion strain to amplify approximately one kb upstream (5' flank) and one kb downstream (3' flank) of the deletion or insertion site (see Appendix D for all primers). Each 5' forward primer and 3' reverse primer contains overhangs with homology to yeast vector pRS426 (leaving the option to create a yeast knockout cassette). Each 5' reverse primer and 3' forward primer contains overhangs with homology to *hph*. For the insertion strain, the 5' and 3' flanks were located adjacent to one another, while the distance between the flanks in each deletion strain is equivalent to the size of the deletion. Each 5' flank was fused to the 5' portion of *hph* by a PCR reaction using the 5' forward primer and the reverse internal *hph* primer. Similarly each 3' flank was PCR-stitched to the 3'portion of *hph* using the forward internal *hph* primer and the 3' reverse primer. The successful integration of the final two final PCR products into the Δ*mus-52* strain (N2931) relies on homologous recombination within the 5' and 3' genomic flanks in addition to the overlap of *hph*. Transformants were selected for growth on medium containing hygromycin and were screened for correct integration by Southern blotting (see Appendix E for primers used to generate Southern blot probes and restriction digests used in Southern blots). Confirmed transformants were crossed to wild-type strain N3752 and progeny containing the deletion were confirmed by Southern blotting.

**Construction of Strains Bearing Segments of H3K27me3 at *his-3***

Primers were designed to have restriction sites built into the overhangs. Segments of an H3K27me3 region were subcloned into pCR (Life Technologies TA Cloning Kit, K2030-40) and then cloned into the *his-3*-targeting vector pBM61. Each vector was linearized and 300 ng of DNA was transformed into N5739. Transformants were screened by Southern blotting for integration at *his-3* and crossed to N625, a *his-3* strain, to generate homokaryons. Progeny were confirmed by Southern blotting.

**Construction of Strains Bearing Segments of H3K27me3 at *csr-1***

3 kb fragments of an H3K27me3 domain, along with 5' and 3' flanks were amplified by PCR. Fragments were purified from a 1.5% agarose gel using the QIAquick Gel Extraction Kit (Qiagen, 28704). The 5' flank, 3' flank and each 3 kb fragment were separately transformed into a *mus-52* strain bearing a deletion of the H3K27me3 domain (N5547). Tranformants were selected on Vogel's medium containing cyclosporin and screened by Southern blot. Transformants were crossed to N3752 to obtain homokaryons. Progeny were screened by Southern blot and spot tested on Vogel's media, with and without basta, to evaluate whether progeny were *mus-52*$^{+}$.

**Chromatin Immunoprecipitation (ChIP)**

5 ml Vogel's sucrose cultures were grown overnight, shaking at 32 °C. Chromatin was cross-linked for ten min in 0.5% formaldehyde and quenched with fresh 2.5 M glycine. Tissue was disrupted by sonication for thirty pulses before chromatin was sheared using the bioruptor for 15 min with a cycle of 30 sec on followed by 30 sec off,

at high power. The following antibodies were used: anti-H3K27me3 (Active Motif 39535), anti-H3K9me3 (Active Motif 39161) and anti-H3K4me2 (Active Motif 391410). 2 µl of antibody was added to each sample and incubated at 4 °C overnight with rotation. 20 µl of Protein A/G Plus Agarose beads (Santa Cruz, sc-2003) were added and incubated with rotation for 3 h at 4 °C. Beads were washed as previously described (52) and decrosslinked overnight. Samples were treated with Proteinase K for 2 h at 50 °C before DNA was purified using the QIAquick PCR Purification Kit (Qiagen, 28106). Purified DNA was eluted in either 25 µl of water, in preparation for ChIP-seq, or 50 µl of water, when prepared exclusively for qChIP. qChIP was performed as in (82) using the SYBR FAST ABI Prism qPCR Kit (KAPA, KK4605).

ChIP samples were normalized to background levels of either H3K27me3 or H3K9me3 at histone H4 (3998, 3999) for most experiments or to the enrichment of H3K27me3 at sub-telomere 1L (3565, 3566) for insertion and deletion strains.

**Preparation of ChIP-seq Libraries for Sequencing**

Approximately 10 ng of DNA was used in creating ChIP-seq libraries. Each library was prepared using the Illumina Tru-Seq Kits A and B (Illumina, IP-202-1012 and IP-202-1024) according to the manufacturer's instructions. DNA was first end-repaired and 3'-adenylated before the ligation of Illumina Tru-seq barcodes. The DNA was size-fractionated on a 2% agarose gel. "Invisible" fragments between 250-400 bp were excised and purified using the MinElute Gel Extraction Kit (Qiagen, 28606). Purified DNA was eluted in 23 microliters of water. Final libraries were PCR-amplified using

one cycle of 98 °C for 30 sec, 18 cycles of 98 °C for 10 sec, 60 °C for 30 sec and 72 °C for 30 sec and a final extension at 72 °C for 5 min.

**Construction of Ectopic Integration Strains**

Each of the H3K27me3 segments was separately co-transformed with the *bar* gene and basta-resistant transformants were screened by Southern blot. All co-transformations were performed in a host strain containing a deletion of the entire 47.4 kb domain (N4933). Each of the transformation strains was micro-conidiated to purify nuclei.

## Bridge to Chapter IV

Chapter III described crosstalk between facultative and constitutive heterochromatin. I next discuss histone deacetylation, which has connections to both facultative and constitutive heterochromatin. For example, in mammals and *D. melanogaster*, PRC2 contains the histone deacetylase, Rpd3. The homolog of Rpd3 in *Neurospora* is HDA-3. In Chapter IV, I explore HDA-3-associated proteins in greater detail and identify two HDA-3 containing complexes.

# CHAPTER IV

# CHARACTERIZATION OF TWO HDA-3 CONTAINING COMPLEXES

This chapter describes unpublished work co-authored by Dani Keahi, Shane Van der Zwan, Heejeung Yoo, Eric U. Selker. Eric U. Selker and I designed the experiments. I performed the affinity purifications of NPF and HDA-3 and Larry David (OHSU) performed mass spectrometry to identify proteins that associated with NPF and HDA-3. Dani Keahi and Shane Van der Zwan assisted in creating the 3xFLAG- and 3xHA-tagged strains that were used for co-immunoprecipitation experiments. Heejeung Yoo and I performed the co-immunoprecipitation (Co-IP) experiments and nuclei isolations.

## Introduction

The nucleosome consists of two copies each of histones H2A, H2B, H3 and H4, and 146 base-pairs of DNA wound around its core. It is a barrier to transcription, inhibiting activator binding, initiation and elongation (122). Some posttranslational modifications of histones, such as acetylation, alter the charge of the histone tails. According to the "charge hypothesis," nonacetylated histone tails are more tightly bound to DNA due to their positive charge while histone acetylation neutralizes the positive charge of histone tails, loosening DNA-protein interactions to facilitate transcription (123, 124). Indeed, lysine acetylation is mostly associated with active genes (122). Acetylation is a reversible modification, with addition of acetyl groups by histone acetyltransferases (HATs) and their removal by histone deacetylases (HDACs).

Mammalian HDACs are divided into four major families defined by structural homology (Classes I, II and IV) or $NAD^+$-dependence (Class IV). Rpd3 is the founding member of the class I Rpd3/HDA1 family, characterized by its HDAC domain located toward the amino terminus and a carboxy-terminal tail (125). HDACs typically have low substrate specificity, Rpd3 deacetylates multiple histone residues, K7 on H2A, K11 and 16 on H2B, K9, 14, 18, 23 and 27 on H3 and K5, 8 and 12 on H4 (126).

Rpd3 and its binding partner, Sin3, form multisubunit complexes that are conserved from fungi to mammals. While plants and animals each contain one Rpd3/Sin3 complex, both budding and fission yeast contain two distinct Rpd3-containing complexes, scRpd3L/spRpd3I and scRpd3S/spRpd3II. The scRpd3L/spRpd3I and scRpd3S/spRpd3II complexes consist of a three subunit core: Rpd3/Clr6, Sin3/Pst1/2 and Ume1/Prw1, with additional subunits specific to each complex. scRpd3L/spRpd3I additionally contains Sds3 and Pho23/Png2 and scRpd3L also contains Sap30, Dep1, Cti6, Rxt2, Rxt3, Ash1 and Ume6 (127). scRpd3S/spRpd3II contains RcoI/Cph1/2 and Eaf3/Alp13 and is recruited to transcribed regions.

The elongating form of RNA Polymerase II (phosphorylated at serine-2) recruits Set2, the H3K36 methyltransferase, to open reading frames (ORFs) (128). Methylated H3K36 subsequently recruits scRpd3S via the chromodomain of Eaf3 and in a manner dependent upon the PHD domain of RcoI (129). Notably, one human homolog of Eaf3, mortality factor on human chromosome 4 (MORF4), lacks a chromodomain, suggesting that the MORF4-containing complex may use a different targeting mechanism (130). The resulting deacetylation of histones within gene bodies, catalyzed by Rpd3-containing complexes ultimately results in transcriptional suppression within affected genes (131).

H3K36me3 distribution is subsequently correlated with histone deacetylation, though the removal of either the Rpd3S-specific Eaf3 or RcoI did not recapitulate the transcriptional silencing observed from a loss of H3K36me3 or Set2 (132). Eaf3 is also part of the lysine acetyltransferase complex, NuA4, and there is some controversy as to whether $Eaf3^{NuA4}$ also binds to H3K36me3, thus competing with Rpd3S for binding (129, 133).

Rpd3 is not restricted solely to HDAC complexes. *D. melanogaster* PRC2 exists in at least two forms, a 600 kilo-Dalton complex, the most prevalent form, and a one mega-Dalton complex. RPD3 is considerably more prevalent in the larger complex, while the presence of Rpd3 in the smaller complex is somewhat controversial (13, 134). It has been proposed that histone deacetylation by RPD3 is a prerequisite for stable PRC2-mediated silencing (13, 134).

It has previously been reported that HDA-3 is required for the deacetylation of certain residues on histone H3, namely H3K9, H3K14, H3K18, H3K23 and H327 as well as deacetylation of histone H4 (109). HDA-3 also has a role in DNA methylation in *N. crassa*, since mutation of *hda-3* results in a partial loss of DNA methylation (109). While the majority of sites of constitutive heterochromatin were unaffected in an $hda\text{-}3^{RIP1}$ strain, there were two regions that showed a partial loss of DNA methylation (109).

## Results

### Identification of HDA-3-Associated Proteins

To identify proteins associated with HDA-3, the protein was endogenously tagged at its amino terminus with a 3xFLAG epitope, driven by the quinic acid (*qa-2*) promoter. The 3xFLAG-HDA-3 strain conidiates poorly compared to wild-type (Fig. 28). Since *hda-3* is an essential gene, presumably this phenotype is due to the 3xFLAG epitope interfering with, but not totally disrupting, the function(s) of HDA-3. Purification of HDA-3 by anti-3xFLAG affinity gel and mass spectrometry identified homologs to two related *S. cerevisiae* histone deacetylase complexes, Rpd3S and Rpd3L, and we named these putative *Neurospora* HDA-3 complexes HDA-3S and HDA-3L. The shared core between *S. cerevisiae* Rpd3S and Rpd3L consists of Rpd3, Sin3 and Ume1 and were identified in our purification as HDA-3 (NCU00824), Sin3 (NCU02578) and NPF (NCU06679).

Most accessory proteins unique to either Rpd3S or Rpd3L were identified in our purification (Table 5), with the exception of homologs to Ash1 and Ume6, which were not found in our purification. In addition to HDAC complexes, we identified all eight subunits of a chaperone-folding TCP1 Ring Complex (TriC), known to fold Rpd3 and many other eukaryotic proteins (135).

Next, we affinity purified 3xFLAG-tagged NPF, expressed using the *qa-2* inducible promoter. We detected HDA-3S and HDA-3L subunits in our NPF purification, validating our HDA-3 purification results. We also identified two members of the putative *Neurospora* Chromatin Assembly Factor-1 (CAF-1), *cac-1* and *cac-2*

(NCU04198 and NCU08357, respectively) (46). CAF-1 is conserved from budding yeast to animals and deposits histones H3 and H4 onto newly synthesized DNA (136). We did not detect PRC2 members, despite the presence of NPF in the purification of PRC2 subunit EED (Chapter I). Presumably this is because PRC2 subunits are less abundant than HDA-3-associated proteins. We also detected the theta subunit of TriC in our NPF purification, although at much lower coverage compared to our HDA-3 purification.

We previously reported that *N. crassa* HDA-3 contains a catalytic histone deacetylase (HDAC) domain located towards the amino terminus that is well conserved between budding and fission yeasts ((109) and Fig. 29). To evaluate the conservation of HDA-3 associated proteins, we aligned their sequences relative to other organisms (Fig. 29). The remaining noncatalytic subunits also show conservation within predicted domains in *Neurospora*.

In attempts to confirm the association of HDA-3 with proteins identified by affinity purification, we fused 3xFLAG and/or 3xHA epitopes to the amino-termini of putative HDA-3S complex members and performed Co-IPs with either 3xFLAG- or 3xHA-HDA-3. As with the 3xFLAG-HDA-3 strain, both the 3xFLAG and 3xHA-tagged members of the putative HDA-3 containing complexes exhibit severe growth defects (Fig. 28), again suggesting that the epitope tags partially disrupt the complex. By Co-IP, we confirmed the *in vivo* interaction of HDA-3 with the other two core members of the HDA-3S/L complexes, NPF and Sin3.

We next confirmed the interaction of HDA-3 with two putative subunits that are thought to be exclusive to each HDA-3S complex, RcoI (NCU0423) and CDP-6 (homolog of *S. cerevisiae* Eaf3, NCU06788) (Fig. 31). Finally, we confirmed that an

interaction did not exist between a member of HDA-3L, Sds3 (NCU01599) and a member of HDA-3S, CDP-6, that are thought to be exclusive to each complex (Fig. 31). Our results therefore suggest that *Neurospora* HDA-3 forms two separate HDAC complexes, as in *S. cerevisiae* and *S. pombe*.

**Some Deletions of HDA-3 Complex Subunits Have Growth Defects**

Two core members of the HDA-3-containing complexes are essential, HDA-3 and Sin3, and we obtained strains containing deletions of the corresponding genes (NCU00824 encodes *hda-3* and NCU002578 encodes *Sin3*) as heterokaryons from the *Neurospora* knockout project (47). Homokaryotic strains were available for deletions of genes encoding the remaining members of the HDA-3S complex, RcoI (gene NCU00423) and Eaf3 (gene NCU06788), as well as for genes encoding subunits specific to the HDA-3L complex: Sds3 (gene NCU01599), Sap30 (gene NCU05240) and Pho23 (gene NCU03461). We also obtained a homokaryotic strain containing a deletion of the third core member, *npf*, the homolog of *S. cerevisiae* UmeI (82), which we also used in the work described in Chapter II. Strains containing deletions of genes encoding two subunits specific to the HDA-3L complex, Sds3 and Pho23, exhibit slower growth rates compared to wild-type (Fig. 28), which is comparable to the rate of growth in a strain containing the deletion of *npf*, as we have also previously shown [(82) and Fig. 30].

**Deletions of HDA-3-Associated Proteins Do Not Display Increased Acetylation**

We have previously reported that a RIP'd allele of *hda-3* increases global acetylation levels of histone H3K9, K14, K18, K23, K27 and histone H4 (109). To

evaluate the contributions of HDA-3S/L complex members to global acetylation levels, we isolated nuclei from deletion strains to assess global acetylation levels at H3K4, H3K9 and K3K18. Surprisingly, we did not observe a significant increase in acetylation at any of the residues we tested relative to wild-type (Fig. 32). Unfortunately, we were unable to include the *hda-3*$^{RIP1}$ strain from Smith *et al*. as a control for these experiments, since it could not be revived from our *Neurospora* strain collection.

## Discussion

The acetylation of histones is regulated by opposing activities of histone acetyltransferases (HATs) and histone deacetylases (HDACs). Histone deacetylation is thought to be involved in several silencing mechanisms. In *Neurospora*, treatment with (R)-trichostatin A, an HDAC inhibitor, resulted in the selective loss of DNA methylation and reactivation of the *hph* and *am* genes (137). In *Drosophila*, HDAC1 associates with SU(VAR)3-9, suggesting that the deacetylation of H3K9 prepares histones for methylation by SU(VAR)3-9 (138). The inclusion of histone deacetylases in H3K9-specific methyltransferase complexes may be limited to certain systems, since the purifications of DCDC in *Neurospora* have not identified any HDACs.

Histone deacetylation also appears to be involved in facultative heterochromatin. It has been reported that the methylation state of H3K27 influences acetylation at H3K27. The knockdown of E(Z), the mammalian H3K27-specific methyltransferase, simultaneously decreases the trimethylation while increasing the acetylation of H3K27 (139). Also, the *Drosophila* one mega-Dalton PRC2 complex contains Rpd3, a homolog

of *N. crassa* HDA-3 (13, 14), and both mammalian HDAC1 and HDAC2 associate with EED (15). The authors of these reports have speculated that a possible role for Rpd3 and its homologs in PRC2 is to prepare histones for stable and heritable gene repression by trimethylating H3K27 (13). HDACs have not been identified in plant PRC2 complexes, but there is evidence of histone deacetylase activity at H3K27me3 targets such as the *FLC* flowering locus (140).

HDA-3 was absent from both our purification of EED (Chapter II). We speculated that HDA-3 might be limited to a subset of PRC2 complexes and was therefore undetected in our purification. To further investigate whether HDA-3 was present in *Neurospora* PRC2, we affinity-purified 3xFLAG-HDA-3. Our purification did not detect proteins exclusive to PRC2 (SET-7, EED and SUZ12), reinforcing the idea that HDA-3 is not a member of PRC2 (Table 5). We detected NPF in our HDA-3 purification, however, which we previously detected in our affinity purification of 3xFLAG-EED (Table 4). NPF is a component of several complexes, in addition to PRC2, including NuRD, NURF, CAF-1 and, most pertinent to this chapter, two Sin3-containing HDAC complexes (136).

To validate the detection of NPF in our purification of HDA-3, we affinity-purified 3xFLAG-NPF (Table 5). As expected, the purification of NPF detected HDA-3, while PRC2 subunits were curiously absent. Upon inspection of our HDA-3 and NPF purifications, we observed an overlapping set of proteins that were close homologs to two Sin3-containing HDAC complexes, both highly conserved in budding and fission yeasts (Table 5), called Rpd3S/L in *S cerevisiae*. The Rpd3S complex is distinguished from the

Rpd3L complex by the inclusion of Eaf, a chromodomain protein, and RcoI. We named these *Neurospora* complexes HDA-3L and HDA-3S.

Our purifications did not detect all known members of HDA-3L. Ash1 and Ume6, both DNA-binding repressors were both absent from both the HDA-3 and NPF purifications. While *N. crassa* does not contain a close homolog to Ash1, it does appear to have two relatively close homologs to Ume6 (NCU05767 and NCU07374), which were not detected by mass spectrometry in either of our purifications. Our results suggest that there are variations in complex compositions between species.

To confirm the results of our purifications, we constructed strains 3xFLAG- and 3xHA-tags at the amino-terminus of HDA-3S and HDA-3 subunits in order to perform Co-IP experiments (Fig. 31). The quinic acid inducible promoter, *qa-2*, drives the expression of each of our epitope-tagged proteins. We tagged all members of the HDA-3S complex, including the core of proteins shared between the HDA-3S and HDA-3L complexes (HDA-3, NPF and Sin3). Our Co-IP experiments successfully detected the interaction of HDA-3 with NPF and Sin3 (Fig. 31). We also detected an interaction between HDA-3 and CDP-6. The strain containing 3xFLAG-RcoI (N5454) only weakly expresses its epitope tag, despite its overexpression by the *qa-2* promoter. As a result, our attempts to demonstrate the interaction by Co-IP between HDA-3 and RcoI were unsuccessful.

We had considerable difficulty generating homokaryotic strains containing epitope-tags of most subunits exclusively present in the HDA-3L complex, such as 3xFLAG-tagged Sap30, Cti6 and Dep1. The crosses of transformants containing these epitope tags to a wild-type strain were barren. Heterokaryotic transformants have been

deposited in the collection (N5456, N5459 and N5460). We did successfully create homokaryotic strains of one member exclusively present in HDA-3L, Sds3, which we tagged with both 3xFLAG and 3xHA. This led us to perform a Co-IP experiment between Sds3 and CDP-6, which is presumably exclusively found in the HDA-3S complex. As expected, we did not detect an interaction of these proteins (Fig. 31).

Histone hyper-acetylation at several residues has previously been reported that in an *hda-3*$^{RIP1}$ strain (141). Surprisingly, we did not detect increases in acetylation in strains containing deletions of either HDA-3S or HDA-3L subunits (Fig. 32). It is possible that the heterokaryotic Δ*hda-3* strain masked an increase in acetylation. Unfortunately, since *hda-3* is an essential gene, we were unable to use a homokaryotic Δ*hda-3* strain for western blots. It is also possible that the non-catalytic subunits of the complexes, all of which are homokaryotic strains (with the exception of the Δ*sin3* strain), are not required for the HDAC activity of the complex. The *hda-3*$^{RIP1}$ strain was not available to be used as a positive control in our western blots due to its absence from our strain collection. For use in future studies, we revived uncharacterized alleles of RIP'd alleles of *hda-3* which might be used as suitable controls once their *hda-3* alleles have been sequenced to determine the extent of their mutation(s).

## Materials and Methods

### *Neurospora* Strains and Methods

*Neurospora* strains were grown, maintained and crossed according to standard procedures (62). The Δ*hda-3*, Δ*npf*, Δ*sin3*, Δ*sds3*, Δ*sap30*, Δ*pho23*, Δ*rco1* and Δ*cdp-6*

strains were made by the *Neurospora* gene knockout project (47) and obtained from the Fungal Genetic Stock Center (FGSC; www.fgsc.net). Strains are listed in Appendix C.

**Construction of Epitope-Tagged Strains at Native Loci**

Endogenous 3xFLAG and 3xHA epitope tags were integrated at the amino terminus of each protein essentially as previously described (142) with some modifications. At each gene, a 5' flank upstream of the start codon and a 3' flank immediately after the start codon were amplified by PCR. Instead of cloning these flanks into a yeast vector as described in (142), we PCR-amplified the 5' flank with the epitope-containing plasmid, using the forward primer of the 5' flank and internal *hph* primer, to create a single product containing *hph* and the 3' flank. In a separate reaction, an internal *hph* primer was used with the reverse primer of the 3' flank to amplify a single product containing *hph* and the 3' flank. The two resulting PCR products were directly transformed into the host strain (N2930) and transformants were selected on medium containing hygromycin. To confirm integration, genomic DNA was isolated by standard procedures (143) and strains were confirmed by Southern blotting (117). Strains were crossed to a *mus-52*$^{+}$ strain (N3753) to obtain *mus-52*$^{+}$ homokaryons.

Strains used for Co-IP experiments were generated by crossing strains containing either 3xFLAG or 3xHA epitope tags in a single strain to one another. Progeny were screened by Southern blot using *hph* as a probe.

**Affinity Purification**

Conidia from a 250 ml solid culture were used to inoculate a 1 L liquid culture of Vogel's with 1.5% glucose and 0.4% quinic acid, shaken overnight at 32 °C. 3xFLAG-HDA-3 and 3xFLAG-NPF were affinity-purified essentially as previously described (78) except that tissue was ground in liquid nitrogen. To precipitate proteins, one volume of 100% Trichloroacetic acid (TCA) was added to four volumes of protein sample and incubated on ice for ten min. Samples were spun for 5 min at 14,000 RPM and the supernatant was removed. The pellet was washed twice with cold acetone and dried in a 95 °C heat block to remove residual acetone. Precipitated samples were analyzed by mass-spectrometry (Larry David, OHSU).

**Co-Immunoprecipitation (Co-IP) Assay**

5 ml liquid Vogel's medium supplemented with 1.5% glucose and 0.4% quinic acid were grown for two days, shaking, at 32 °C in order to obtain a sufficient amount of tissue. Co-IP experiments were performed as previously described (76).

**Nuclei Isolation and Western Blotting**

Nuclei were isolated essentially as in (49) except that one liter cultures were grown and tissue was pulverized in liquid nitrogen and stored at -80 °C until use. Five grams of ground tissue was used per sample. 40 ml of Buffer A (1M sorbitol, 7% Ficoll, 20% glycerol, 5 mM $MgAc_2$, 3 mM $CaCl_2$ and 50 mM Tris HCl pH 7.5) was added to the tissue. Next, 70 ml of Buffer B (10% glycerol, 5 mM $MgAc_2$ and 25 mM Tris-HCl pH 7.5) was slowly added. Samples were each divided into two tubes and 15 ml of 1:1.7

Buffer A:Buffer B was added to each tube. Samples were then centrifuged at 4,000 rpm for 7 min at 4 °C in a swinging bucket rotor. The supernatant was layered over 5 ml Buffer C (1 M sucrose, 10% glycerol 5 mM $MgAc_2$ and 25 mM Tris-HCl pH 7.5). Samples were again centrifuged, this time at 7,000 rpm for 15 min at 4 °C in a swinging bucket rotor. The supernatant was decanted from each sample and both pellets were resuspended in 700 µl of Nuclei Storage Buffer (25% glycerol, 5 mM $MgAc_2$, 0.1 mM EDTA, 3 mM DTT and 25 mM Tris-HCl pH 7.5). 0.2 ml of each resuspended pellet was aliquoted and flash-frozen in liquid nitrogen. Samples were stored at -80 °C. In preparation for western blotting, samples were centrifuged at 10,000 rpm for 5 min at 4 °C. The supernatant was removed, and pellets were resuspended in 200 ul $H_2O$. Qubit fluorometric quantitation (Life Technologies) was used to quantify protein concentration. 10 µg of protein used for each 5% acrylamide stacking, 12% acrylamide resolving gel. Membranes were probed with antibodies against H3K4me2 (Active Motif, 39141), H3K4ac (Active Motif, 39381), H3K9ac (Active Motif, 39137) and H3K18ac (Active Motif, 39587).

## APPENDIX A

## FIGURES

### Figures for Chapter II

**Fig. 1 (see next page). Genome-wide H3K27me3 ChIP-Seq analysis of wild-type, Δ*set-7,* and Δ*npf* strains.** (A) The distribution of H3K27me3 in the wild-type strain (blue) grown in Bird's medium, displayed above the predicted genes (green ticks), is represented to scale on the seven LGs of *N. crassa*. Below the genes, the absence of H3K27me3 enrichment in a Δ*set-7* strain (gray) and the regionally-affected H3K27me3 distribution in a Δ*npf* strain (inverted black traces) are displayed. LG I is divided at the right end of its centromere into IL and IR. Red arrows indicate the locations of primer sets used for qChIP experiments. (B) Part of the right arm of LG V near the telomere (dotted line) is expanded to detail mutually exclusive H3K27me3 and H3K9me3 domains. H3K9me3 data for the whole genome is presented in Fig 3. (C) Relative H3K27me3 enrichment was determined by qChIP at the telomeres of LG I (IL and IR) and at two genic regions sporting H3K27me3 in LG VII for wild-type and for strains deleted for genes encoding the PRC2 subunits. (D) H3K27me3 ChIP-Seq read densities for wild-type, Δ*set-7* and Δ*npf* for the regions assayed by qChIP (primers indicated by red arrows).

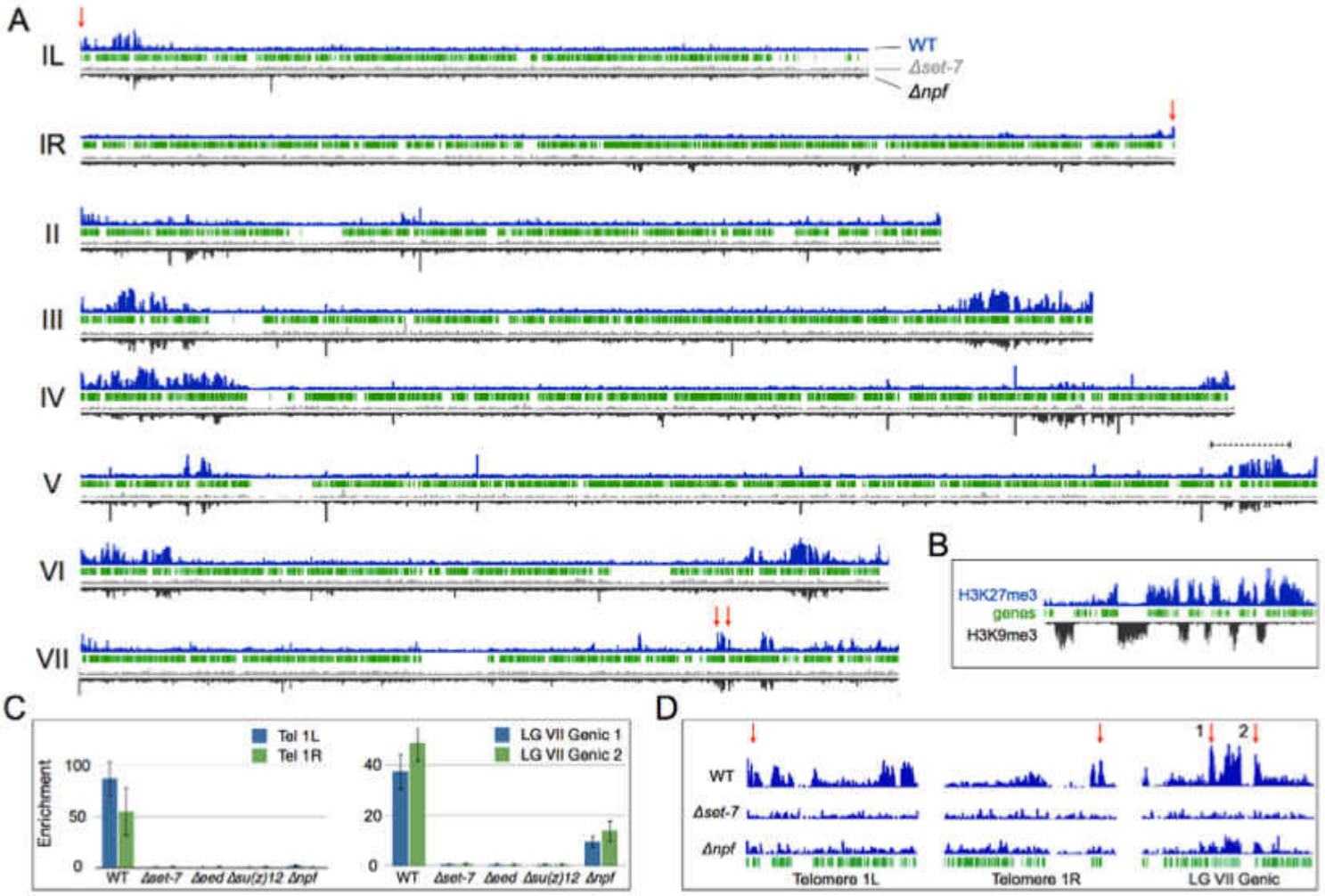
A
IL
IR
II
III
IV
V
VI
VII
WT
Δset-7
Δnpf
B
H3K27me3
genes
H3K9me3
C
Tel 1L
Tel 1R
Enrichment
100
50
0
WT
Δset-7
Δeed
Δsu(z)12
Δnpf
LG VII Genic 1
LG VII Genic 2
40
20
0
D
WT
Δset-7
Δnpf
1
2
Telomere 1L
Telomere 1R
LG VII Genic

**Fig. 2 (see next page). H3K27me3 domains are reproducibly detected.** (A) The H3K27me3 ChIP-Seq read density profile (upper track) closely matches that obtained by ChIP-chip for LG VII (lower track). (B) H3K27me3 ChIP-Seq read density is shown for the seven LGs of *N. crassa* for cultures grown in Bird's medium (blue above the genes) and in Vogel's medium (inverted, blue below the genes). Virtually identical profiles were obtained.

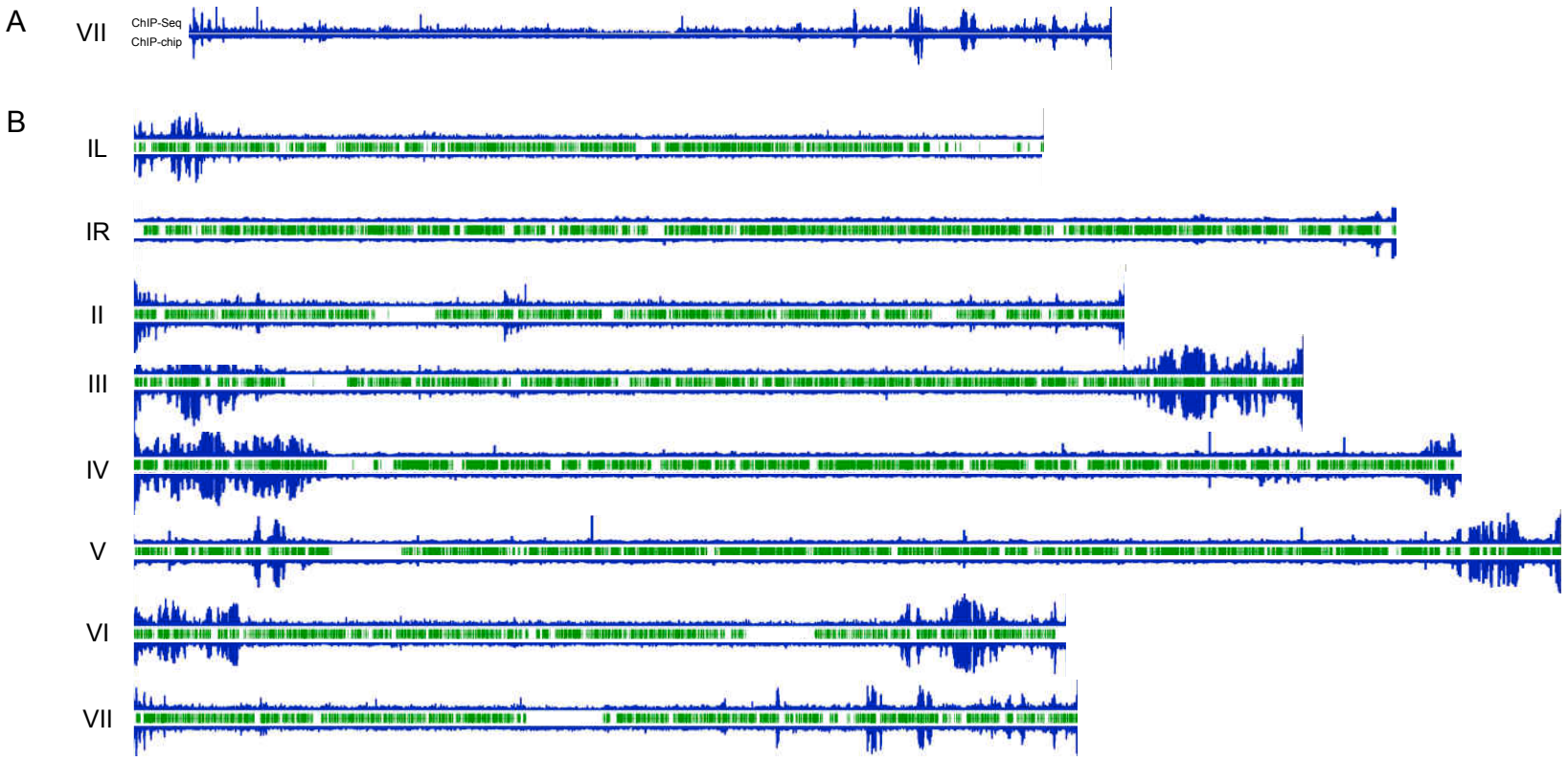
A
VII
ChIP-Seq
ChIP-chip
B
IL
IR
II
III
IV
V
VI
VII

**Fig. 3 (see next page). Genome-wide distribution of H3K27me3 and H3K9me3 in *N. crassa*.** (A) Predicted genes (vertical green lines), distribution of H3K27me3 (blue traces above genes) and H3K9me3 (black traces below genes) are represented to scale on the seven LGs of *N. crassa*. The largest chromosome, LG I, is divided at the right end of its centromere into IL and IR. (B) A portion of the right arm of LG V near the telomere is expanded to detail mutually exclusive H3K27me3 and H3K9me3 domains.

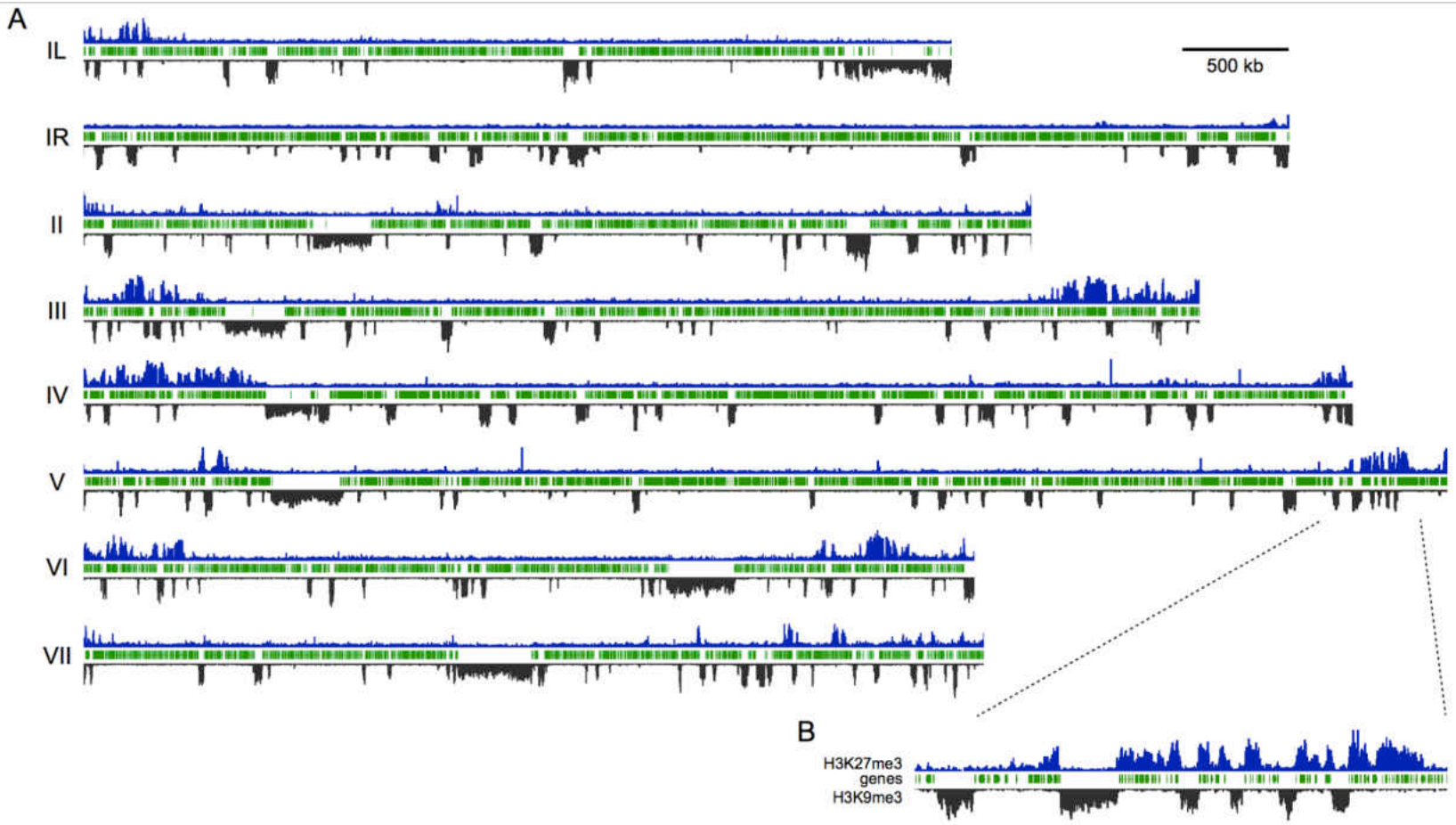
A
IL
IR
II
III
IV
V
VI
VII
500 kb
B
H3K27me3
genes
H3K9me3

**Fig. 4. Predicted lengths of proteins encoded by H3K27me3-marked and unmarked genes of *N. crassa*.** Predicted lengths of proteins encoded by H3K27me3-marked and unmarked genes of *N. crassa*. Box-and-whisker plot of protein lengths show a significantly shorter average length for H3K27me3 marked genes ($P<2\times10^{-16}$, t-test).

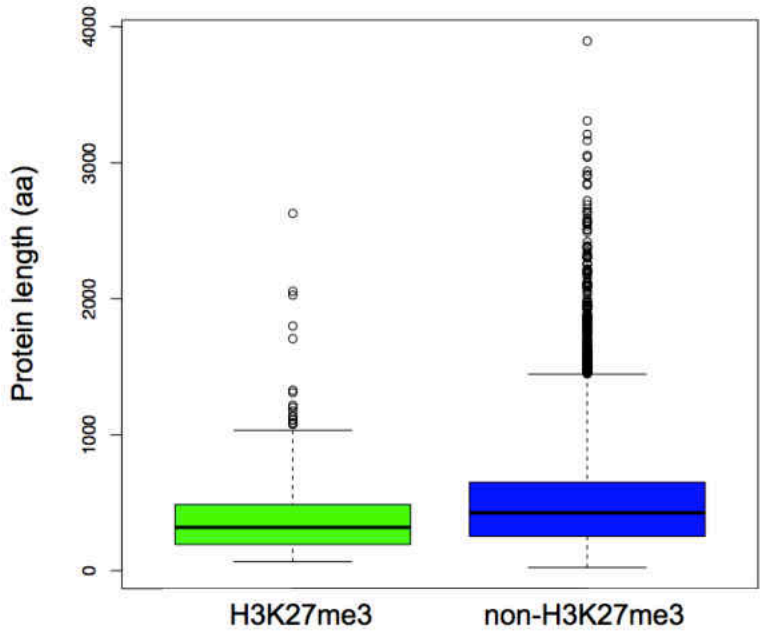

**Fig. 5. Functional Category (FunCat) classification of *N. crassa* H3K27me3 genes.** Functional Category (FunCat) classification of *N. crassa* H3K27me3 genes. (A) Pie chart displaying the FunCat classification of all *N. crassa* predicted genes. (B) Pie chart displaying the FunCat classification of *N. crassa* genes found within H3K27me3 domains.

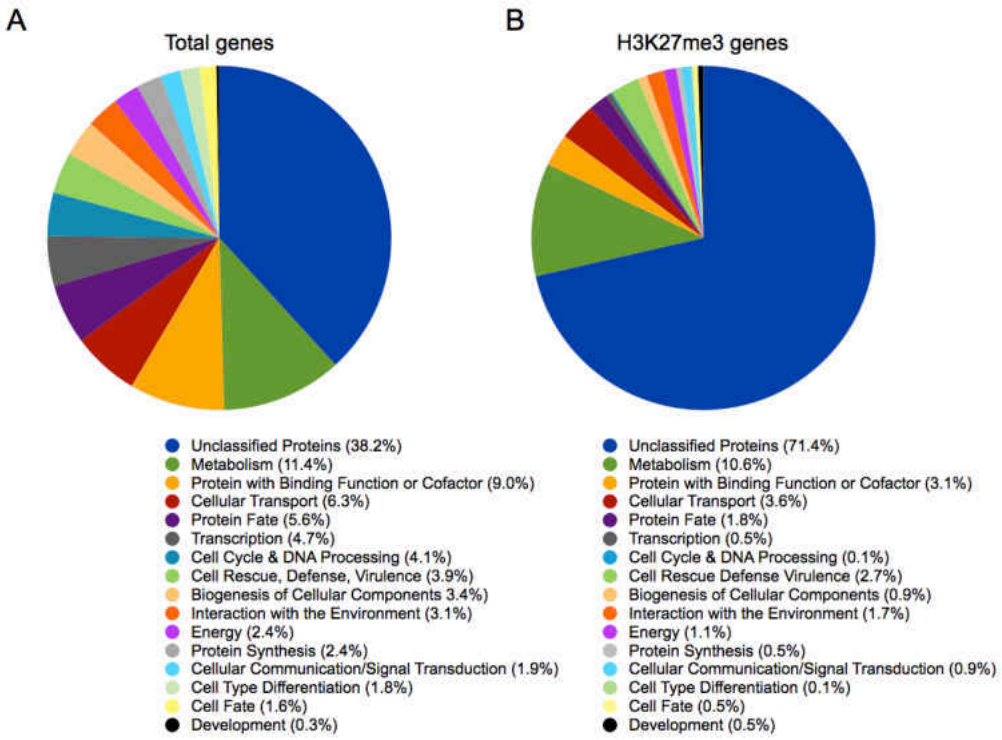

**Fig. 6. Conservation of H3K27me3 genes in *Neurospora* species.** (A) The phylogenetic tree depicts the classification of *Neurospora* species and their relationship to common model organisms. The pie charts illustrate conservation of *N. crassa* orthologs within H3K27me3 domains (H3K27me3 genes) or outside H3K27me3 domains (non-H3K27me3 genes). (B) Conservation and H3K27me3 status of *N. crassa* genes with or without H3K27me3 relative to *N. tetrasperma* and *N. discreta*.

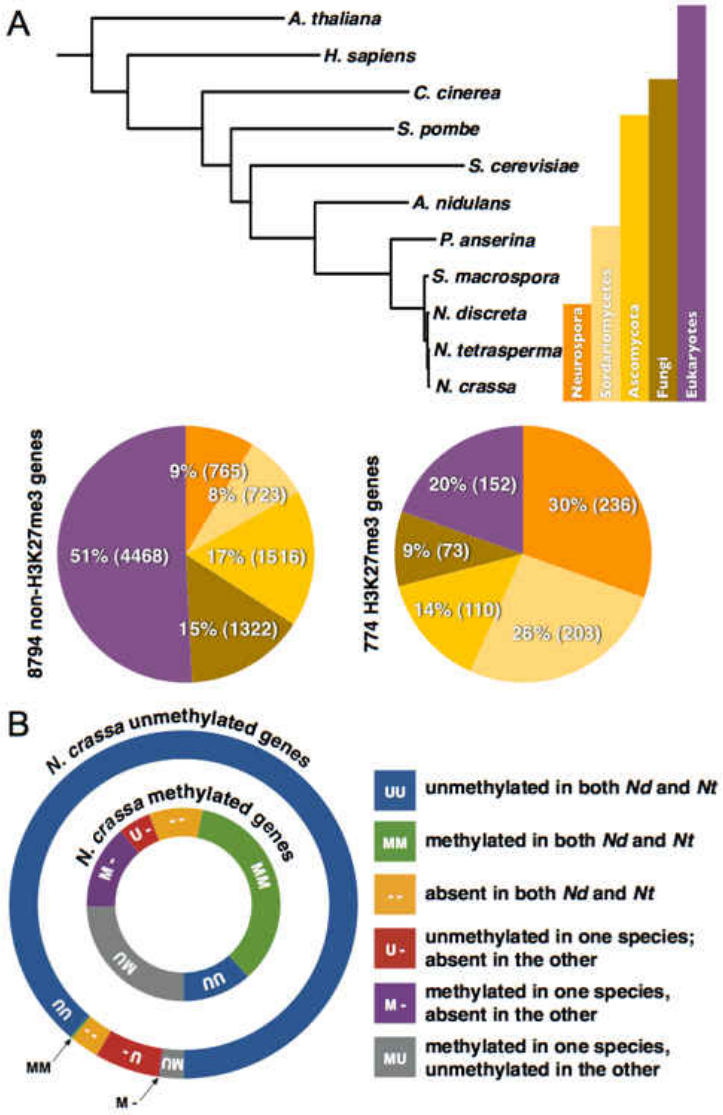

**Fig. 7. Domain structures of the four core subunits of the *N. crassa* PRC2 complex.** SET-7, the closest *Neurospora* homolog of *Drosophila* E(Z), contains the presumptive histone H3K27 methyltransferase domain (SET; blue pentagon); EED and NPF each possess multiple WD40 repeat domains (green triangles); *N. crassa* SU(Z)12 has a presumptive zinc-binding domain (blue rectangle).

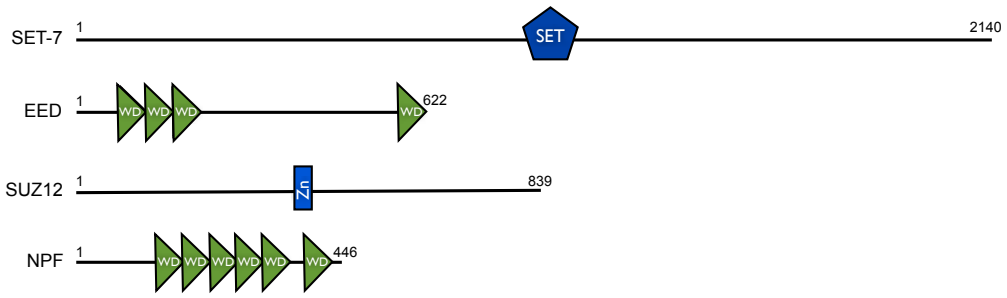

**Fig. 8 (see pages 76-78). Multiple alignments of the PRC2 subunits.** The protein sequence from each of the *N. crassa* PRC2 subunits was aligned to corresponding homologs from *Mus musculus*, *Drosophila melanogaster*, *Arabidopsis thaliana*, and *Caenorhabditis elegans* using ClustalWS. (A) Alignment of *N. crassa* SET-7 with homologs. ClustalWS alignments from *N. crassa* (XP_965043), *M. musculus* (AAH16391), *D. melanogaster* (NP_524021), *A. thaliana* (AEC07449) and *C. elegans* (O17514). The SET domain (V1040 to L1173, E = 3.38e-29) is indicated by the black line. (B) Alignment of *N. crassa* EED with homologs. ClustalWS alignments from *N. crassa* (XP_962071), *M. musculus* (NP_068676), *D. melanogaster* (AAA86427), *A. thaliana* (AEE76418) and *C. elegans* (Q9GYS1). Four WD40 domains are indicated by the black lines (S77 to D125, E = 7.96e+00; Q128 to S168, E = 1.74e-08; A175 to T216, E = 1.01e-04; E575 to Q618, E = 2.38e+01). (C) Alignment of *N. crassa* SUZ12 with homologs. ClustalWS alignments from *N. crassa* (XP_963451), *M. musculus* (AAH64461), *D. melanogaster* (Q9NJG9) and *A. thaliana* (AED96057). The zinc finger domain is indicated by the black line (L403 to H425, E = 2.12e+01). (D) Alignment of *N. crassa* NPF with homologs. ClustalWS alignments from *N. crassa* (XP_960994), *M. musculus* (AAC52970), *D. melanogaster* (AAF55146) and *A. thaliana* (AED97021). Five WD40 domains are indicated by the black lines (R130 to D169, E = 3.21e-01; T180 to D220, E = 1.02e-05; Q230 to D270, E = 9.94e-01; T276 to D317, E = 5.86e-06; M321 to D361, E = 2.14e-08; P378 to K418, E = 4.48e-02).

A

B

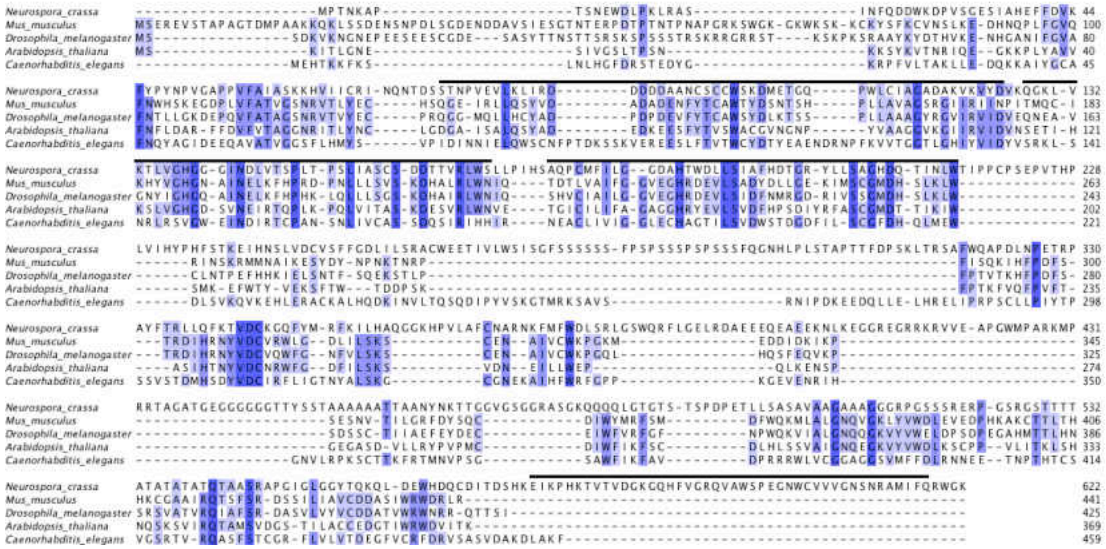

C

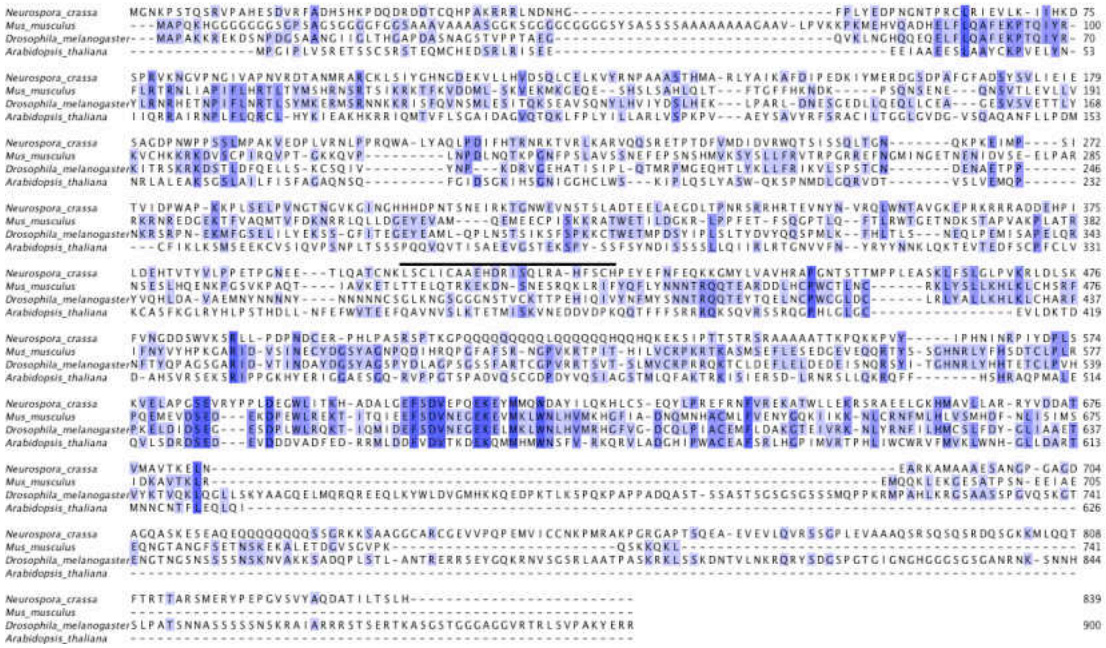

D


Neurospora_crassa
Mus_musculus
Drosophila_melanogaster
Arabidopsis_thaliana

**Fig 9. Linear growth rates of PRC2 subunit deletion mutants.** (A) The linear growth rate for wild-type and PRC2 deletion mutant strains was measured by growth in race tubes on Vogel's solid medium (44). (B) The linear growth rate was measured for four wild-type and four Δ*npf* strains on Vogel's solid medium (44).

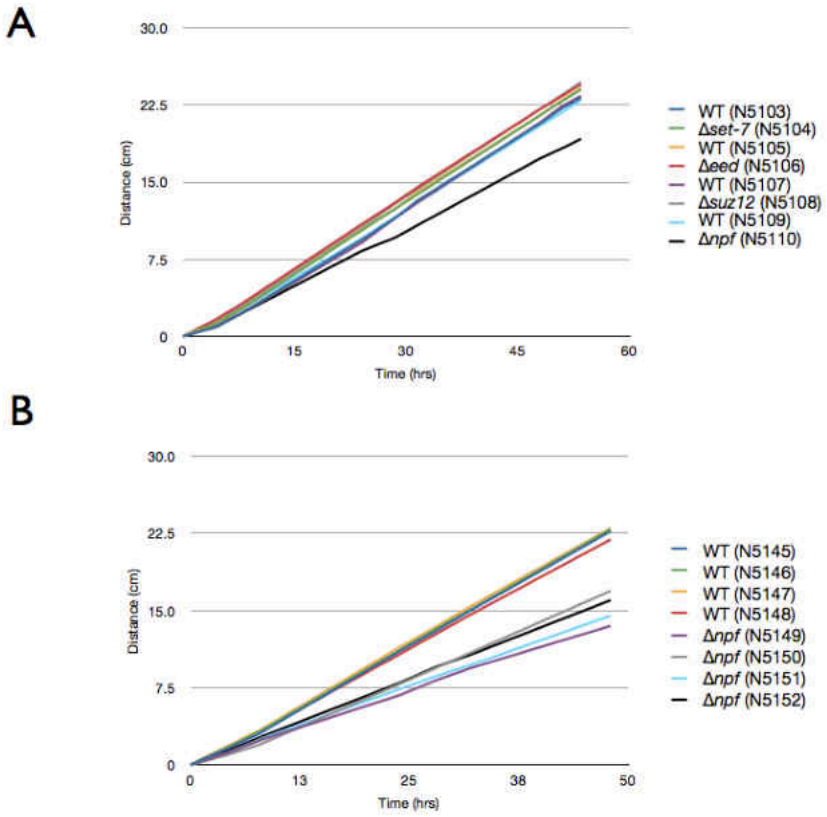

**Fig. 10 (see next page). Deletion of *set-7* de-represses a subset of *Neurospora* genes.** (A) RNA-seq read densities for wild-type (black) and Δ*set-7* (green) are displayed below the genes (green ticks) for LG V; H3K27me3 enrichment (blue) is included for reference. (B) Two genes (NCU08907 and NCU11087) within an H3K27me3 domain are expanded along with the corresponding RNA-seq reads. Northern confirmation of increased NCU08907 expression in a Δ*set-7* mutant; 18S rRNA stained with methylene blue is shown as a loading control. (C) Transcript abundance, expressed as Fragments Per Kilobase of exon per Million fragments mapped (FPKM), plotted *vs.* H3K27me3 level (reads) for genes contained within H3K27me3 domains (blue circles), genes partially contained in H3K27me3 domains (H3K27me3 "border" genes; black diamonds) and for genes outside of H3K27me3 domains (non-H3K27me3 genes; green crosses). The *set-7* upregulated genes that were verified by Northern blots are indicated by red dots.

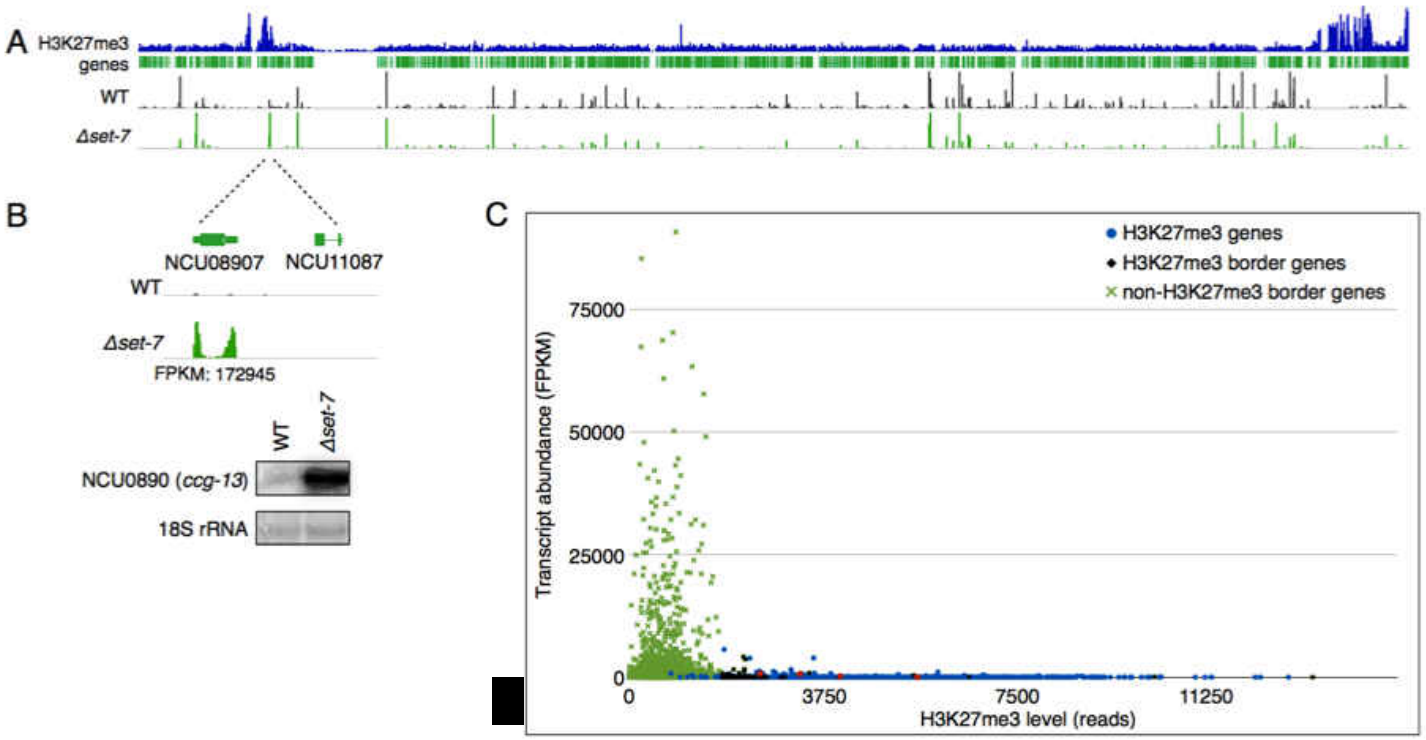
A
H3K27me3
genes
WT
Δset-7
B
NCU08907
NCU11087
WT
Δset-7
FPKM: 172945
WT
Δset-7
NCU0890 (ccg-13)
18S rRNA
C
H3K27me3 genes
H3K27me3 border genes
non-H3K27me3 border genes
Transcript abundance (FPKM)
75000
50000
25000
0
0
3750
7500
11250
H3K27me3 level (reads)

**Fig. 11. Increased expression of H3K27me3 genes in the Δ*set-7* mutant.** Northern blots show the increased expression of three additional genes (NCU05897, NCU11292 and NCU08541) in the Δ*set-7* strain. 18S rRNA stained with methylene blue is shown as a loading control.

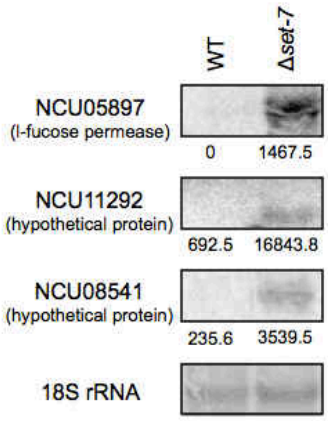

**Fig. 12. Functional Category (FunCat) classification of genes showing increased expression of 130 upregulated genes in the Δ*set-7* strain.**

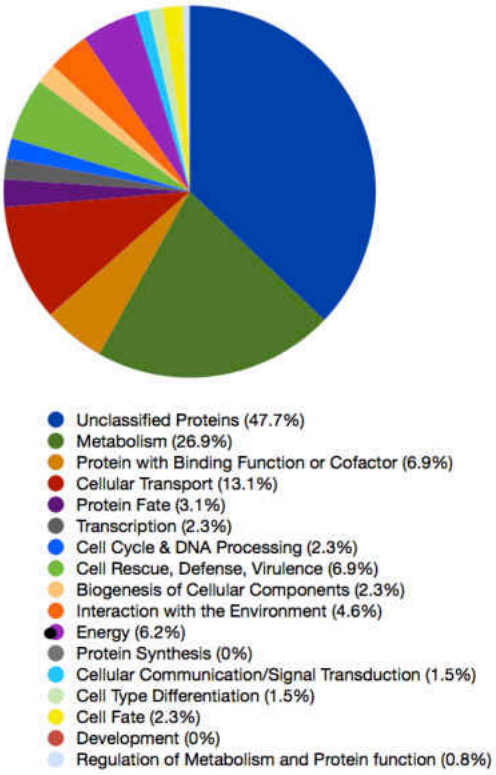


**Fig. 13. Proportion of *N. crassa* H3K27me3-marked and -unmarked genes relative to their conservation in two other *Neurospora* species, *N. tetrasperma* (*N.t.*) and *N. discreta* (*N.d.*)**

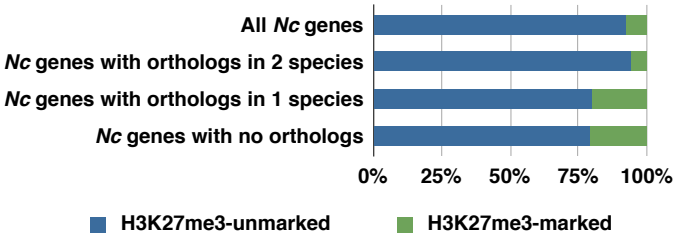

## Figures for Chapter III

**Fig. 14 (see next page). ChIP-seq analysis of H3K27me3 in wild-type and strains containing deletions of genes encoding DCDC subunits.** (A) The wild-type distributions of H3K27me3 (blue track) and H3K9me3 (inverted green track) on LG I are displayed above the distributions of H3K27me3 in Δ*dim-5*, Δ*dim-7*, Δ*dim-9*, Δ*cul4* and Δ*dim-8* strains, respectively (black tracks). The bottom track (purple) shows predicted genes. Expanded views are shown at (B) LG IL sub-telomere (C) two genes, NCU06955 and NCU09590, on LG VII and (D) LG IR sub-telomere. (E) H3K27me3 enrichment ChIP-seq for deletions of each of the DCDC members was validated by qChIP. Red arrows above tracks in (B), (C) and (D) indicate the location of qChIP primer pairs. The enrichment of H3K27me3 was normalized to background levels at histone H4.

Fig. 14 A

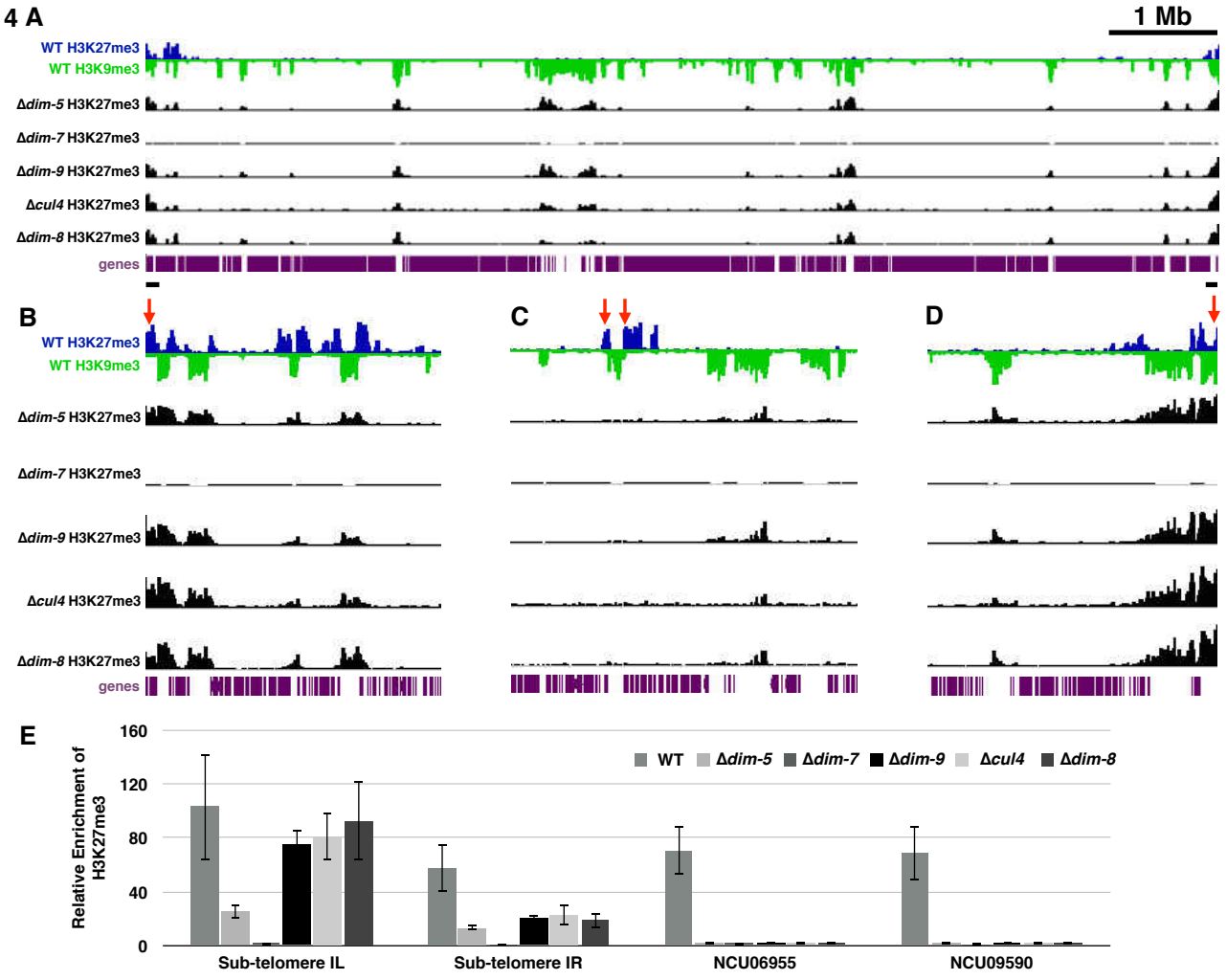
1 Mb
WT H3K27me3
WT H3K9me3
Δdim-5 H3K27me3
Δdim-7 H3K27me3
Δdim-9 H3K27me3
Δcul4 H3K27me3
Δdim-8 H3K27me3
genes
B
C
D
E
Relative Enrichment of H3K27me3
160
120
80
40
0
WT
Δdim-5
Δdim-7
Δdim-9
Δcul4
Δdim-8
Sub-telomere IL
Sub-telomere IR
NCU06955
NCU09590

**Fig. 15 (see next page). ChIP-seq analysis of H3K27me3 at centromeres in Δ*dim-5* and Δ*dim-8* strains.** Centromeres on LG I through VII are shown in (A) through (G), respectively. The wild-type distributions of H3K27me3 (blue track) and H3K9me3 (inverted green track) are shown for comparison. ChIP-seq analyses of H3K27me3 in a Δ*dim-5* strain (mirrored black tracks) and a Δ*dim-8* strain (mirrored red tracks) were each performed twice. Predicted genes are represented by purple rectangles.

Fig. 15

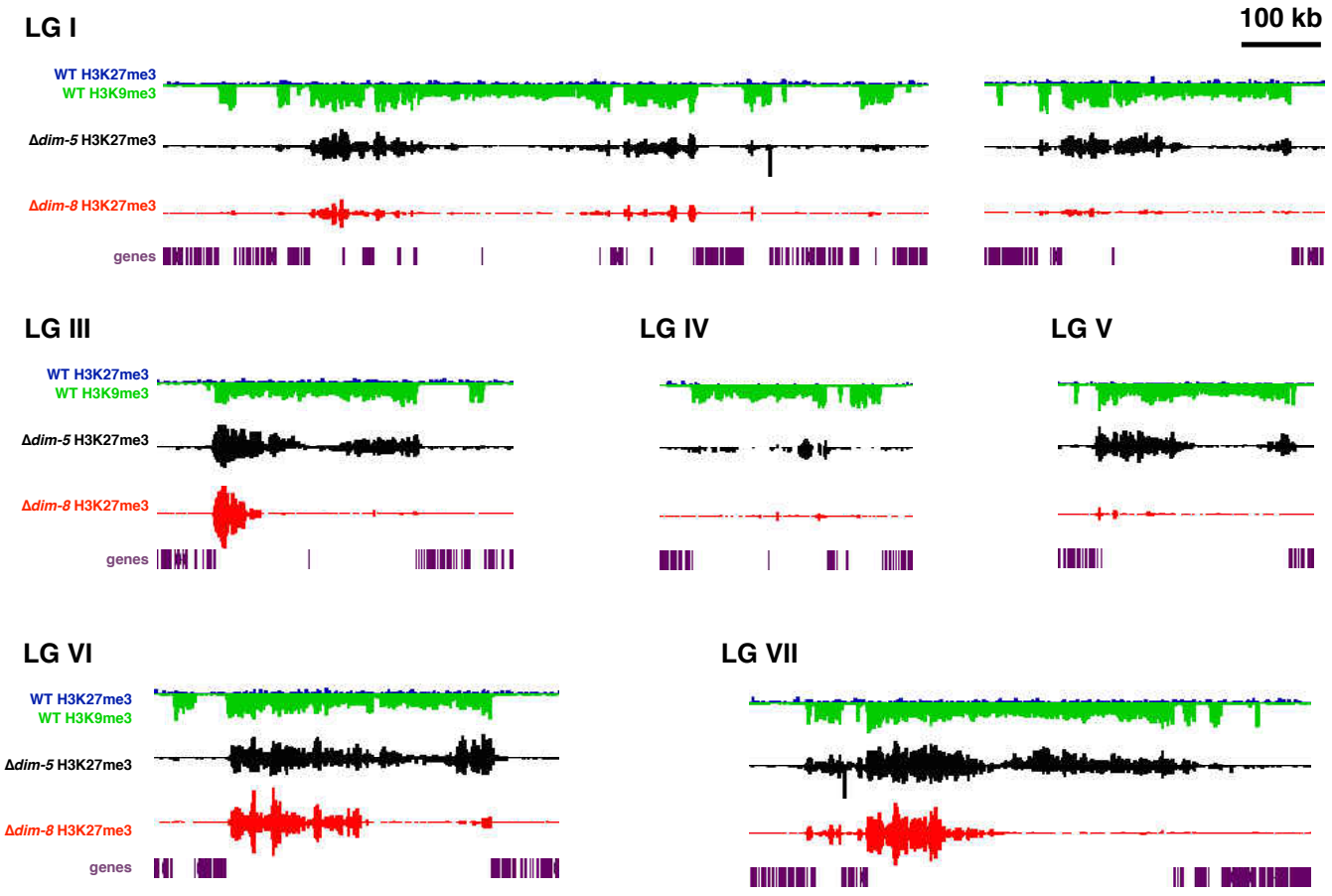
LG I
100 kb
WT H3K27me3
WT H3K9me3
Δdim-5 H3K27me3
Δdim-8 H3K27me3
genes
LG III
LG IV
LG V
LG VI
LG VII

**Fig. 16 (see pages 89-90). The redistribution of H3K27me3 is dependent upon loss of HP1 binding.** (A) The wild-type distributions of H3K27me3 (blue track) and H3K9me3 (inverted green track) on LG I are displayed above the distributions of H3K27me3 in a Δ*dim-5* strain (shown for comparison) and H3K27me3 in Δ*dim-2* strain (both blue tracks). Below are the distributions of H3K27me3 (blue track) and H3K9me3 (inverted green track) in Δ*hpo*. Predicted genes are shown in purple. The redistribution of H3K27me3 in Δ*dim-5* and Δ*hpo* strains but not a Δ*dim-2* strain is highlighted by expansions of H3K27me3 ChIP-seq at (B) LG IL sub-telomere (C) two genes on LG VI, NCU06955 and NCU09590, and (D) LG IR sub-telomere. The decrease in H3K9me3 in a Δ*hpo* strain relative to wild-type is demonstrated in expansions of H3K9me3 ChIP-seq analysis at (B) LG IL sub-telomere, (E) 8:A6, a relatively small region of constitutive heterochromatin and (F) the centromere of LG I highlight the loss or reduction of H3K9me3 in Δ*hpo*. (G) qChIP verified H3K27me3 ChIP-seq at sub-telomere IL, sub-telomere IR and two genes on LG VII. Red arrows indicate the locations of primer pairs used in H3K27me3 qChIP. (H) H3K9me3 ChIP-seq results were verified by qChIP at regions of constitutive heterochromatin, namely 8:A6, sub-telomere IL and two sites on centromere I. Gray arrows indicate the locations of primer pairs used in H3K9me3 qChIP experiments. In all qChIP experiments, the enrichment of H3K27me3 and H3K9me3 were each normalized to background at histone H4.

Fig. 16

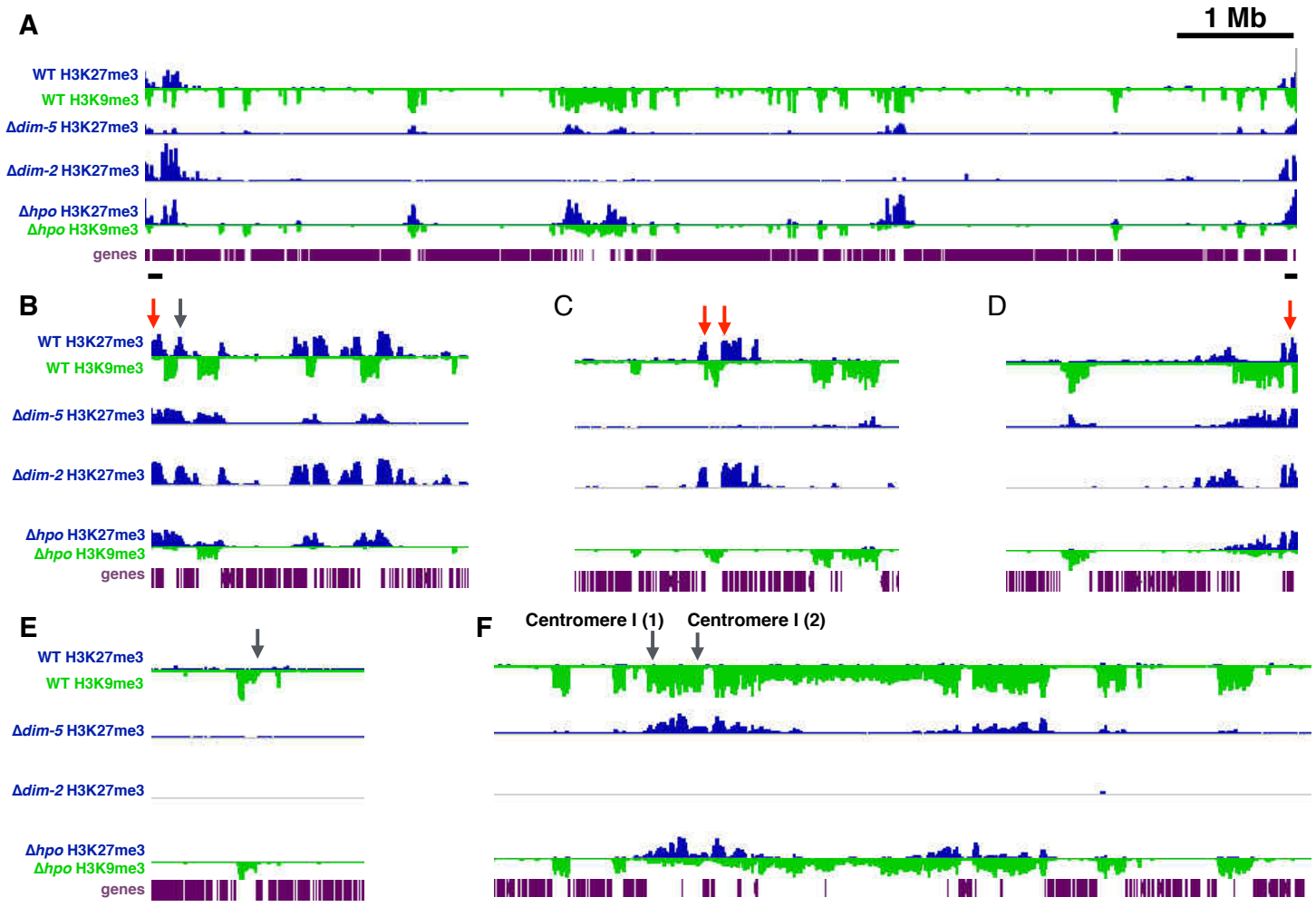
A
1 Mb
WT H3K27me3
WT H3K9me3
Δdim-5 H3K27me3
Δdim-2 H3K27me3
Δhpo H3K27me3
Δhpo H3K9me3
genes
B
C
D
E
F
Centromere I (1)
Centromere I (2)

**Fig. 16**

**G**

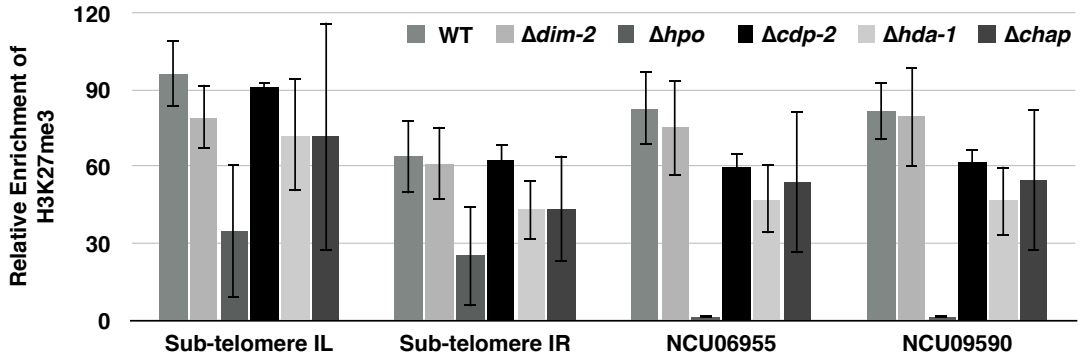
120
90
60
30
0
Relative Enrichment of H3K27me3
WT
Δdim-2
Δhpo
Δcdp-2
Δhda-1
Δchap
Sub-telomere IL
Sub-telomere IR
NCU06955
NCU09590

**H**

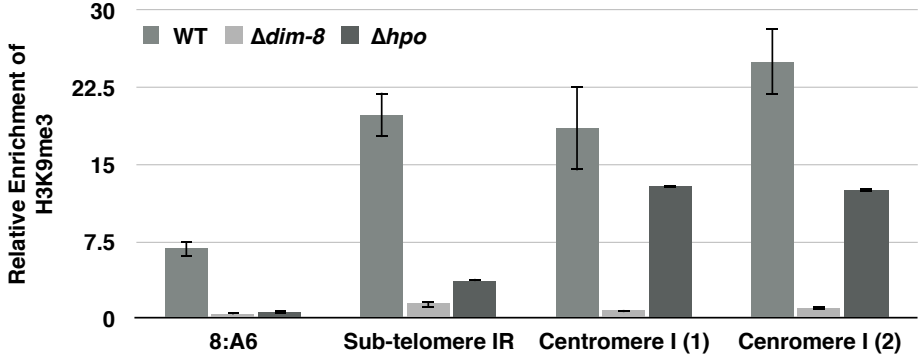
30
22.5
15
7.5
0
Relative Enrichment of H3K9me3
WT
Δdim-8
Δhpo
8:A6
Sub-telomere IR
Centromere I (1)
Cenromere I (2)

**Fig. 17 (see next page). Three novel H3K27me3 peaks on LG VI are observed in two Δ*dim-2* strains relative to the wild-type distribution of H3K27me3.** (A) Tracks displaying the wild-type distributions of H3K27me3 (blue track) and H3K9me3 (inverted green track) are displayed above the distributions of H3K27me3 in two Δ*dim-2* strains (N1850 and N1851, black tracks). Purple boxes represent predicted genes. (B) Expansion of a region containing novel H3K27me3 peaks in Δ*dim-2* strains.

Fig. 17

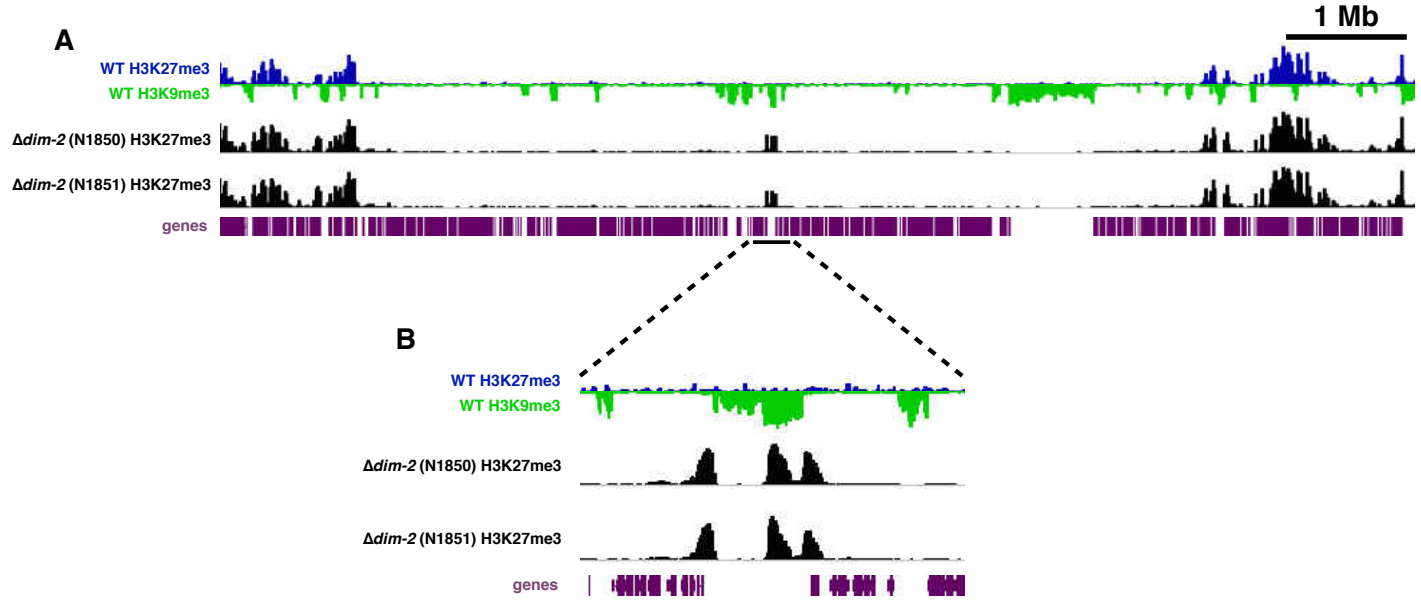
A
1 Mb
WT H3K27me3
WT H3K9me3
Δdim-2 (N1850) H3K27me3
Δdim-2 (N1851) H3K27me3
genes
B
WT H3K27me3
WT H3K9me3
Δdim-2 (N1850) H3K27me3
Δdim-2 (N1851) H3K27me3
genes

**Fig. 18 (see pages 94-95). *hH3*$^{R8A}$ and *hH3*$^{S10A}$ strains show a regional loss of H3K9me3 and a redistribution of H3K27me3.** (A) The wild-type distributions of H3K27me3 (blue track) and H3K9me3 (inverted green track) on LG I are shown for comparison above distributions of H3K27me3 (blue tracks) and H3K9me3 (inverted green tracks) for *hH3*$^{R8A}$ and *hH3*$^{S10A}$, respectively. Predicted genes are shown in purple. The redistributions of H3K27me3 in both the *hH3*$^{R8A}$ and *hH3*$^{S10A}$ strains are highlighted by expansions of H3K27me3 ChIP-seq at (B) sub-telomere IL, (C) two genes on LG VII, NCU06955 and NCU09590, and (D) sub-telomere IR. The significant reduction of H3K9me3 in the *hH3*$^{R8A}$ and *hH3*$^{S10A}$ strains are depicted in (B) sub-telomere IL, (E) 8:A6 and (F) the centromere on LG I. (G) H3K27me3 ChIP-seq analysis was verified by qChIP using the primers pairs indicated by red arrows in (B), (C) and (D). (H) H3K9me3 ChIP-seq was verified by qChIP using the primer pairs indicated by gray arrows in (B), (E) and (F). In all qChIP experiments, H3K27me3 enrichment was normalized to background at histone H4.

Fig. 18

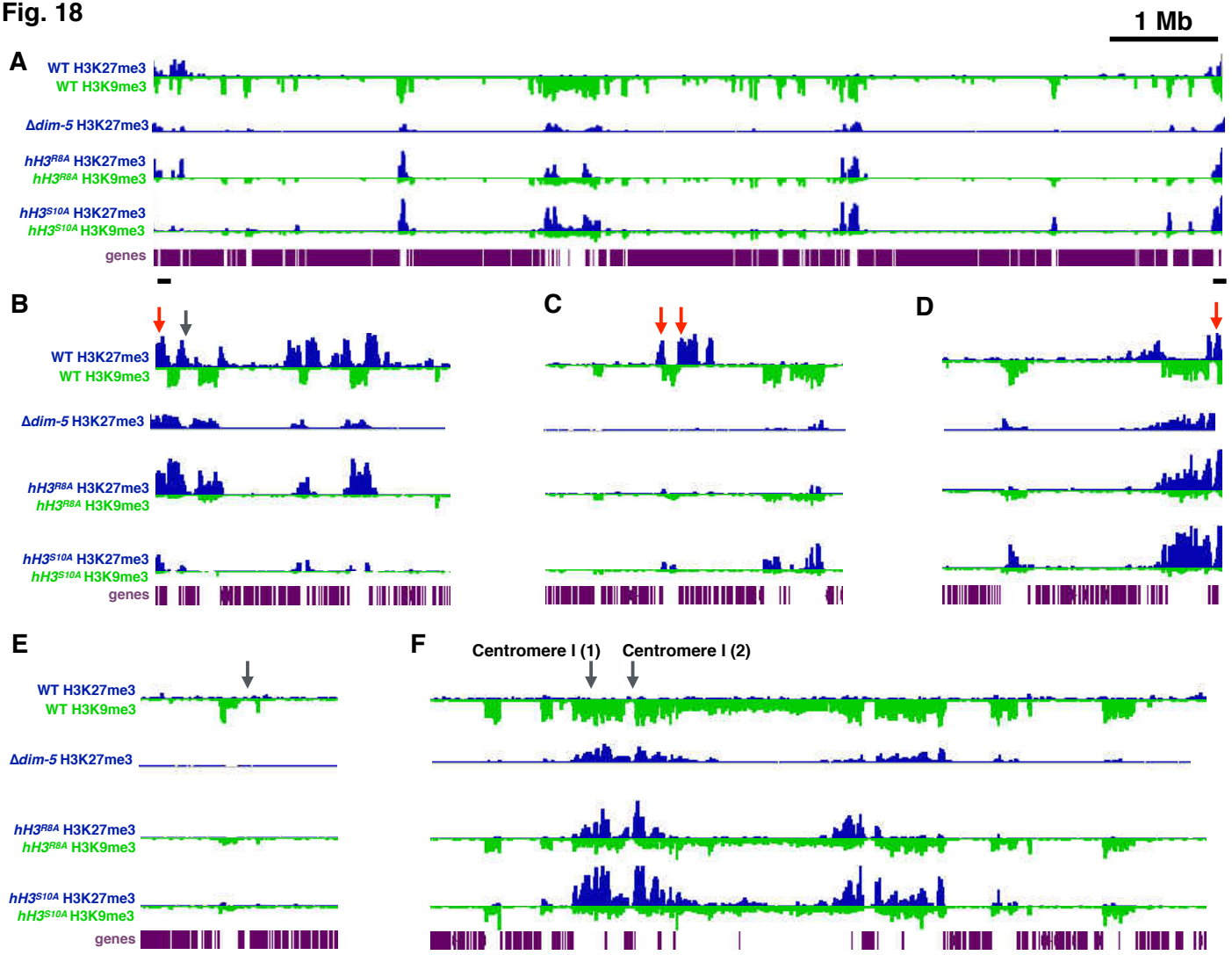
1 Mb
A
WT H3K27me3
WT H3K9me3
Δdim-5 H3K27me3
hH3R8A H3K27me3
hH3R8A H3K9me3
hH3S10A H3K27me3
hH3S10A H3K9me3
genes
B
C
D
E
F
Centromere I (1)
Centromere I (2)

**Fig. 18**

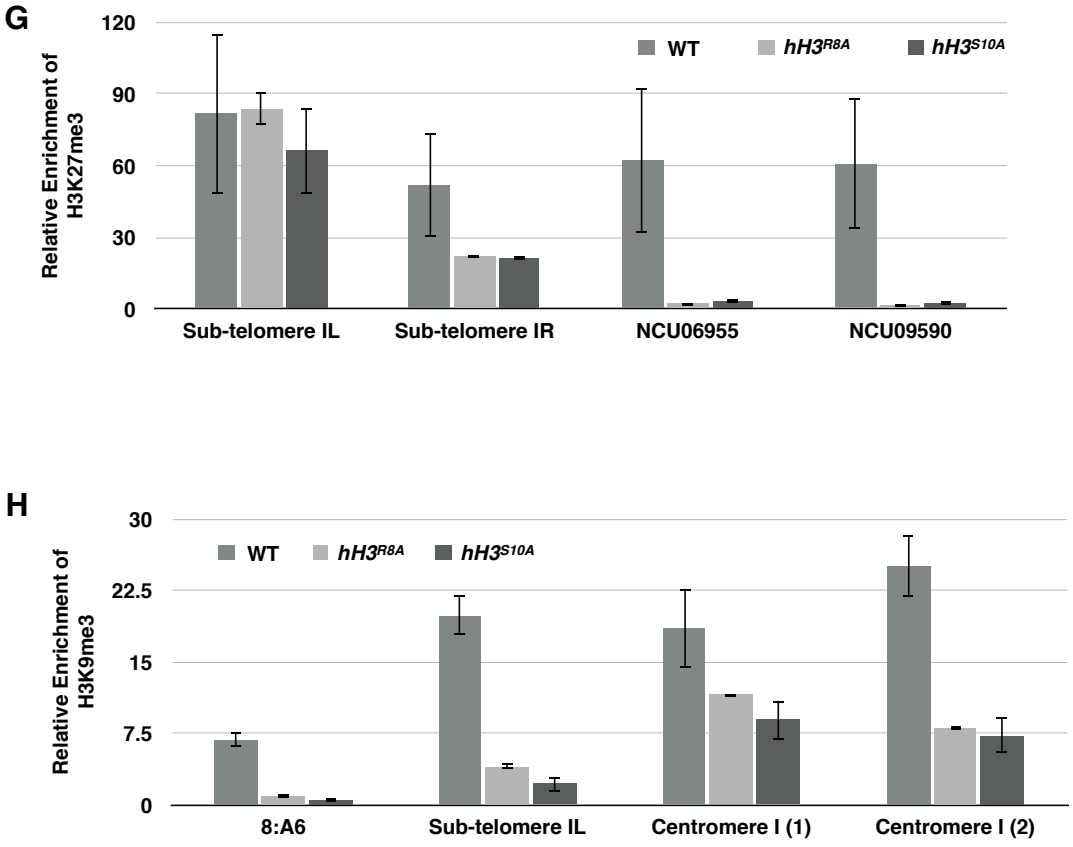
G
120
90
60
30
0
Relative Enrichment of H3K27me3
WT
hH3R8A
hH3S10A
Sub-telomere IL
Sub-telomere IR
NCU06955
NCU09590
H
30
22.5
15
7.5
0
Relative Enrichment of H3K9me3
WT
hH3R8A
hH3S10A
8:A6
Sub-telomere IL
Centromere I (1)
Centromere I (2)

**Fig. 19 (see next page). H3K27me3 is significantly depleted in *hH3*$^{R2L}$ and *hH3*$^{A7M}$ strains.** (A) The wild-type distributions of H3K27me3 (blue track) and H3K9me3 (inverted green track) on LG I are shown for comparison above distributions of H3K27me3 (blue tracks) in *hH3*$^{R2L}$ and *hH3*$^{A7M}$ strains, respectively. Predicted genes are shown in purple. Expansions of ChIP-seq are shown at (B) sub-telomere IL, (C) two genes on LG VII, NCU06955 and NCU09590, (D) sub-telomere IR. (E) The reduction of H3K27me3 in both the *hH3*$^{R2L}$ and *hH3*$^{A7M}$ relative to a wild-type strain at sub-telomeres IL and IR, NCU06955 and NCU09590 were confirmed by qChIP. Red arrows in (B), (C) and (D) indicate the location of primers pairs used for H327me3 qChIP experiments. In all qChIP experiments, H3K27me3 enrichment was normalized to background at histone H4.

Fig. 19

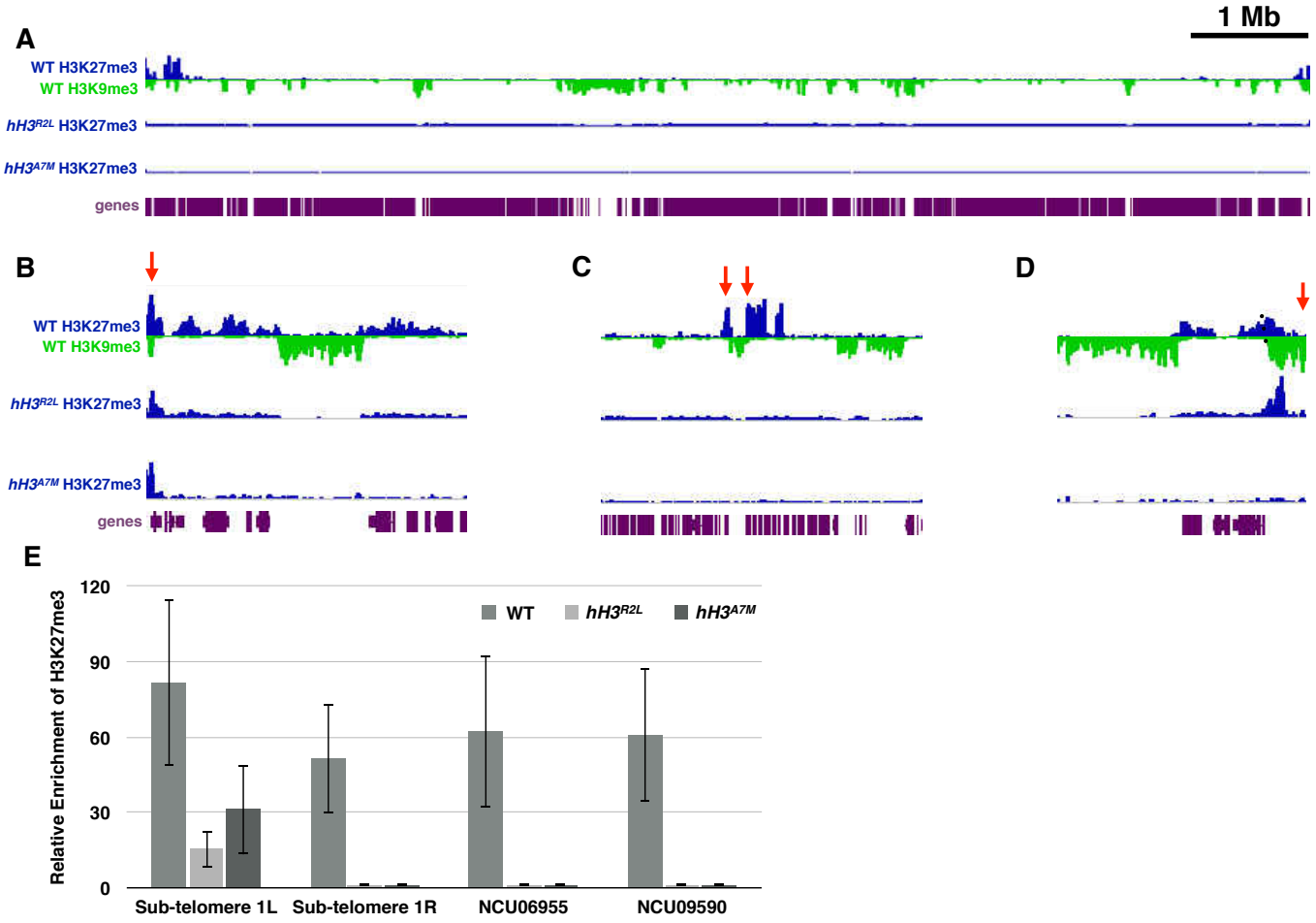
A
1 Mb
WT H3K27me3
WT H3K9me3
hH3R2L H3K27me3
hH3A7M H3K27me3
genes
B
C
D
E
Relative Enrichment of H3K27me3
120
90
60
30
0
WT
hH3R2L
hH3A7M
Sub-telomere 1L
Sub-telomere 1R
NCU06955
NCU09590

**Fig. 20 (see next page). The distribution of H3K9me3 is not altered by the absence of H3K27me3 in Δ*set-7* and Δ*eed* strains.** (A) ChIP-seq on LG I of H3K27me3 (blue track) and H3K9me3 (inverted green track) displayed above H3K9me3 ChIP-seq in Δ*set-7* and Δ*eed* strains. Predicted genes are shown in purple. Expansions of H3K9me3 ChIP-seq analysis are shown at (B) sub-telomere IL, (C) two regions on the LG I centromere and (D) 8:A6, a region of constitutive heterochromatin. (E) H3K9me3 ChIP-seq analysis was validated by qChIP experiments at regions highlighted in (B) through (D). Red arrows indicate the locations of primer pairs used in qChIP experiments. In all qChIP experiments, H3K9me3 enrichment was normalized to background at histone H4.

Fig. 20

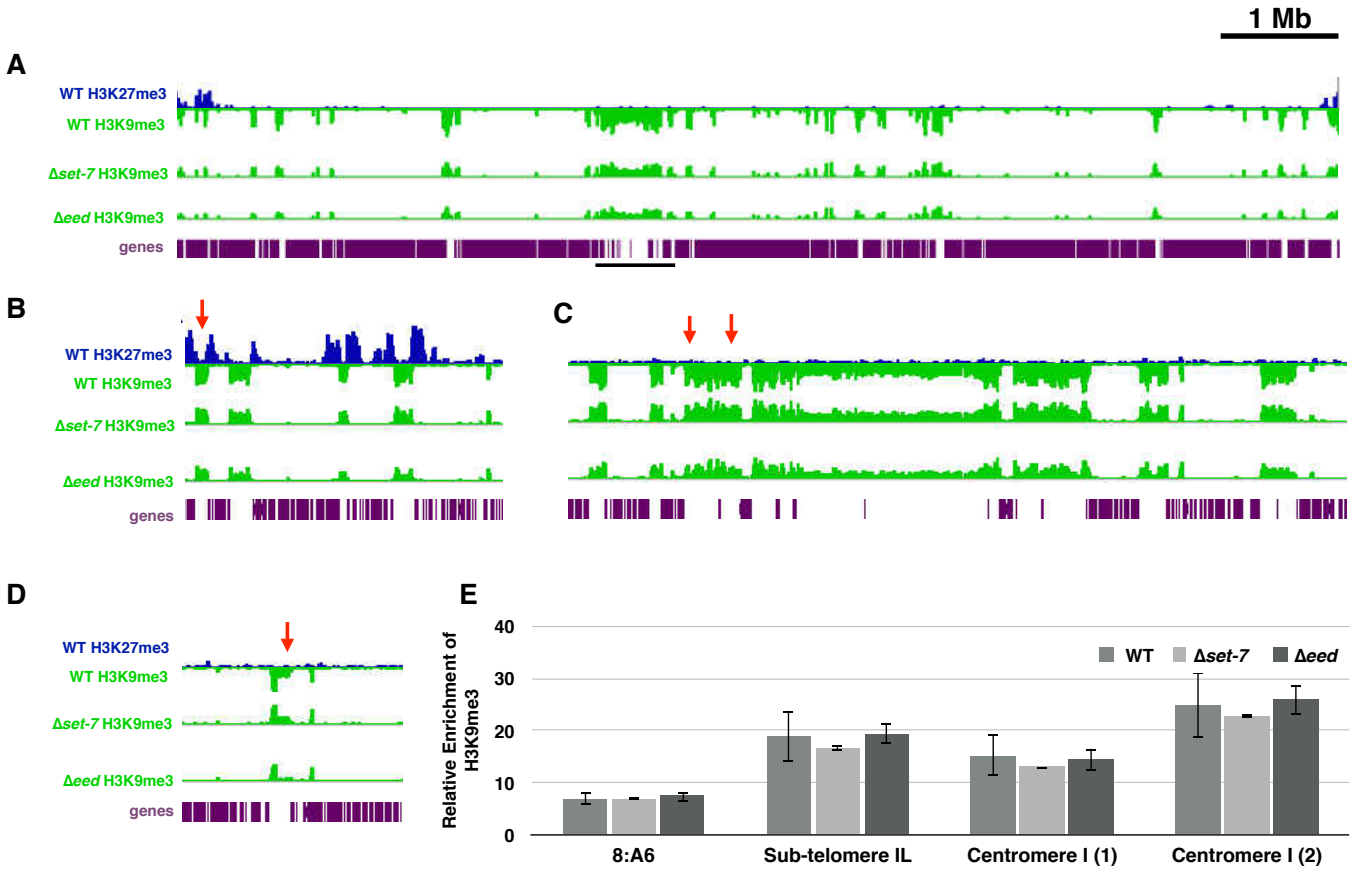
1 Mb
A
WT H3K27me3
WT H3K9me3
Δset-7 H3K9me3
Δeed H3K9me3
genes
B
C
D
E
Relative Enrichment of H3K9me3
40
30
20
10
0
WT
Δset-7
Δeed
8:A6
Sub-telomere IL
Centromere I (1)
Centromere I (2)

**Fig. 21 (see pages 101-107). Summary of H3K27me3 and H3K9me3 ChIP-seq analysis for all seven linkage groups.** H3K27me3 distribution in wild-type and strains containing deletions of *dim-5*, *dim-7*, *dim-8*, *dim-9*, *cul4*, *dim-2* and *hpo* and histone H3 substitutions for R8A, S10A, R2L and A7M are shown for all seven linkage groups (blue tracks). H3K9me3 distribution in wild-type and strains containing deletions of *hpo*, *set-7* and *eed* and histone H3 R8A and S10A substitutions (green tracks). H3K4me3 distribution in wild-type (red track) and predicted genes (purple track) are shown for comparison.

Fig. 21

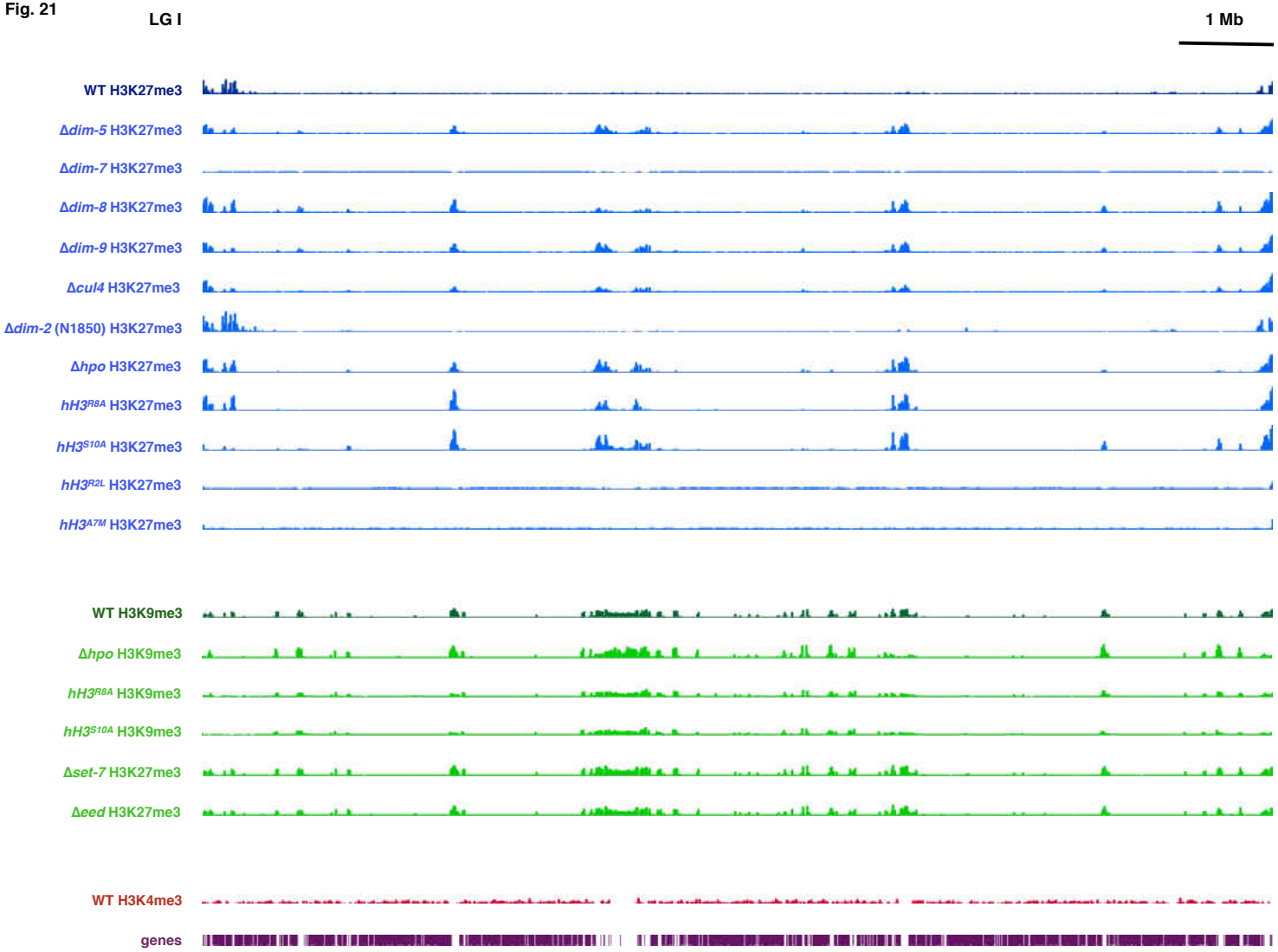
LG I
1 Mb
WT H3K27me3
Δdim-5 H3K27me3
Δdim-7 H3K27me3
Δdim-8 H3K27me3
Δdim-9 H3K27me3
Δcul4 H3K27me3
Δdim-2 (N1850) H3K27me3
Δhpo H3K27me3
hH3R8A H3K27me3
hH3S10A H3K27me3
hH3R2L H3K27me3
hH3A7M H3K27me3
WT H3K9me3
Δhpo H3K9me3
hH3R8A H3K9me3
hH3S10A H3K9me3
Δset-7 H3K27me3
Δeed H3K27me3
WT H3K4me3
genes

Fig. 21

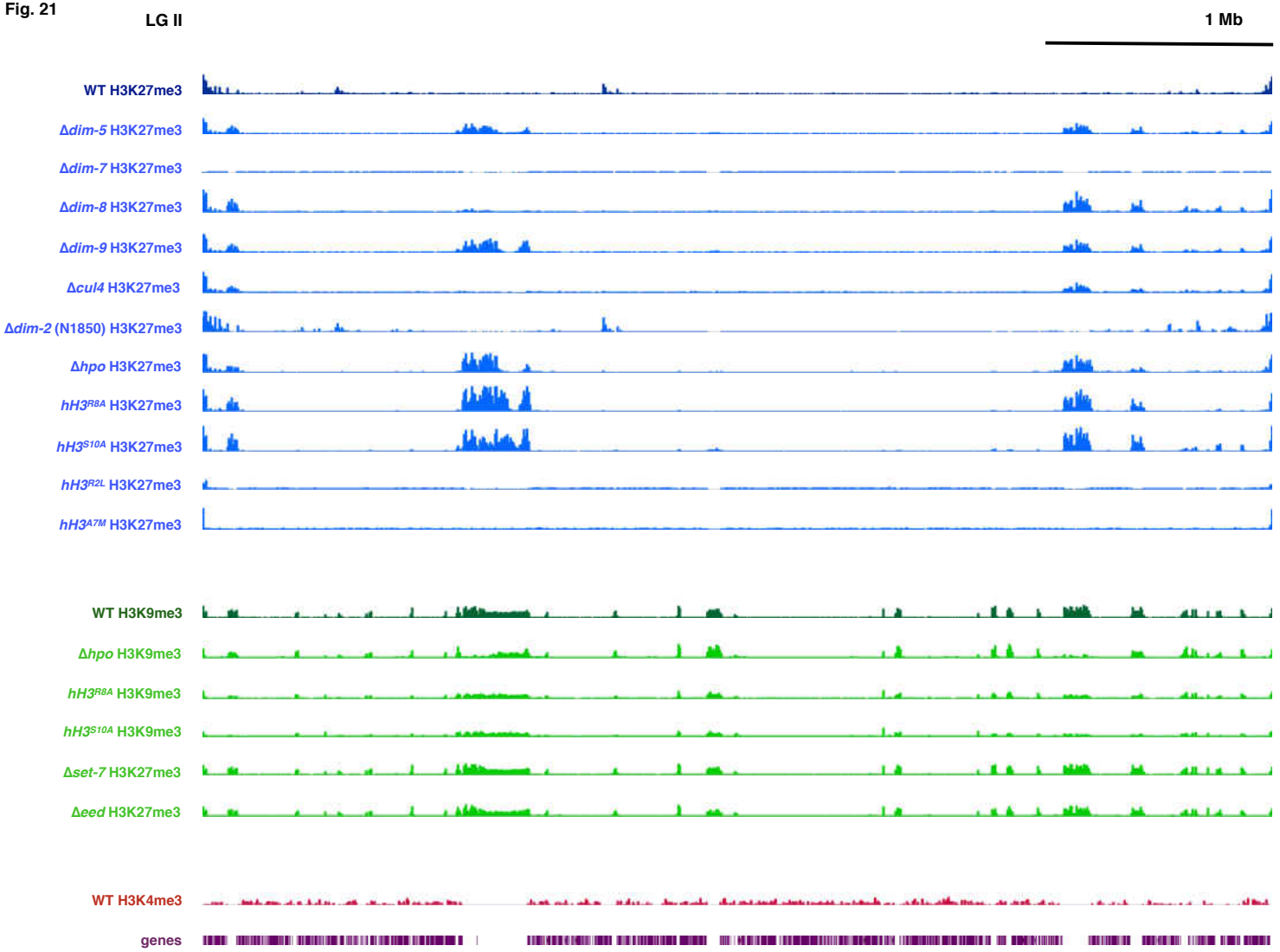
LG II
1 Mb
WT H3K27me3
Δdim-5 H3K27me3
Δdim-7 H3K27me3
Δdim-8 H3K27me3
Δdim-9 H3K27me3
Δcul4 H3K27me3
Δdim-2 (N1850) H3K27me3
Δhpo H3K27me3
hH3R8A H3K27me3
hH3S10A H3K27me3
hH3R2L H3K27me3
hH3A7M H3K27me3
WT H3K9me3
Δhpo H3K9me3
hH3R8A H3K9me3
hH3S10A H3K9me3
Δset-7 H3K27me3
Δeed H3K27me3
WT H3K4me3
genes

Fig. 21

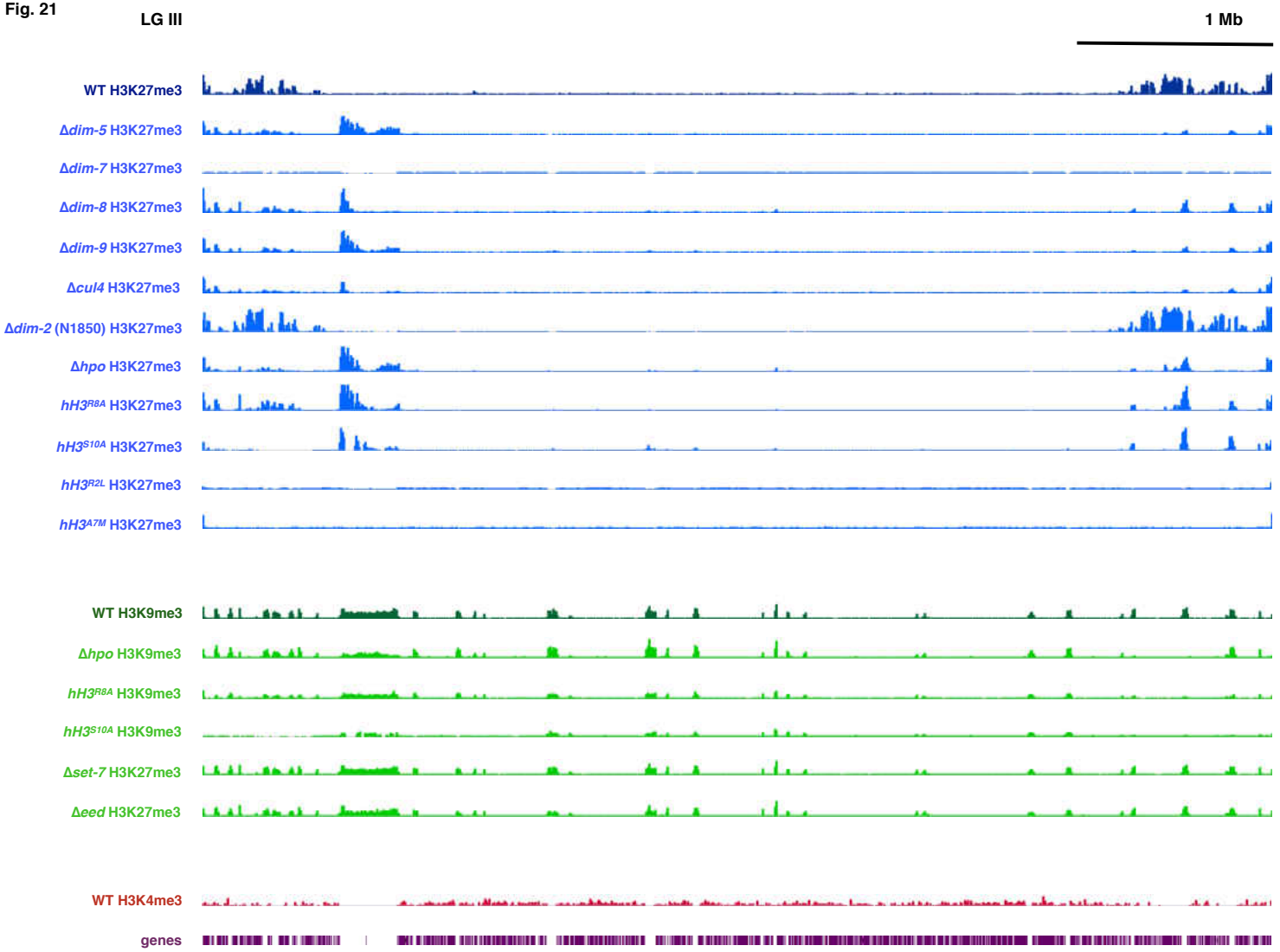
LG III
1 Mb
WT H3K27me3
Δdim-5 H3K27me3
Δdim-7 H3K27me3
Δdim-8 H3K27me3
Δdim-9 H3K27me3
Δcul4 H3K27me3
Δdim-2 (N1850) H3K27me3
Δhpo H3K27me3
hH3R8A H3K27me3
hH3S10A H3K27me3
hH3R2L H3K27me3
hH3A7M H3K27me3
WT H3K9me3
Δhpo H3K9me3
hH3R8A H3K9me3
hH3S10A H3K9me3
Δset-7 H3K27me3
Δeed H3K27me3
WT H3K4me3
genes

Fig. 21

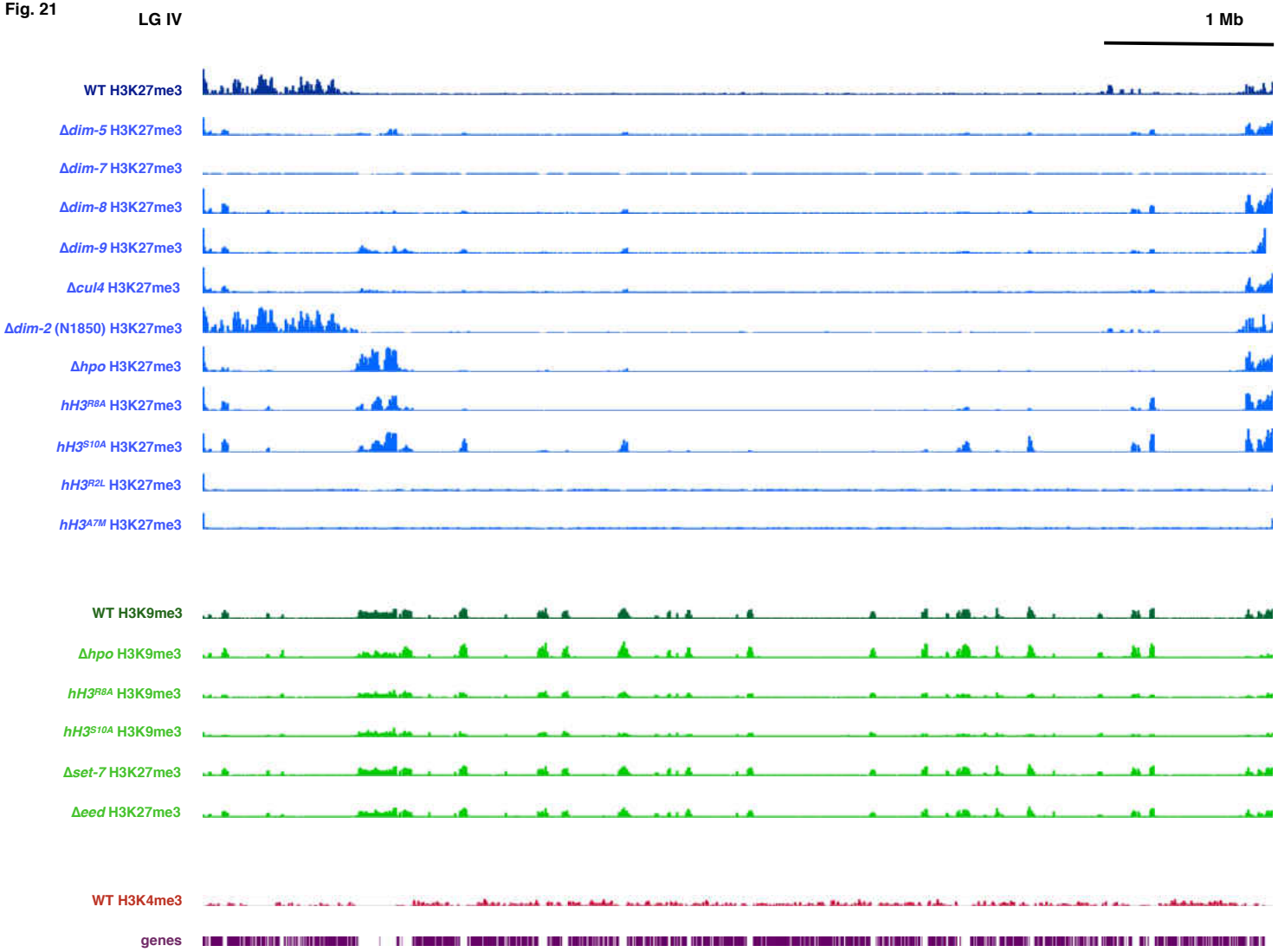
LG IV
1 Mb
WT H3K27me3
Δdim-5 H3K27me3
Δdim-7 H3K27me3
Δdim-8 H3K27me3
Δdim-9 H3K27me3
Δcul4 H3K27me3
Δdim-2 (N1850) H3K27me3
Δhpo H3K27me3
hH3R8A H3K27me3
hH3S10A H3K27me3
hH3R2L H3K27me3
hH3A7M H3K27me3
WT H3K9me3
Δhpo H3K9me3
hH3R8A H3K9me3
hH3S10A H3K9me3
Δset-7 H3K27me3
Δeed H3K27me3
WT H3K4me3
genes

Fig. 21

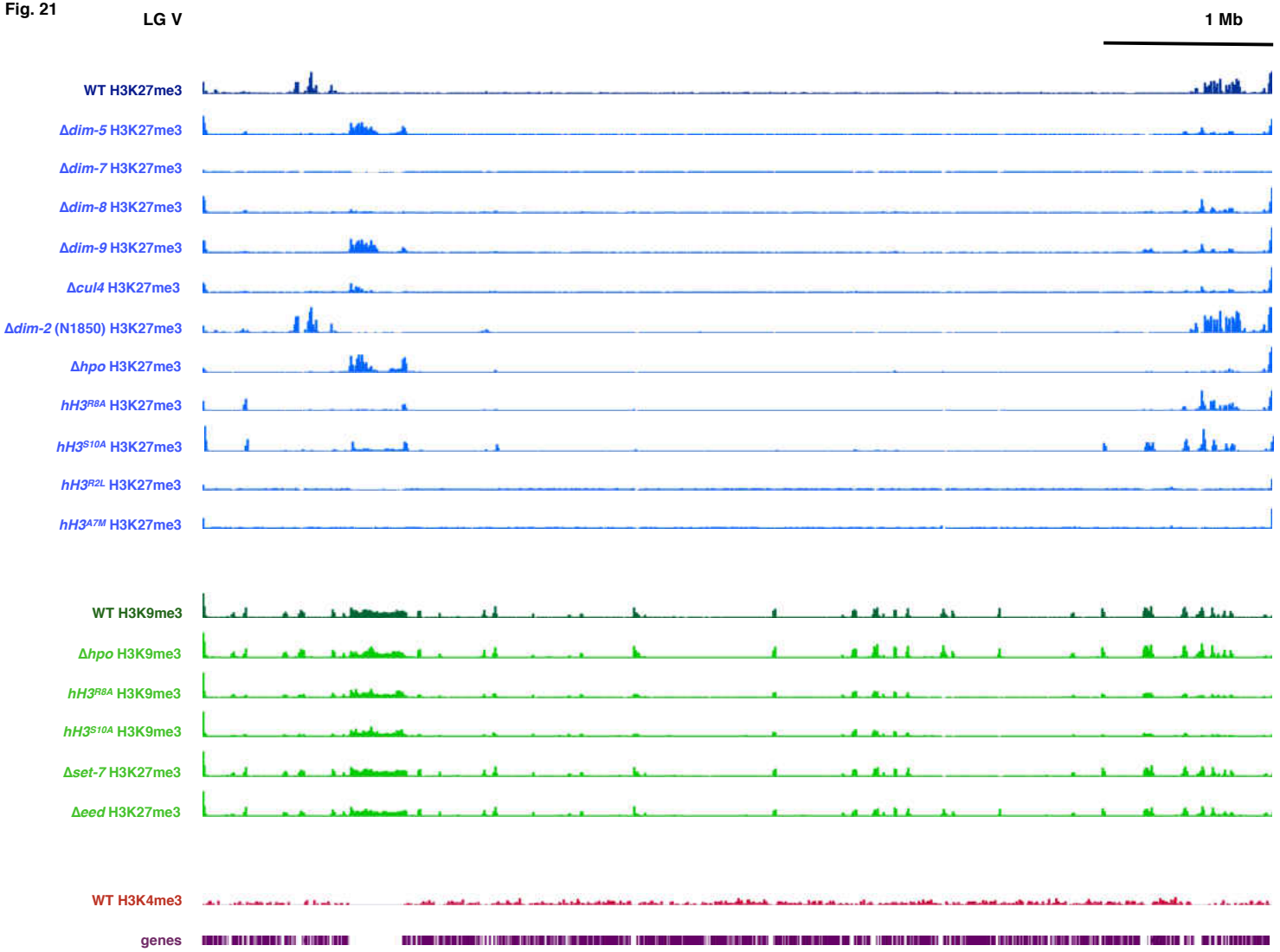
LG V
1 Mb
WT H3K27me3
Δdim-5 H3K27me3
Δdim-7 H3K27me3
Δdim-8 H3K27me3
Δdim-9 H3K27me3
Δcul4 H3K27me3
Δdim-2 (N1850) H3K27me3
Δhpo H3K27me3
hH3R8A H3K27me3
hH3S10A H3K27me3
hH3R2L H3K27me3
hH3A7M H3K27me3
WT H3K9me3
Δhpo H3K9me3
hH3R8A H3K9me3
hH3S10A H3K9me3
Δset-7 H3K27me3
Δeed H3K27me3
WT H3K4me3
genes

Fig. 21

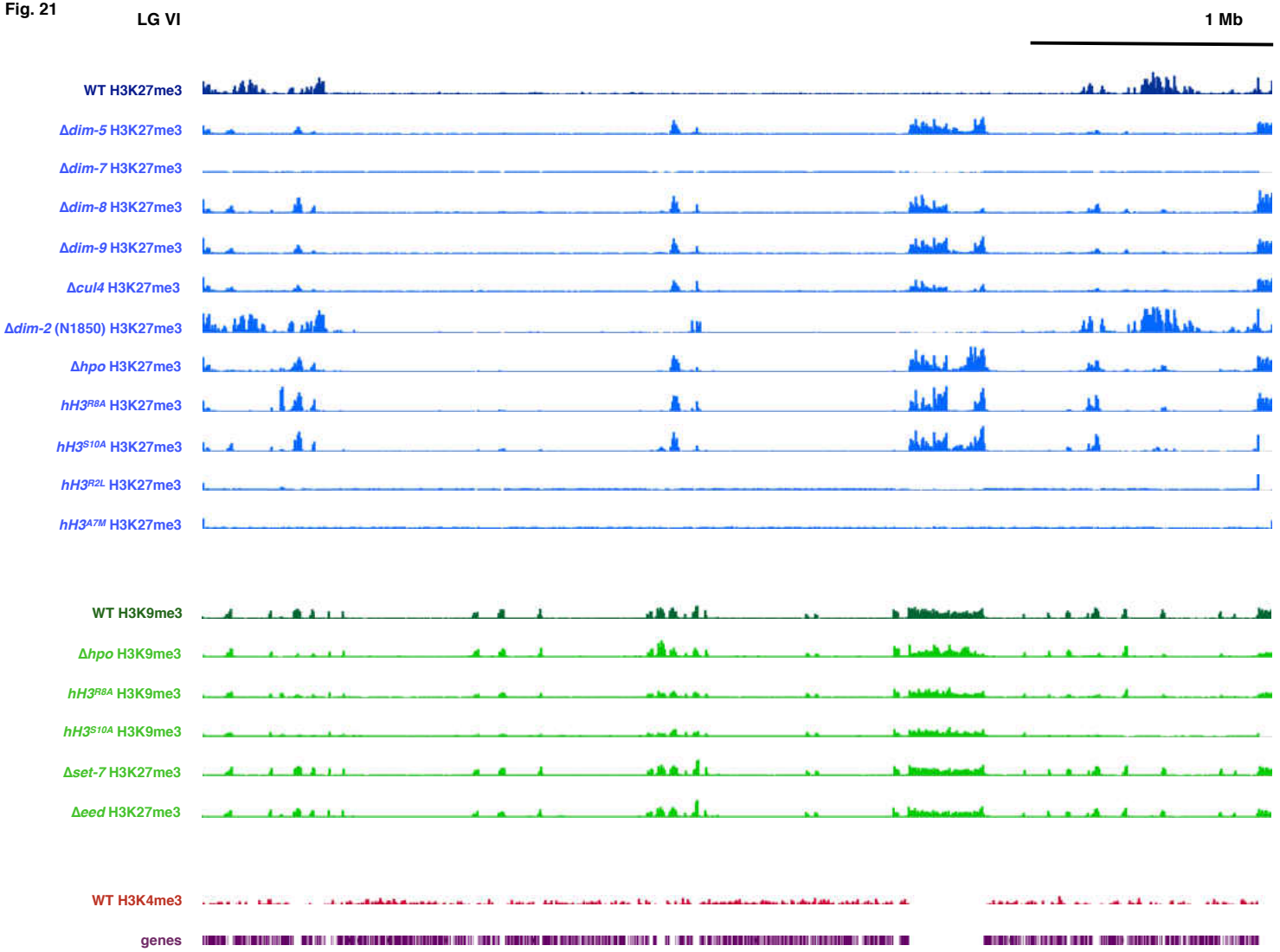
LG VI
1 Mb
WT H3K27me3
Δdim-5 H3K27me3
Δdim-7 H3K27me3
Δdim-8 H3K27me3
Δdim-9 H3K27me3
Δcul4 H3K27me3
Δdim-2 (N1850) H3K27me3
Δhpo H3K27me3
hH3R8A H3K27me3
hH3S10A H3K27me3
hH3R2L H3K27me3
hH3A7M H3K27me3
WT H3K9me3
Δhpo H3K9me3
hH3R8A H3K9me3
hH3S10A H3K9me3
Δset-7 H3K27me3
Δeed H3K27me3
WT H3K4me3
genes

Fig. 21

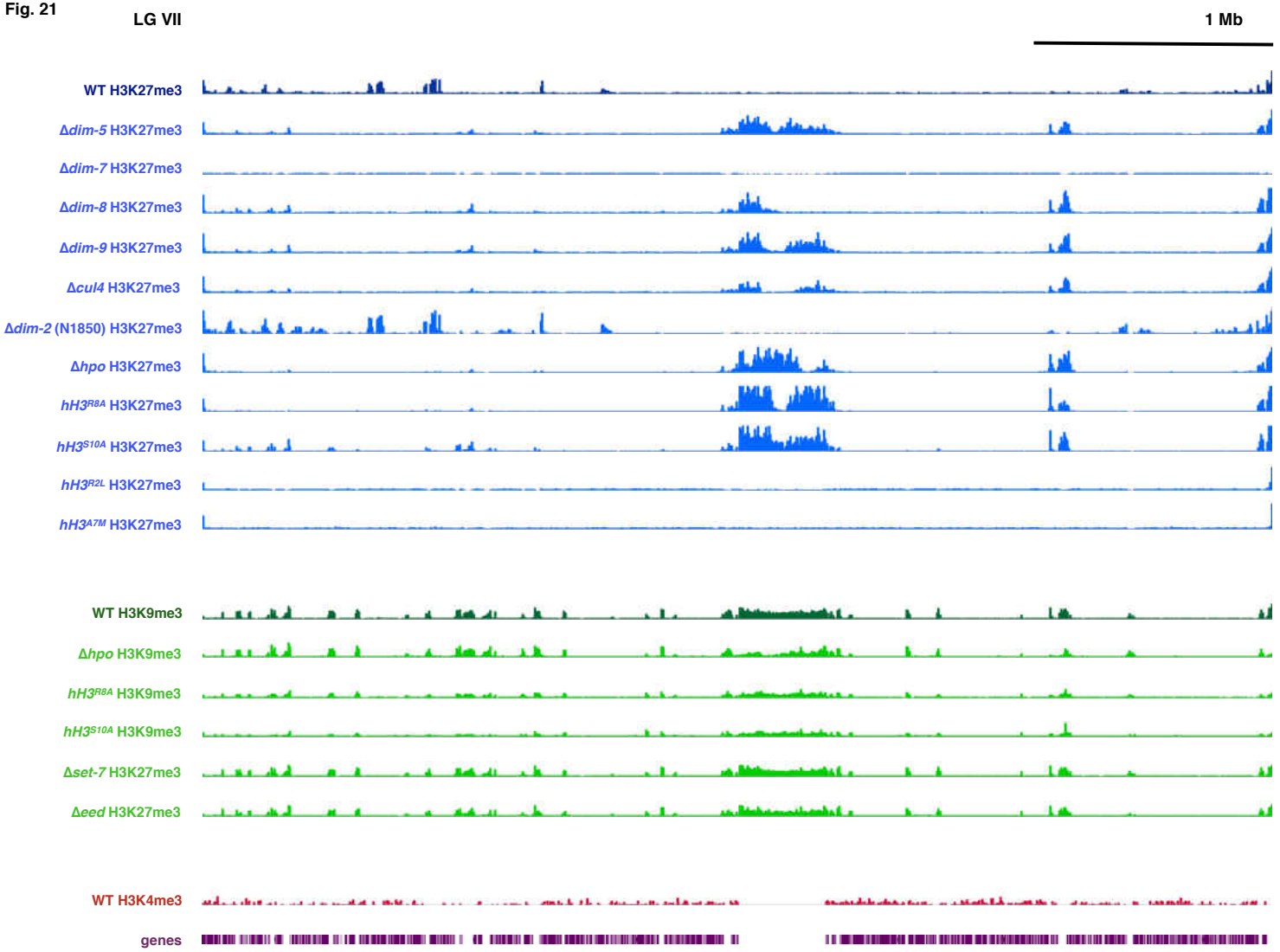
LG VII
1 Mb
WT H3K27me3
Δdim-5 H3K27me3
Δdim-7 H3K27me3
Δdim-8 H3K27me3
Δdim-9 H3K27me3
Δcul4 H3K27me3
Δdim-2 (N1850) H3K27me3
Δhpo H3K27me3
hH3R8A H3K27me3
hH3S10A H3K27me3
hH3R2L H3K27me3
hH3A7M H3K27me3
WT H3K9me3
Δhpo H3K9me3
hH3R8A H3K9me3
hH3S10A H3K9me3
Δset-7 H3K27me3
Δeed H3K27me3
WT H3K4me3
genes

**Fig. 22 (see pages 109-111). Summary of biological replicates of H3K27me3 ChIP-seq analysis for Δ*dim-5* and Δ*dim-8* strains across all seven linkage groups.** The distributions of H3K27me3 (blue track) and H3K9me3 (inverted green track) are shown for comparison. Below are two biological replicates of H3K27me3 in Δ*dim-5* (strain N3944, black and inverted gray tracks) and Δ*dim-8* (strain N3403, red and inverted light red tracks). Next, H3K27me3 ChIP-seq analysis is displayed in two strains (N1850 and N1851), each containing a deletion of *dim-2* (orange and inverted light orange tracks).

Fig. 22

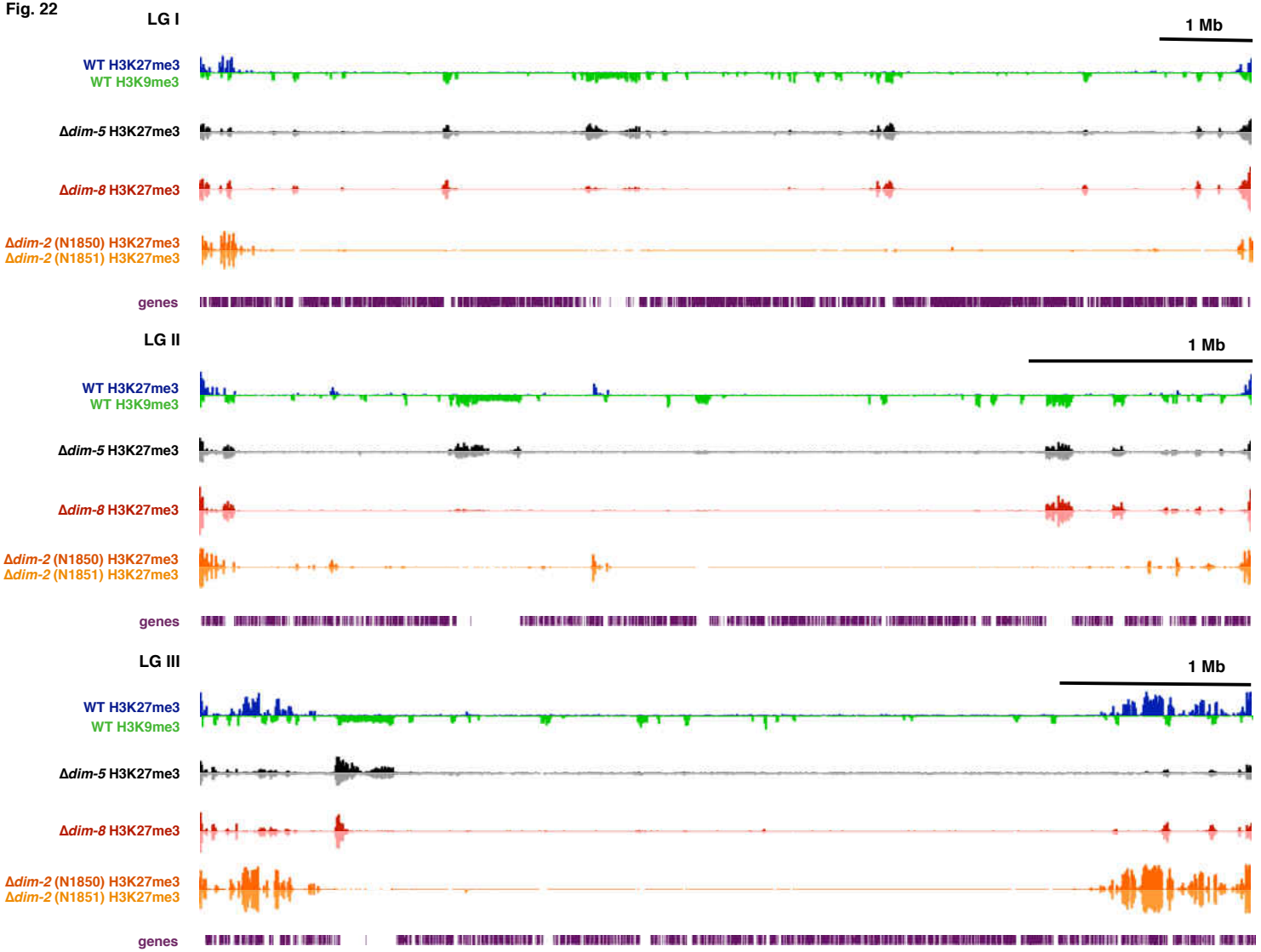
LG I
1 Mb
WT H3K27me3
WT H3K9me3
Δdim-5 H3K27me3
Δdim-8 H3K27me3
Δdim-2 (N1850) H3K27me3
Δdim-2 (N1851) H3K27me3
genes
LG II
1 Mb
WT H3K27me3
WT H3K9me3
Δdim-5 H3K27me3
Δdim-8 H3K27me3
Δdim-2 (N1850) H3K27me3
Δdim-2 (N1851) H3K27me3
genes
LG III
1 Mb
WT H3K27me3
WT H3K9me3
Δdim-5 H3K27me3
Δdim-8 H3K27me3
Δdim-2 (N1850) H3K27me3
Δdim-2 (N1851) H3K27me3
genes

Fig. 22

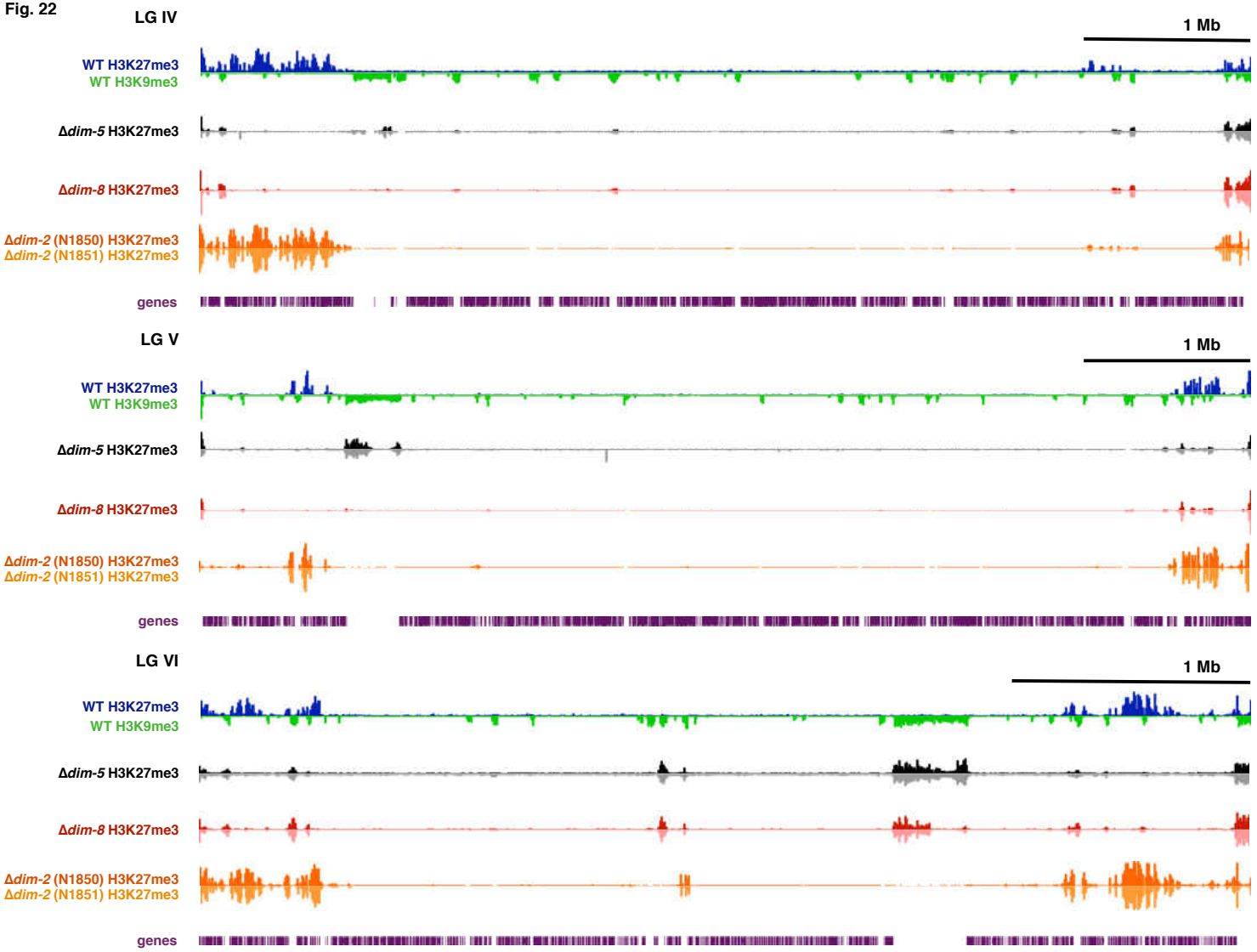
LG IV
1 Mb
WT H3K27me3
WT H3K9me3
Δdim-5 H3K27me3
Δdim-8 H3K27me3
Δdim-2 (N1850) H3K27me3
Δdim-2 (N1851) H3K27me3
genes
LG V
1 Mb
WT H3K27me3
WT H3K9me3
Δdim-5 H3K27me3
Δdim-8 H3K27me3
Δdim-2 (N1850) H3K27me3
Δdim-2 (N1851) H3K27me3
genes
LG VI
1 Mb
WT H3K27me3
WT H3K9me3
Δdim-5 H3K27me3
Δdim-8 H3K27me3
Δdim-2 (N1850) H3K27me3
Δdim-2 (N1851) H3K27me3
genes

Fig. 22

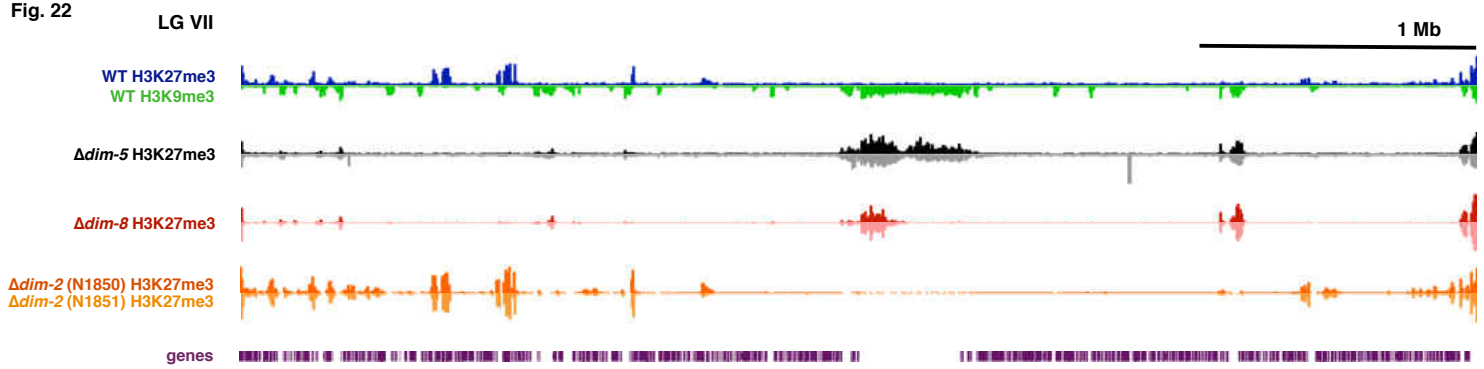
LG VII
1 Mb
WT H3K27me3
WT H3K9me3
Δdim-5 H3K27me3
Δdim-8 H3K27me3
Δdim-2 (N1850) H3K27me3
Δdim-2 (N1851) H3K27me3
genes

**Fig. 23 (see pages 113-116). Three kilobase sequences are not sufficient to trigger *de novo* H3K27me3 at either *his-3* or *csr-1*.** (A) ChIP-seq analysis of H3K27me3 (blue track), H3K9me3 (inverted green track) and H3K4me3 (black track) are displayed above predicted genes (purple track) on LG VI. The black horizontal bar below the predicted genes has been expanded in (B). (B) Eight regions of DNA, labeled "1" through "8," normally marked by H3K27me3 and 3 kb in length, were separately moved to both the *his-3* and *csr-1*. In separate strains, a 12 kb region labeled "9" and a 10 kb region labeled "10" were ectopically integrated. Gray rectangles within each of the fragments indicate the location of primer pairs used in qChIP experiments and are labeled "P1" through "P14." qChIP experiments indicate the absence of ectopic H3K27me3 in strains containing regions 1 through 8, each separately targeted to (C) *his-3* and (D) *csr-1*. (E) The induction of *de novo* H3K27me3 was observed in a strain containing one copy of "9" that has been randomly ectopically targeted. In all qChIP experiments, H3K27me3 enrichment within each of the fragments was normalized to enrichment at sub-telomere IL.

Fig. 23

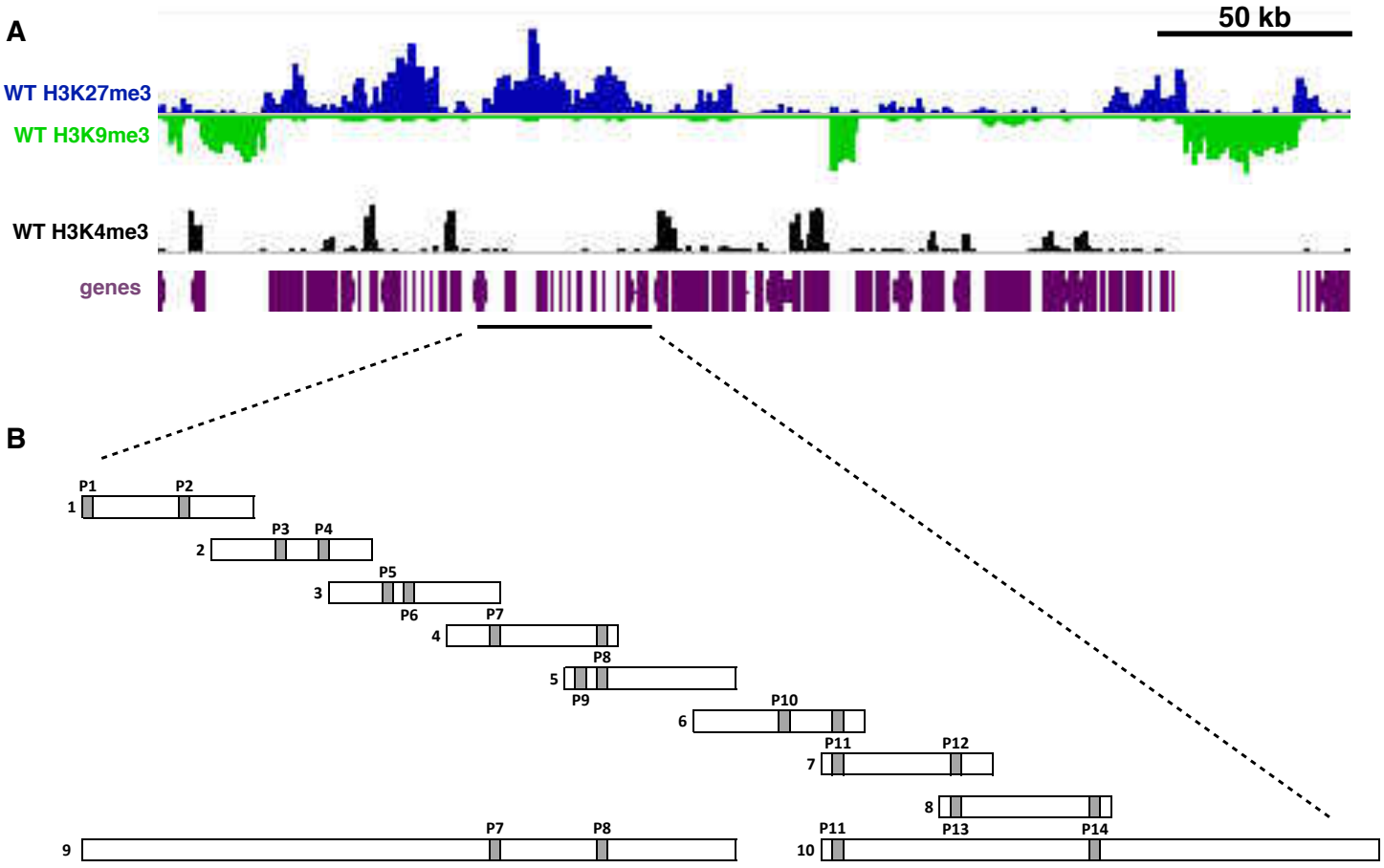
A
50 kb
WT H3K27me3
WT H3K9me3
WT H3K4me3
genes
B
P1
P2
1
P3
P4
2
P5
P6
3
P7
4
P8
P9
5
P10
6
P11
P12
7
8
P7
P8
9
P11
P13
P14
10

**Fig. 23**

**C**

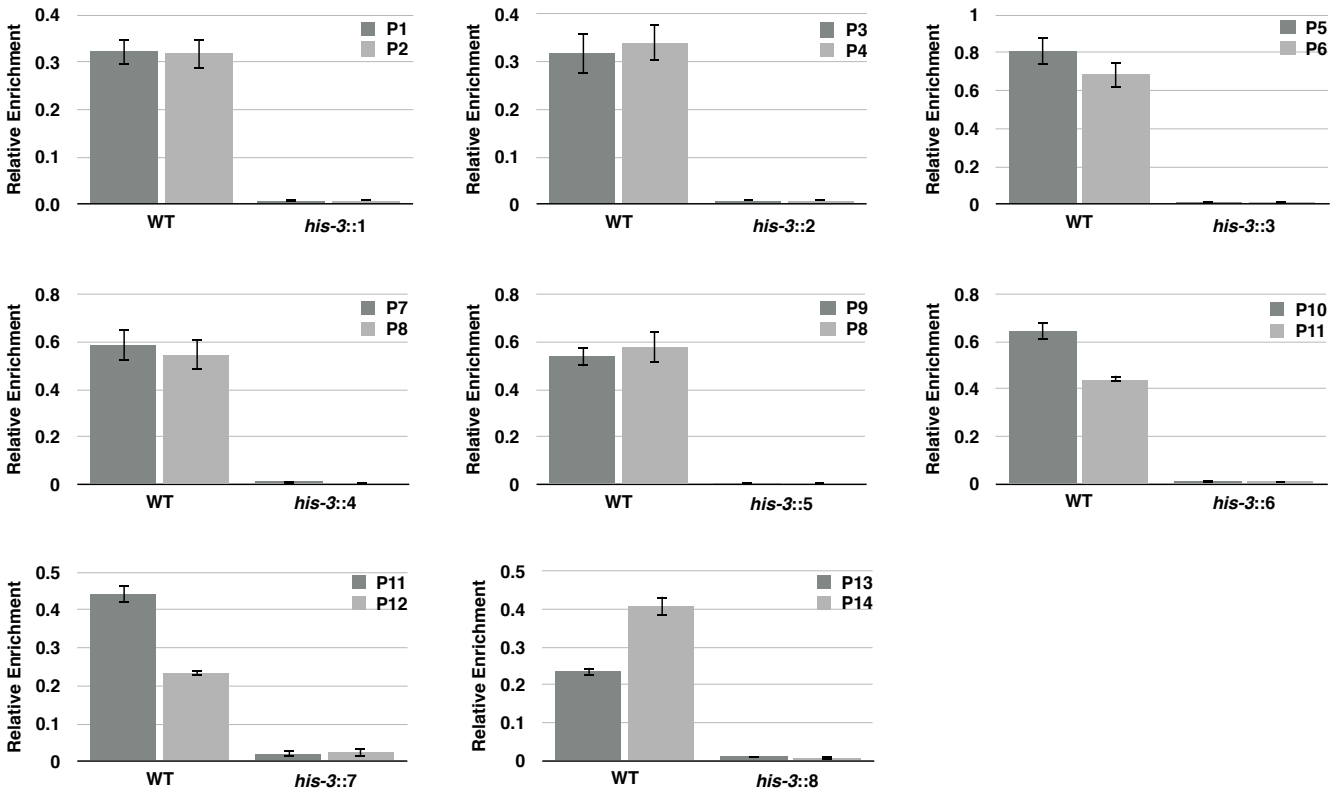
Relative Enrichment
P1
P2
WT
his-3::1
P3
P4
his-3::2
P5
P6
his-3::3
P7
P8
his-3::4
P9
P8
his-3::5
P10
P11
his-3::6
P11
P12
his-3::7
P13
P14
his-3::8

**Fig. 23**

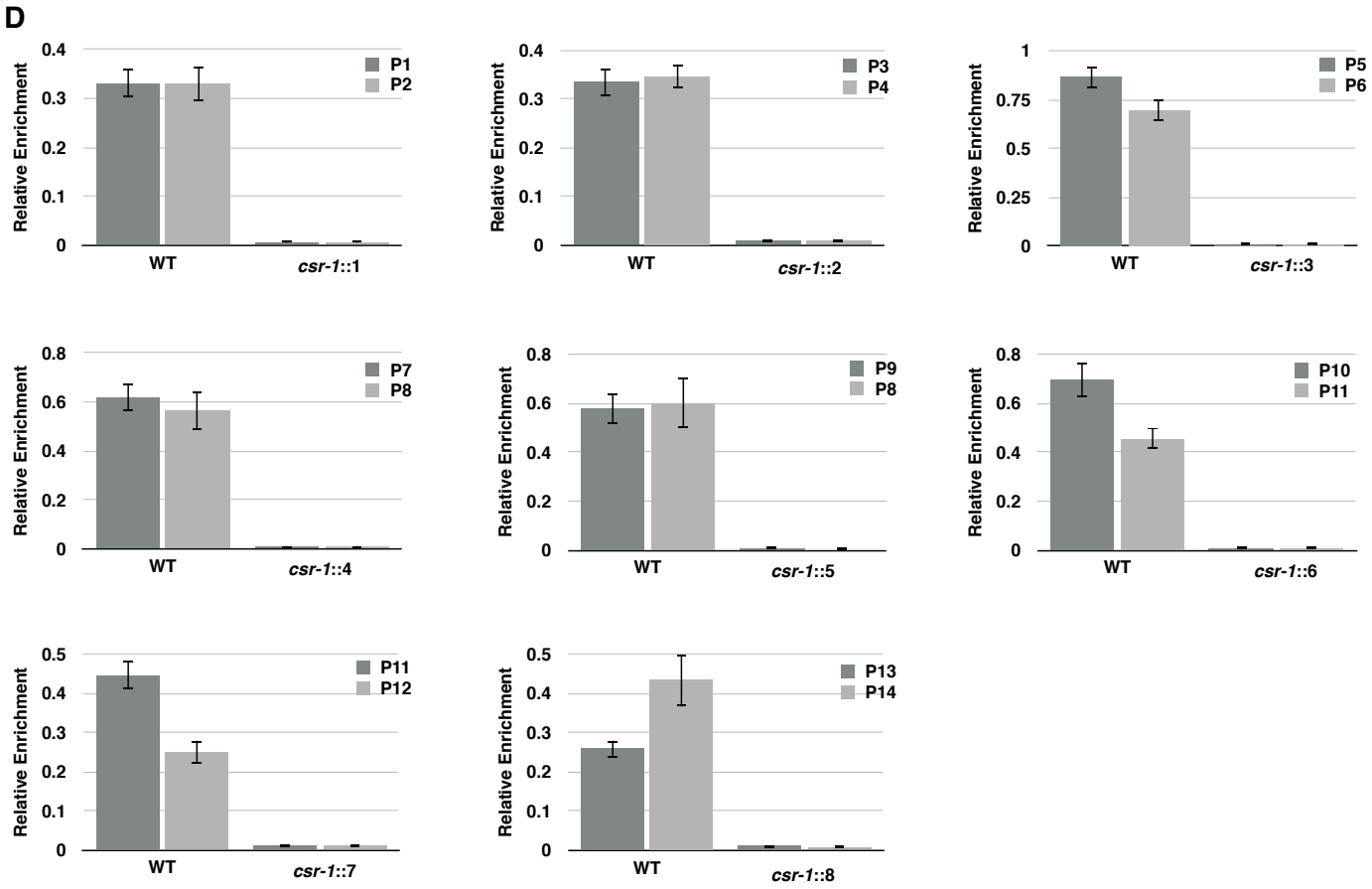
D
Relative Enrichment
P1
P2
WT
csr-1::1
P3
P4
csr-1::2
P5
P6
csr-1::3
P7
P8
csr-1::4
P9
P8
csr-1::5
P10
P11
csr-1::6
P11
P12
csr-1::7
P13
P14
csr-1::8

**Fig. 23**

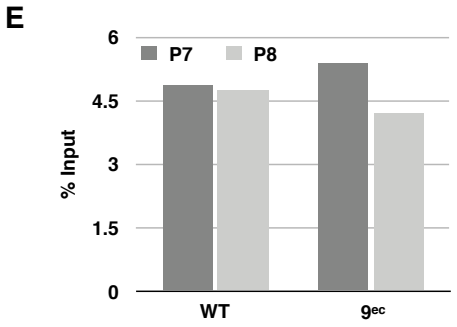

**Fig. 24 (see pages 118-123). A series of deletions within a 47.4 kb H3K27me3 domain in an effort to determine a sequence element required for H3K27me3.** (A) For reference, the distributions of H3K27me3 (blue track), H3K9me3 (inverted green track), H3K4me3 (black track) and predicted genes (purple rectangles) are displayed. (B) Fourteen strains, each containing a deletion of a portion of a 47.4 kb H3K27me3 region (shown in black) and simultaneously replaced with *hph*; intact sequence is indicated by the dashed black line in (A) located below the predicted genes. A strain containing an insertion of *hph* (labeled "Insertion") is used as a control to show that the insertion of *hph* is not sufficient to disrupt H3K27me3. The size of each deletion and its corresponding strain number are listed to the right of each strain. Rectangles located above the deletion strains indicate the locations of primer pairs for qChIP experiments. Blue, white and red rectangles superimposed over each deletion strain indicate the extent to which each deletion has disrupted H3K27me3 enrichment at each primer pair by qChIP (see key on the left). The reduction of H3K27me3 enrichment within each deletion relative to a wild-type strain at each primer pair is indicated as a percentage to the right of the each primer pair. (C) qChIP experiments to determine the extent to which H3K27me3 has been disrupted. Between one and three biological ChIP replicates were performed. Where available, error bars indicate the standard deviation within biological replicates. For all qChIP, H3K27me3 enrichment at locations proximal to the deletion was normalized to enrichment at sub-telomere IL.

Fig. 24

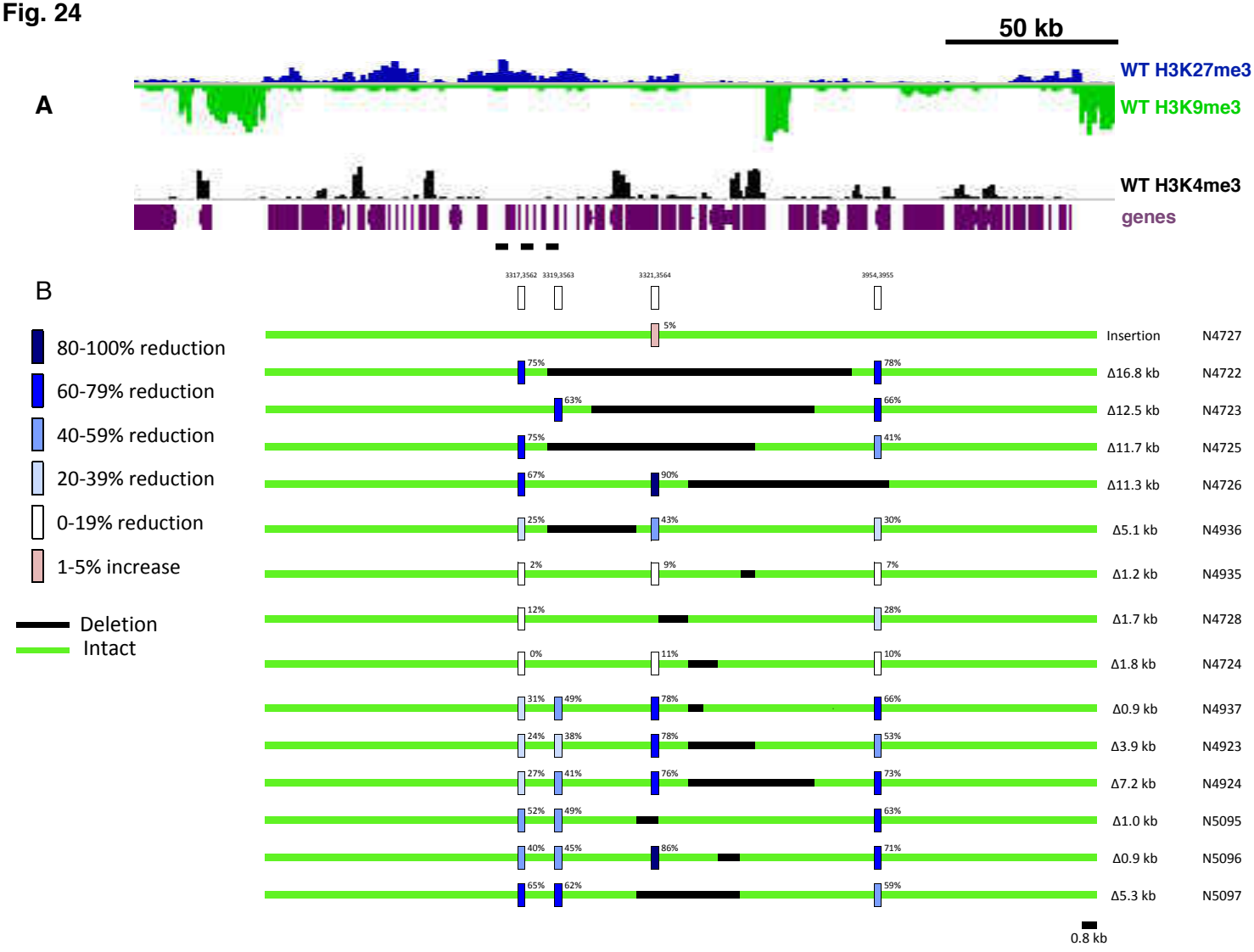
A
50 kb
WT H3K27me3
WT H3K9me3
WT H3K4me3
genes
B
80-100% reduction
60-79% reduction
40-59% reduction
20-39% reduction
0-19% reduction
1-5% increase
Deletion
Intact
3317,3562
3319,3563
3321,3564
3954,3955
Insertion N4727
Δ16.8 kb N4722
Δ12.5 kb N4723
Δ11.7 kb N4725
Δ11.3 kb N4726
Δ5.1 kb N4936
Δ1.2 kb N4935
Δ1.7 kb N4728
Δ1.8 kb N4724
Δ0.9 kb N4937
Δ3.9 kb N4923
Δ7.2 kb N4924
Δ1.0 kb N5095
Δ0.9 kb N5096
Δ5.3 kb N5097
0.8 kb

**Fig. 24 C**

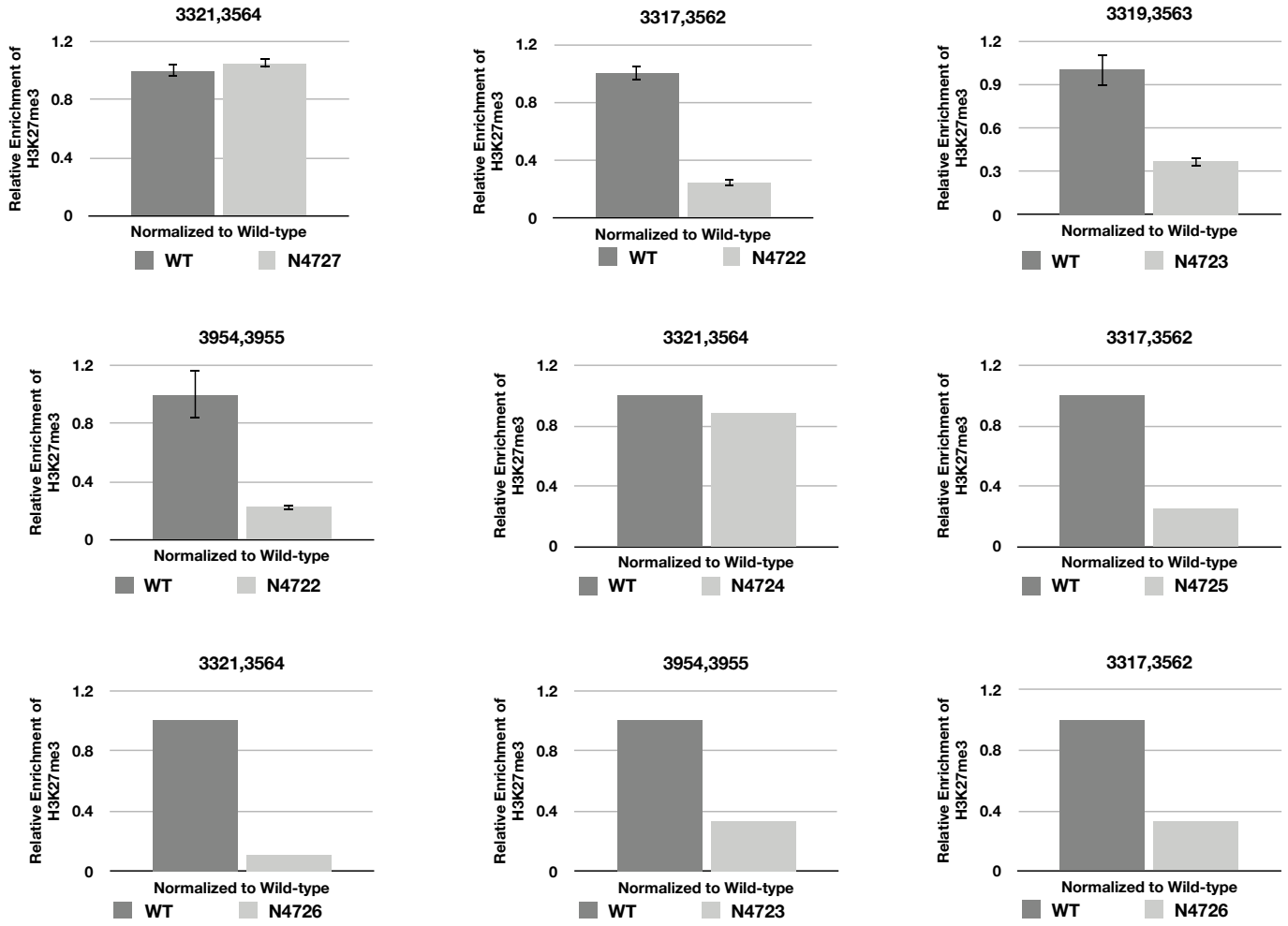
3321,3564
Relative Enrichment of H3K27me3
1.2
0.8
0.4
0
Normalized to Wild-type
WT
N4727
3317,3562
Relative Enrichment of H3K27me3
1.2
0.8
0.4
0
Normalized to Wild-type
WT
N4722
3319,3563
Relative Enrichment of H3K27me3
1.2
0.9
0.6
0.3
0
Normalized to Wild-type
WT
N4723
3954,3955
Relative Enrichment of H3K27me3
1.2
0.8
0.4
0
Normalized to Wild-type
WT
N4722
3321,3564
Relative Enrichment of H3K27me3
1.2
0.8
0.4
0
Normalized to Wild-type
WT
N4724
3317,3562
Relative Enrichment of H3K27me3
1.2
0.8
0.4
0
Normalized to Wild-type
WT
N4725
3321,3564
Relative Enrichment of H3K27me3
1.2
0.8
0.4
0
Normalized to Wild-type
WT
N4726
3954,3955
Relative Enrichment of H3K27me3
1.2
0.8
0.4
0
Normalized to Wild-type
WT
N4723
3317,3562
Relative Enrichment of H3K27me3
1.2
0.8
0.4
0
Normalized to Wild-type
WT
N4726

**Fig. 24 C**

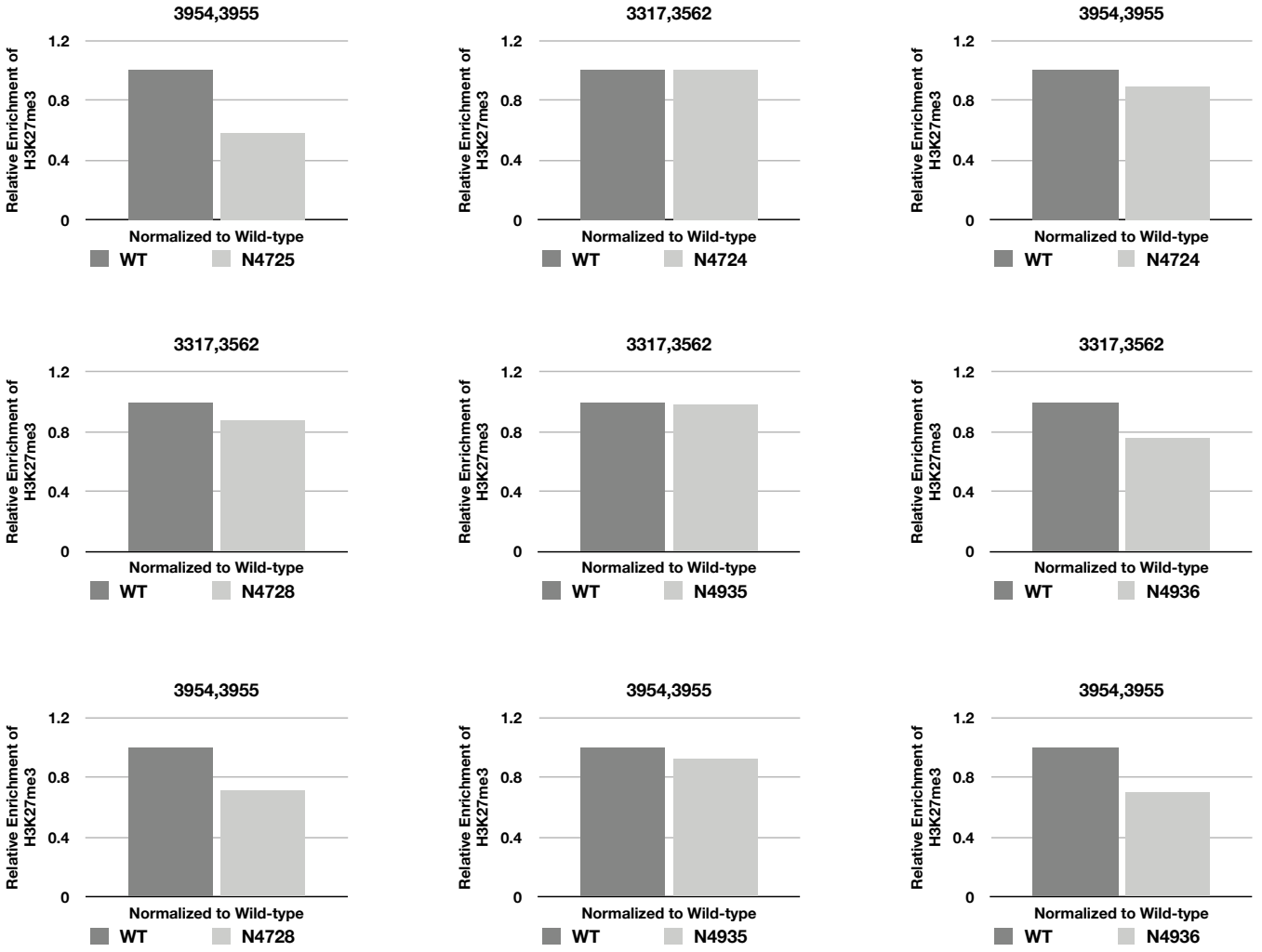
3954,3955
Relative Enrichment of H3K27me3
1.2
0.8
0.4
0
Normalized to Wild-type
WT
N4725
3317,3562
Relative Enrichment of H3K27me3
1.2
0.8
0.4
0
Normalized to Wild-type
WT
N4724
3954,3955
Relative Enrichment of H3K27me3
1.2
0.8
0.4
0
Normalized to Wild-type
WT
N4724
3317,3562
Relative Enrichment of H3K27me3
1.2
0.8
0.4
0
Normalized to Wild-type
WT
N4728
3317,3562
Relative Enrichment of H3K27me3
1.2
0.8
0.4
0
Normalized to Wild-type
WT
N4935
3317,3562
Relative Enrichment of H3K27me3
1.2
0.8
0.4
0
Normalized to Wild-type
WT
N4936
3954,3955
Relative Enrichment of H3K27me3
1.2
0.8
0.4
0
Normalized to Wild-type
WT
N4728
3954,3955
Relative Enrichment of H3K27me3
1.2
0.8
0.4
0
Normalized to Wild-type
WT
N4935
3954,3955
Relative Enrichment of H3K27me3
1.2
0.8
0.4
0
Normalized to Wild-type
WT
N4936

**Fig. 24 C**

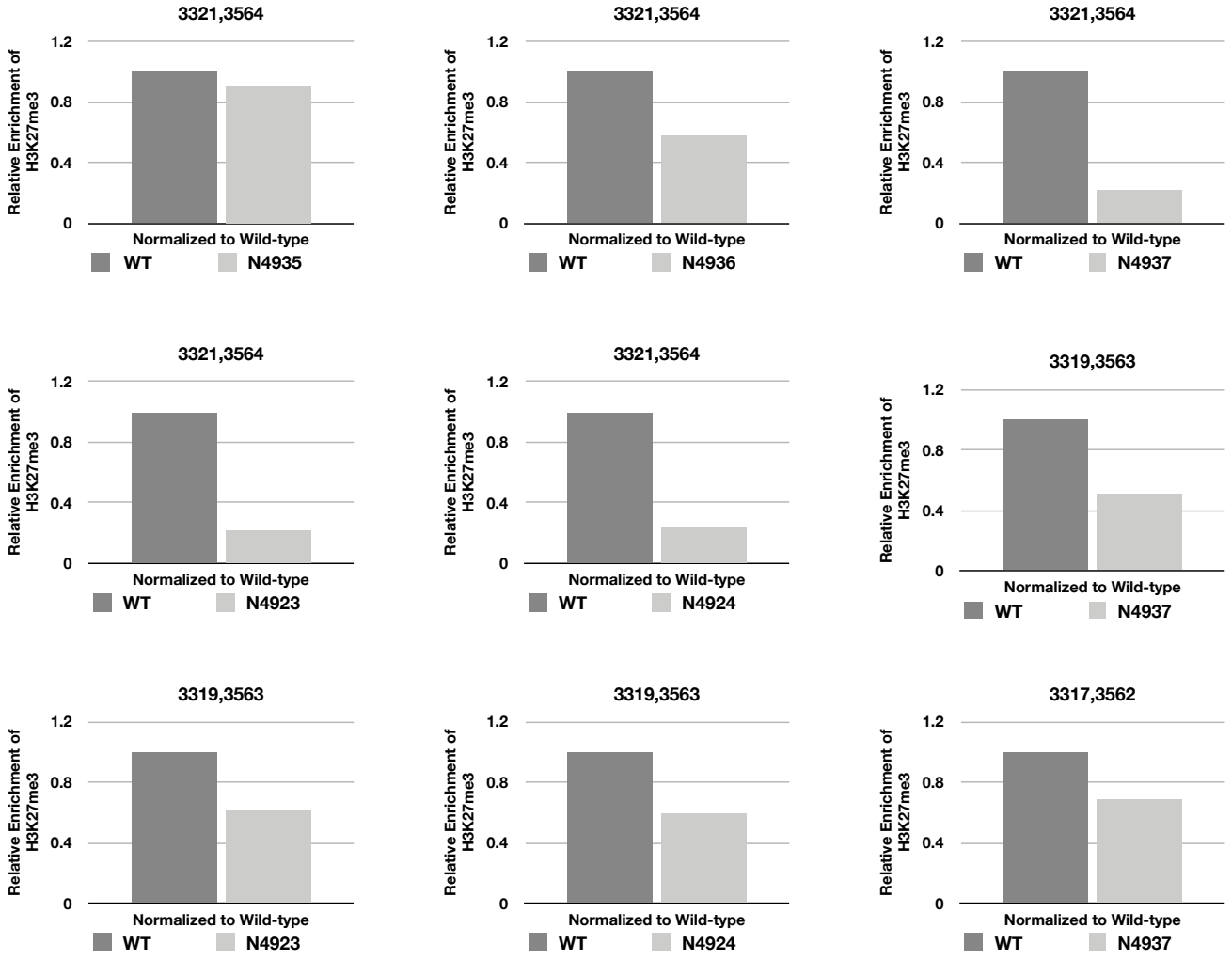
3321,3564
Relative Enrichment of H3K27me3
1.2
0.8
0.4
0
Normalized to Wild-type
WT
N4935
3321,3564
Relative Enrichment of H3K27me3
1.2
0.8
0.4
0
Normalized to Wild-type
WT
N4936
3321,3564
Relative Enrichment of H3K27me3
1.2
0.8
0.4
0
Normalized to Wild-type
WT
N4937
3321,3564
Relative Enrichment of H3K27me3
1.2
0.8
0.4
0
Normalized to Wild-type
WT
N4923
3321,3564
Relative Enrichment of H3K27me3
1.2
0.8
0.4
0
Normalized to Wild-type
WT
N4924
3319,3563
Relative Enrichment of H3K27me3
1.2
0.8
0.4
0
Normalized to Wild-type
WT
N4937
3319,3563
Relative Enrichment of H3K27me3
1.2
0.8
0.4
0
Normalized to Wild-type
WT
N4923
3319,3563
Relative Enrichment of H3K27me3
1.2
0.8
0.4
0
Normalized to Wild-type
WT
N4924
3317,3562
Relative Enrichment of H3K27me3
1.2
0.8
0.4
0
Normalized to Wild-type
WT
N4937

**Fig. 24 C**

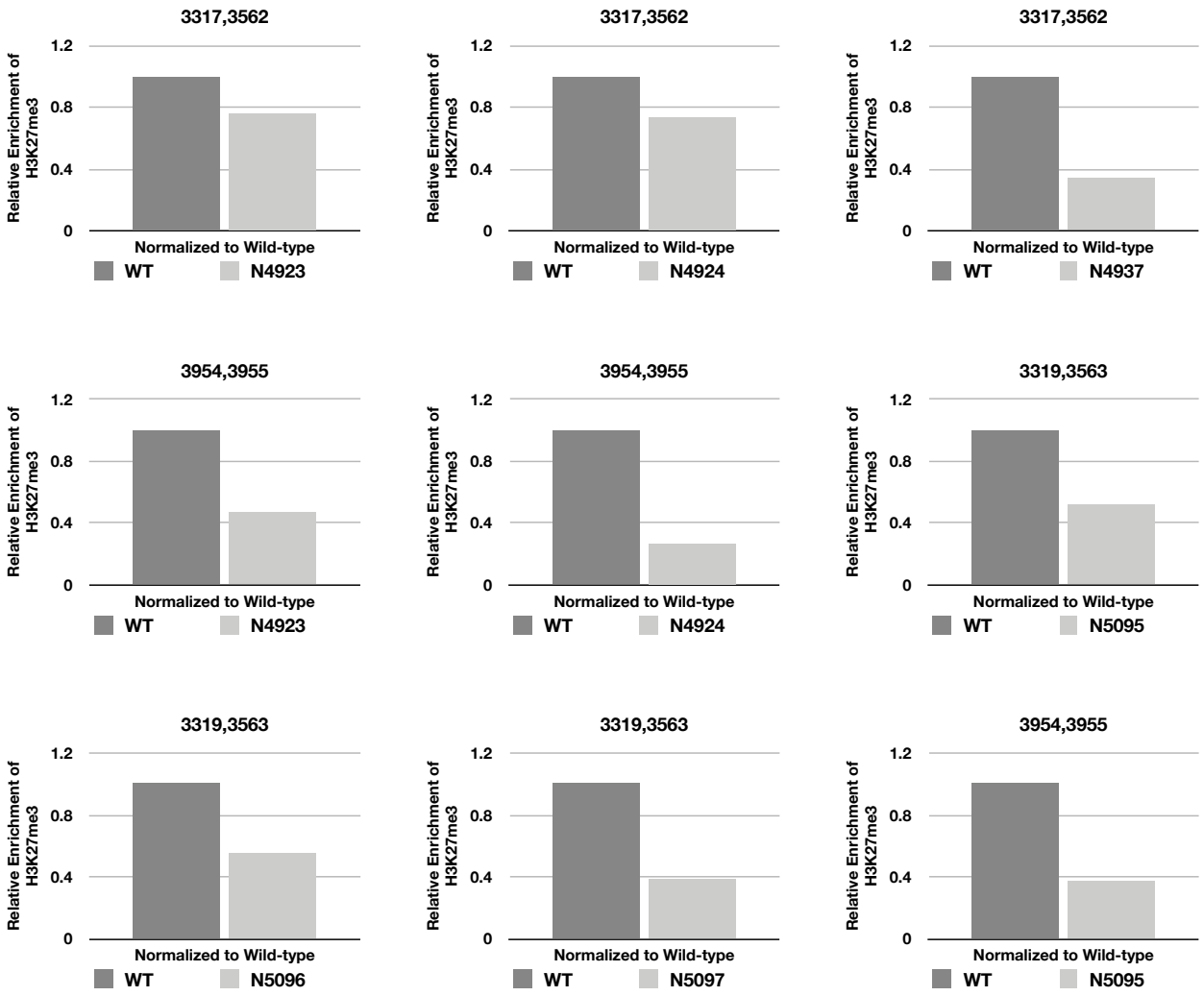
3317,3562
Relative Enrichment of H3K27me3
1.2
0.8
0.4
0
Normalized to Wild-type
WT
N4923
3317,3562
Relative Enrichment of H3K27me3
1.2
0.8
0.4
0
Normalized to Wild-type
WT
N4924
3317,3562
Relative Enrichment of H3K27me3
1.2
0.8
0.4
0
Normalized to Wild-type
WT
N4937
3954,3955
Relative Enrichment of H3K27me3
1.2
0.8
0.4
0
Normalized to Wild-type
WT
N4923
3954,3955
Relative Enrichment of H3K27me3
1.2
0.8
0.4
0
Normalized to Wild-type
WT
N4924
3319,3563
Relative Enrichment of H3K27me3
1.2
0.8
0.4
0
Normalized to Wild-type
WT
N5095
3319,3563
Relative Enrichment of H3K27me3
1.2
0.8
0.4
0
Normalized to Wild-type
WT
N5096
3319,3563
Relative Enrichment of H3K27me3
1.2
0.8
0.4
0
Normalized to Wild-type
WT
N5097
3954,3955
Relative Enrichment of H3K27me3
1.2
0.8
0.4
0
Normalized to Wild-type
WT
N5095

**Fig. 24 C**

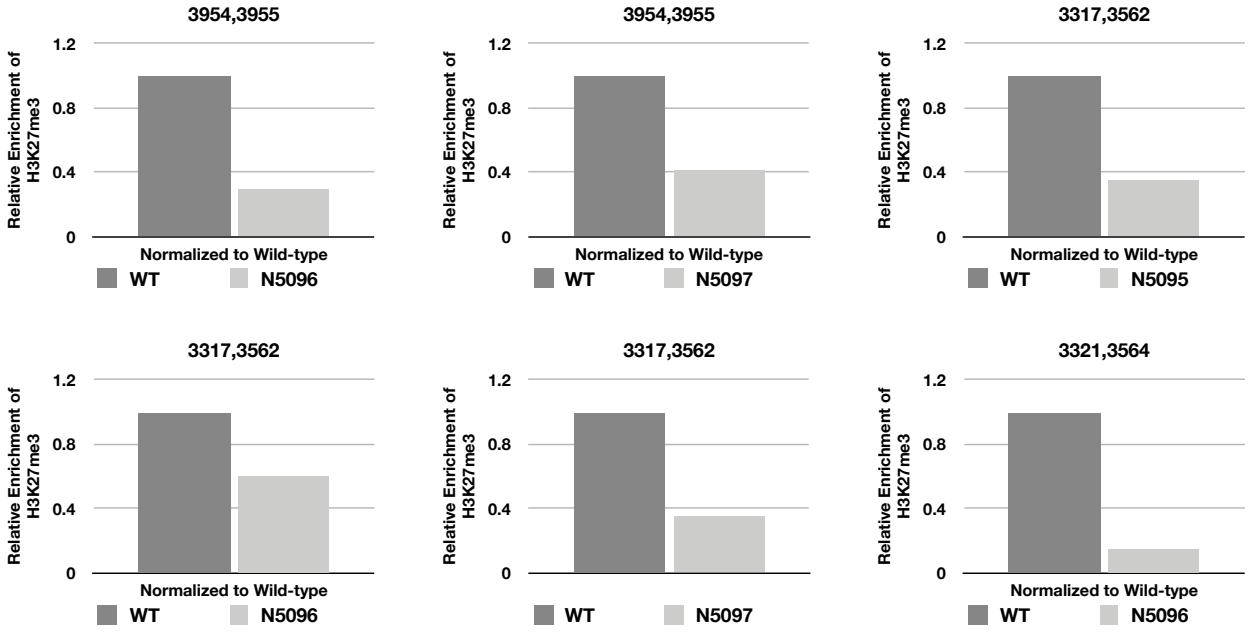
3954,3955
Relative Enrichment of H3K27me3
1.2
0.8
0.4
0
Normalized to Wild-type
WT
N5096
3954,3955
Relative Enrichment of H3K27me3
1.2
0.8
0.4
0
Normalized to Wild-type
WT
N5097
3317,3562
Relative Enrichment of H3K27me3
1.2
0.8
0.4
0
Normalized to Wild-type
WT
N5095
3317,3562
Relative Enrichment of H3K27me3
1.2
0.8
0.4
0
Normalized to Wild-type
WT
N5096
3317,3562
Relative Enrichment of H3K27me3
1.2
0.8
0.4
0
Normalized to Wild-type
WT
N5097
3321,3564
Relative Enrichment of H3K27me3
1.2
0.8
0.4
0
Normalized to Wild-type
WT
N5096

**Fig. 25 (see next page). A pericentric inversion alters the distribution of H3K27me3.** The AR16 strain contains a pericentric inversion in which a distal segment of LG IL is interchanged with LG IR. (A) The blue track indicates H3K27me3 ChIP-seq analysis in a wild-type strain and purple boxes indicate the locations of predicted genes. Each black dashed line indicates the location of the interchanged segments on LG IL and IR. (B) and (C) Expansions of LG IL and IR, respectively, where the distributions of H3K27me3 (blue track) and H3K9me3 (inverted green track) in a wild-type strain and the distribution of H3K27me3 in AR16 (black track). Below, rectangles indicate predicted genes. (B) H3K27me3 ChIP-seq analysis shows a novel H3K27me3 domain in AR16 upstream of the breakpoint on LG IL relative to a wild-type strain. (C) H3K27me3 ChIP-seq analysis shows the absence of an H3K27me3 domain on LG IR in the AR16 strain relative to a wild-type strain

Fig. 25

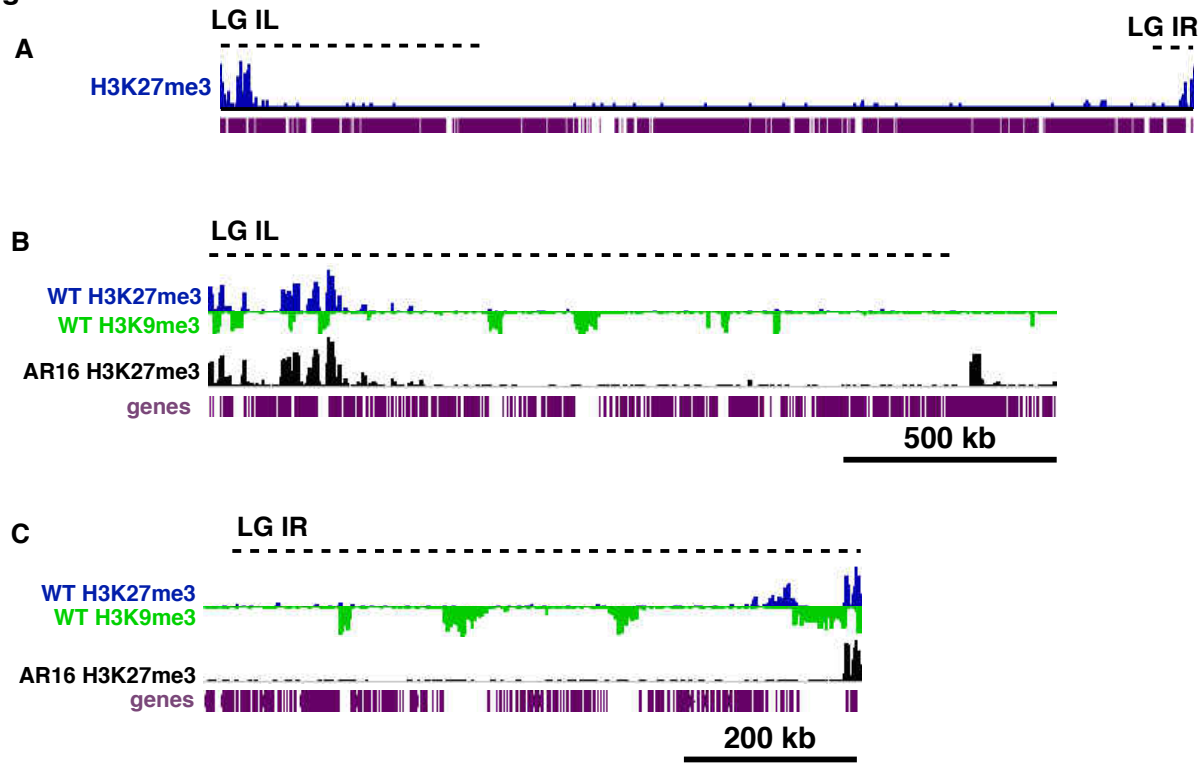
A
LG IL
LG IR
H3K27me3
B
LG IL
WT H3K27me3
WT H3K9me3
AR16 H3K27me3
genes
500 kb
C
LG IR
WT H3K27me3
WT H3K9me3
AR16 H3K27me3
genes
200 kb

**Fig. 26 (see next page). An insertional translocation alters the distribution of H3K27me3.** The OY329 strain contains an insertional translocation in which a segment of LG VIR (about 560 kb, indicated by the black bar below LG VI) is inserted into LG IIIR (the location of the insertion is indicated by a black dashed line). (A) The blue track represents H3K27me3 ChIP-seq analysis in a wild-type strain and relevant genetic markers are indicated below the tracks. (B) Expansion of region indicated by the dashed black line in (A). The distributions of H3K27me3 (blue track) and H3K9me3 (green track) in a wild-type strain are displayed above the distribution of H3K27me3 in OY329 (black track). Predicted genes are represented by purple rectangles. H3K27me3 domains proximal to the telomere in a wild-type strain are absent in OY329, while H3K27me3 domains in OY329 upstream of the translocation breakpoint are absent in a wild-type strain.

Fig. 26

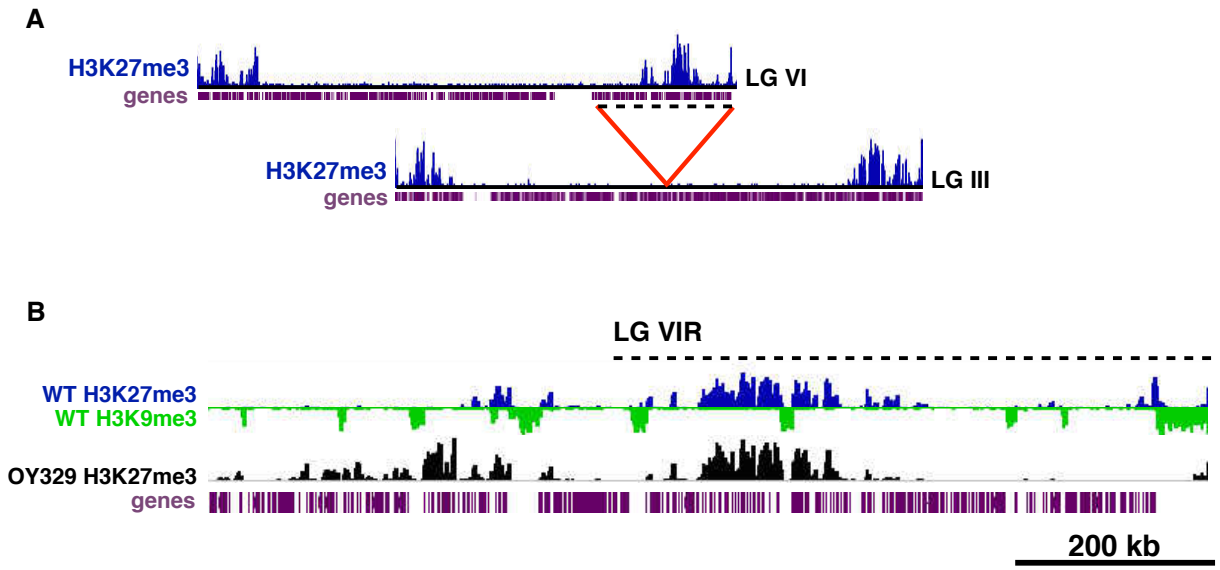
A
H3K27me3
genes
LG VI
H3K27me3
genes
LG III
B
LG VIR
WT H3K27me3
WT H3K9me3
OY329 H3K27me3
genes
200 kb

**Fig. 27. Occasional spreading of H3K27me3 into *hph*.**

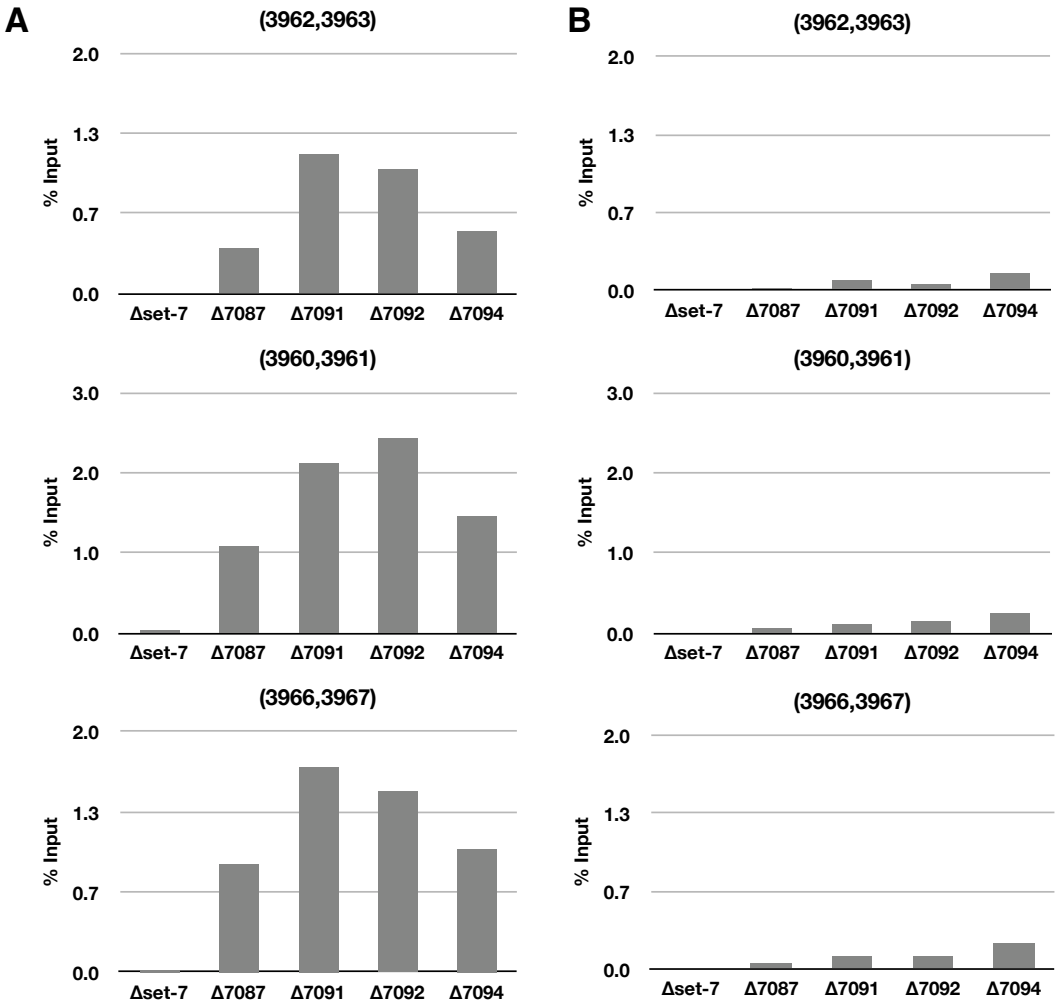

## Figures for Chapter IV

**Fig. 28 (see pages 130-131). Strains containing epitope tags of HDA-3S/L subunits exhibit growth defects.** Strains were grown for ten days at 32 °C on solid Vogel's medium with 1.5% sucrose.

**Fig. 28**

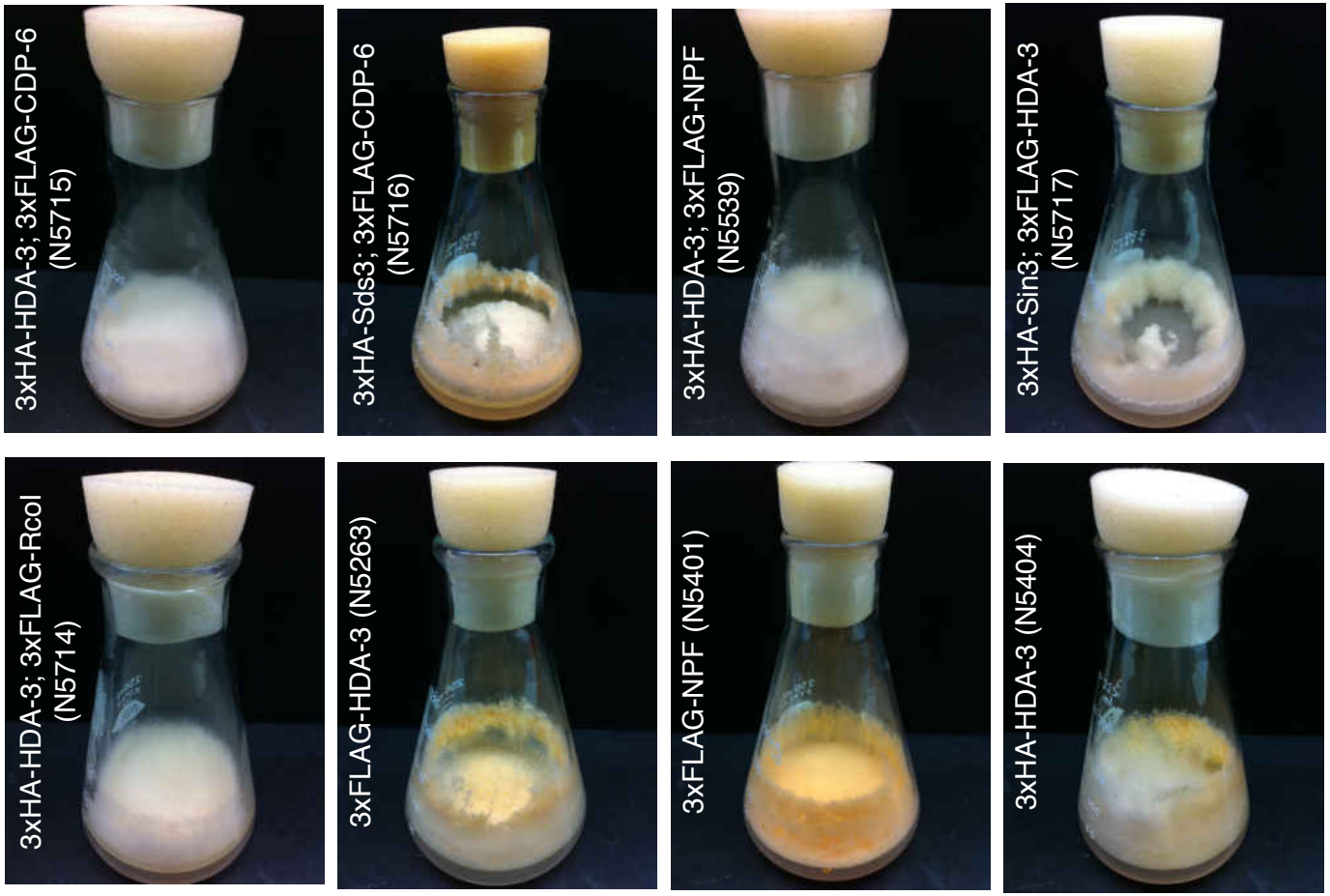
3xHA-HDA-3; 3xFLAG-CDP-6 (N5715)
3xHA-Sds3; 3xFLAG-CDP-6 (N5716)
3xHA-HDA-3; 3xFLAG-NPF (N5539)
3xHA-Sin3; 3xFLAG-HDA-3 (N5717)
3xHA-HDA-3; 3xFLAG-Rcol (N5714)
3xFLAG-HDA-3 (N5263)
3xFLAG-NPF (N5401)
3xHA-HDA-3 (N5404)

**Fig. 28**


3xHA-Sin3 (N5453)
3xFLAG-Rcol (N5454)
3xFLAG-CDP-6 (N5455)
3xHA-Sds3 (N5457)

**Fig. 29 (see pages 133-138). Multiple alignments of HDA-3-containing complex members in *Neurospora*.** The protein sequence for *N. crassa* HDA-3S and HDA-3L subunits was aligned to corresponding homologs using ClustalWS. (A) Alignment of *N. crassa* HDA-3 with homologs. ClustalWS alignments from *N. crassa* (XP_964367.1), *S. cerevisiae* (NP_014069.1), *S. pombe* (NP_595333.1), *M. musculus* (NP_032255.2), *D. rerio* (NP_775343.1), *C. elegans* (NP_506599.1), *D. melanogaster* (NP_647918.2), *A. thaliana* (NP_190054.2). The HDAC domain (V1040 to L1173, E = 3.38e-29) is indicated by the black line. (B) Alignment of *N. crassa* Sin3 with homologs. ClustalWS alignments from *N. crassa* (XP_965709.2), *S. cerevisiae* (NP_014639.1), *S. pombe* (NP_595333.1), *M. musculus* (NP_035508.2), *D. rerio* (NP_001091650.1), *C. elegans* (CAB03984.1), *D. melanogaster* (NP_725189.1) and *A. thaliana* (AEE77930.1). Two PAH domains (P242-P288, 3e-16, and P457-P503, 9.4e-18) and a Sin3 domain (N720-H821, 5.9e-37) are indicated by the black lines. (C) Alignment of *N. crassa* Sds3 with homologs. *N. crassa* (XP_956510.2), *S. cerevisiae* (NP_012182.1), *S. pombe* (NP_594462.1), *M. musculus* (AAM22676.1) and *D. melanogaster* (NP_608325.1). An Sds-like domain (Q40-V438, E=1.2e-54) is indicated by the black line. (D) Alignment of *N. crassa* RcoI with homologs. *N. crassa* (XP_956687.1) and *S. cerevisiae* (NP_013791.1). Two PHD domains (Y898-R942, E=5.96e-12, and I1029-V1078, E=0.000246) are indicated by the black lines. (E) Alignment of *N. crassa* CDP-6 with homologs. *N. crassa* (XP_963629.2) and *S. cerevisiae* (NP_015348.1). The chromo domain (L25 to S87, E=0.000713) is indicated by the black line.

A

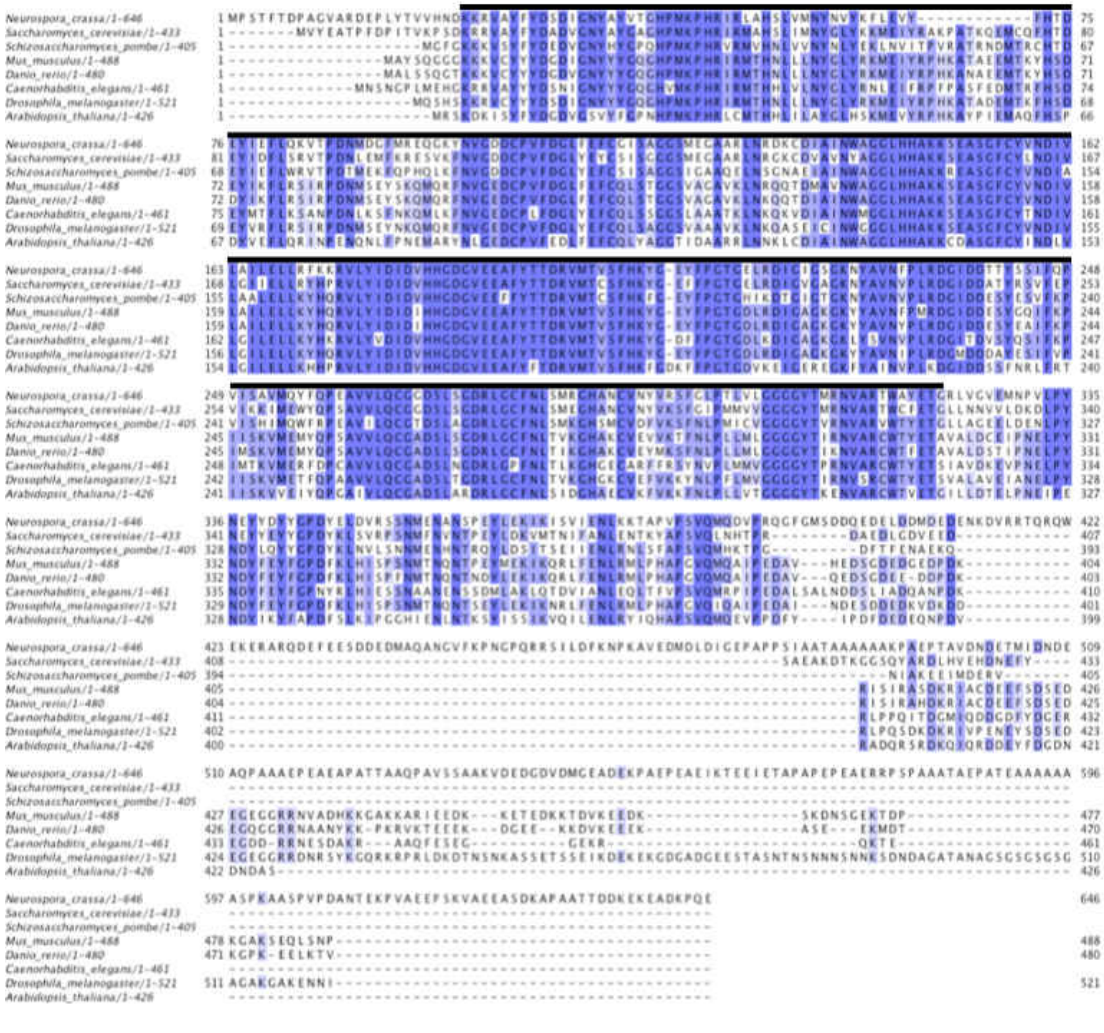
Neurospora_crassa/1-646
Saccharomyces_cerevisiae/1-433
Schizosaccharomyces_pombe/1-405
Mus_musculus/1-488
Danio_rerio/1-480
Caenorhabditis_elegans/1-461
Drosophila_melanogaster/1-521
Arabidopsis_thaliana/1-426

B


Neurospora_crassa/1-1486
Saccharomyces_cerevisiae/1-1536
Schizosaccharomyces_pombe/1-405
Mus_musculus/1-1274
Danio_rerio/1-1276
Caenorhabditis_elegans/1-461
Drosophila_melanogaster/1-1751
Arabidopsis_thaliana/1-426

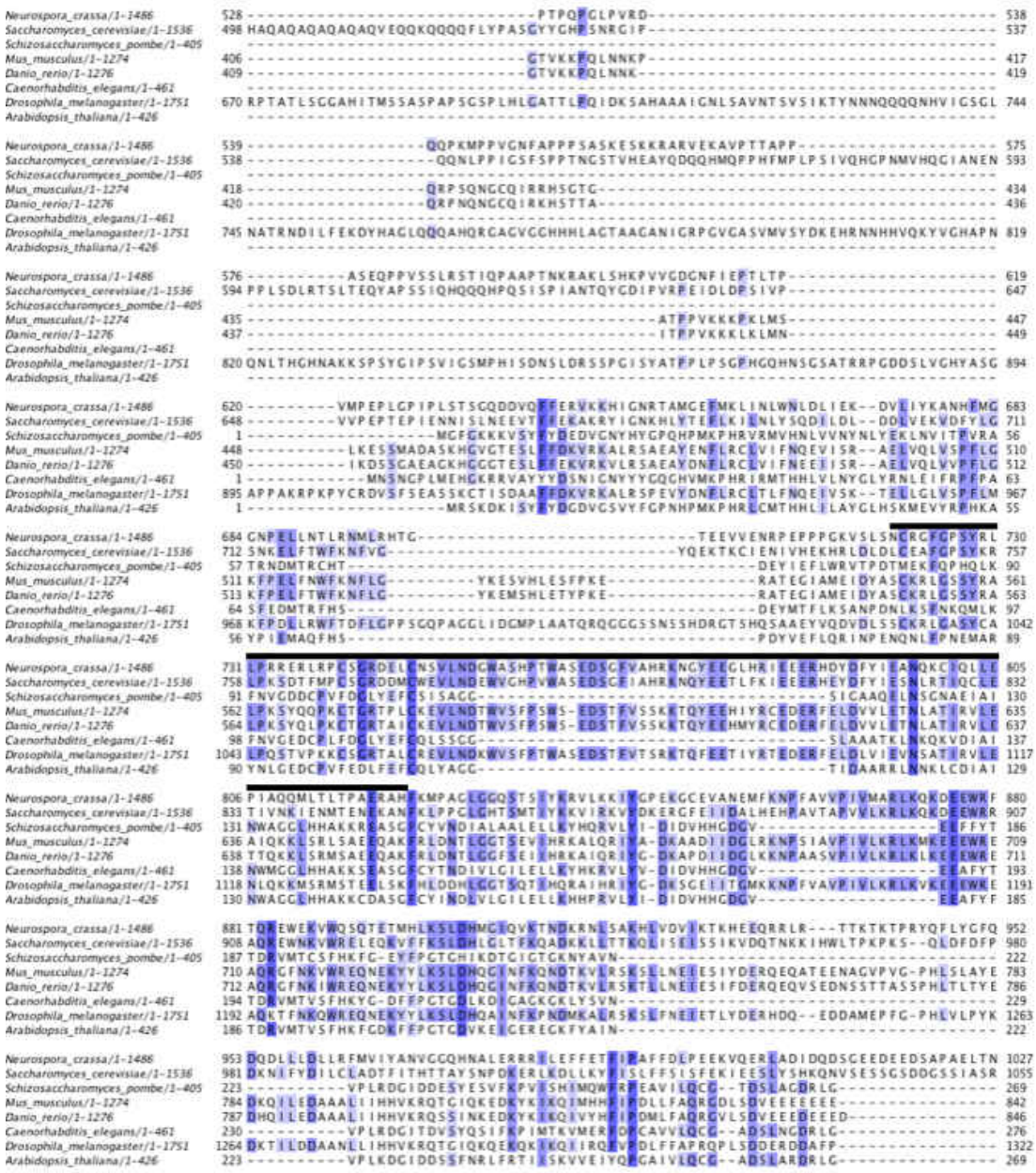
Neurospora_crassa/1-1486
Saccharomyces_cerevisiae/1-1536
Schizosaccharomyces_pombe/1-405
Mus_musculus/1-1274
Danio_rerio/1-1276
Caenorhabditis_elegans/1-461
Drosophila_melanogaster/1-1751
Arabidopsis_thaliana/1-426

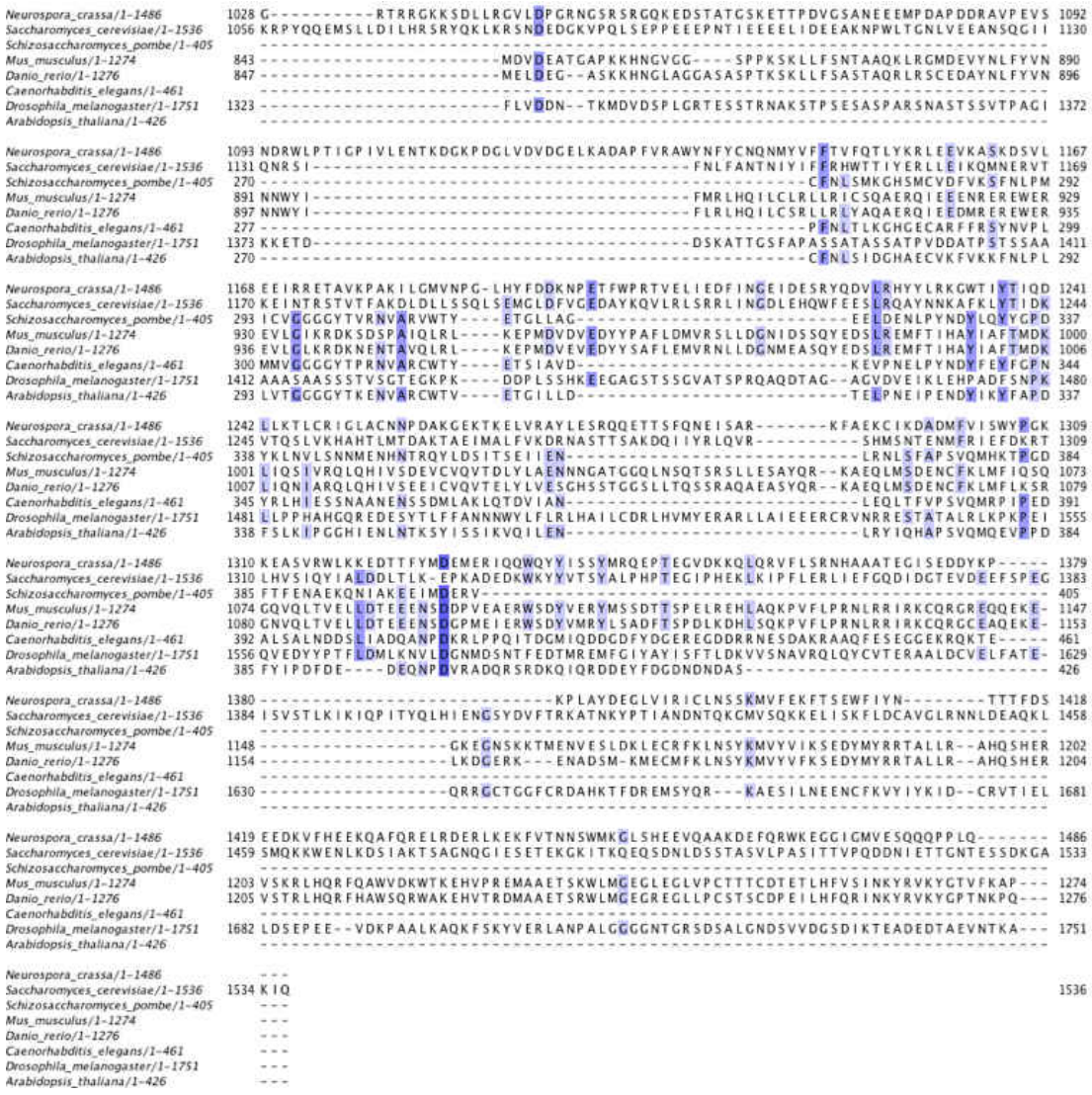
Neurospora_crassa/1-1486
Saccharomyces_cerevisiae/1-1536
Schizosaccharomyces_pombe/1-405
Mus_musculus/1-1274
Danio_rerio/1-1276
Caenorhabditis_elegans/1-461
Drosophila_melanogaster/1-1751
Arabidopsis_thaliana/1-426

C

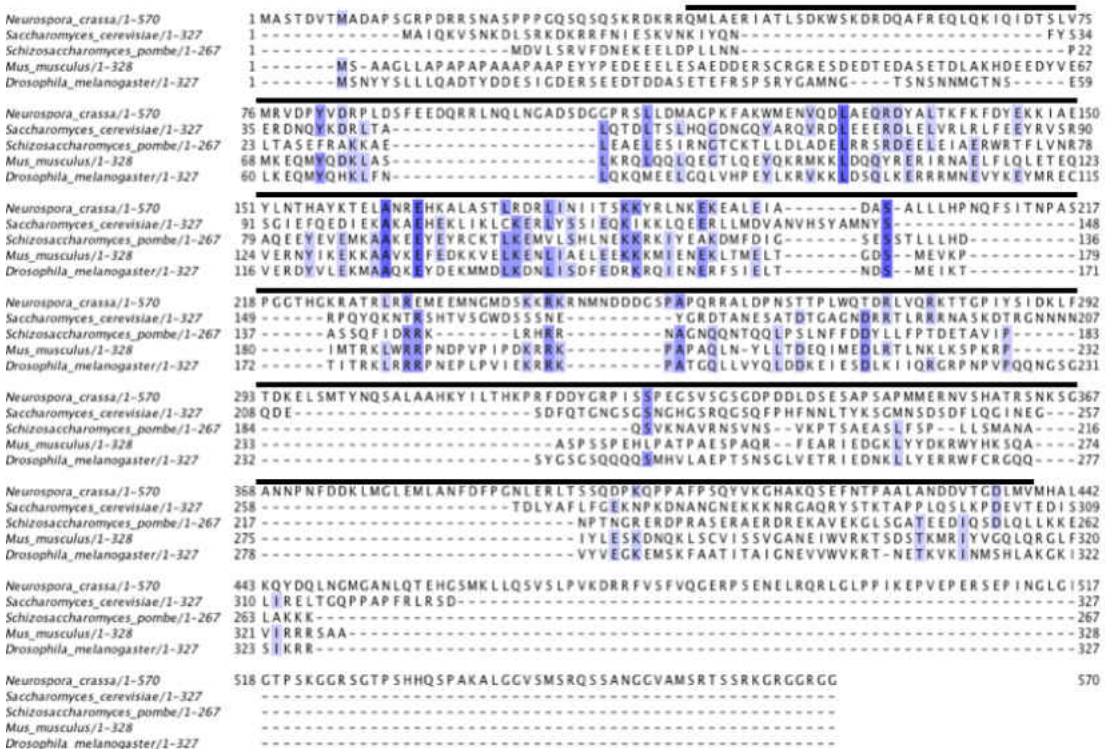
Neurospora_crassa/1-570
Saccharomyces_cerevisiae/1-327
Schizosaccharomyces_pombe/1-267
Mus_musculus/1-328
Drosophila_melanogaster/1-327

D

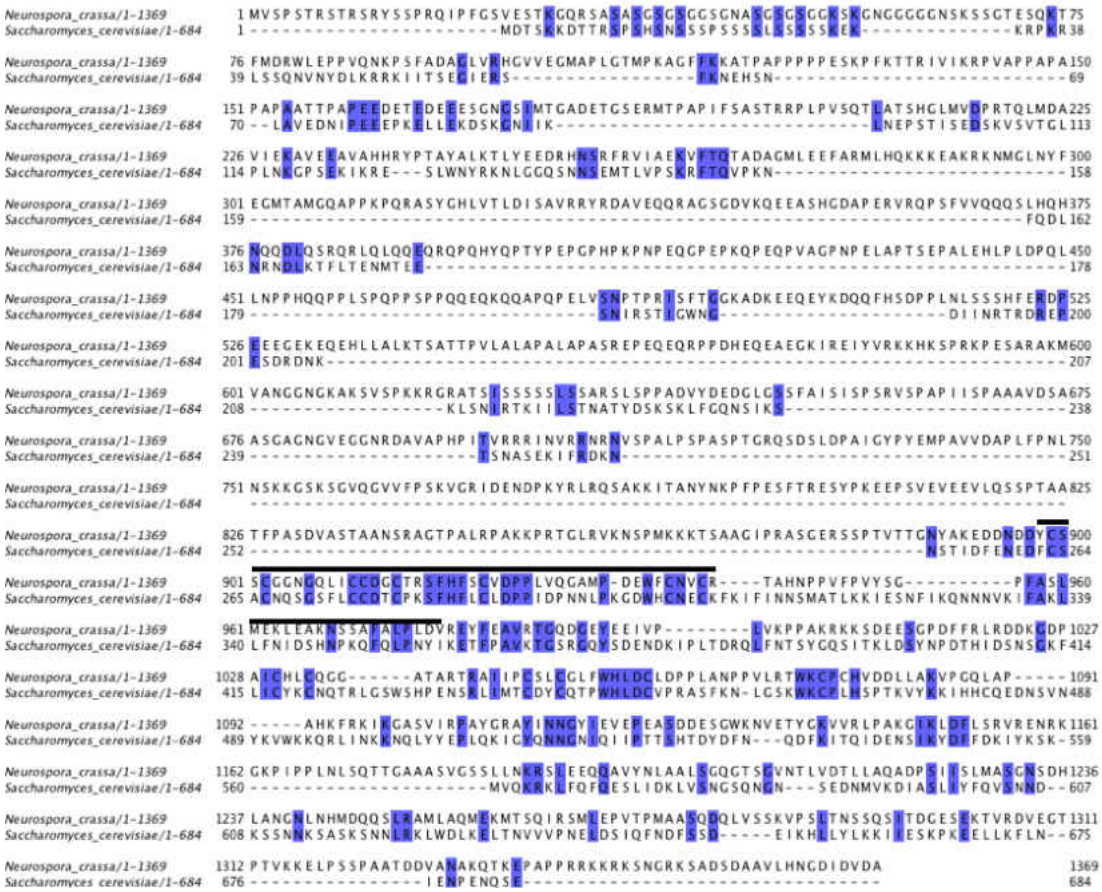
Neurospora_crassa/1-1369
Saccharomyces_cerevisiae/1-684

E


Neurospora_crassa/1-145
Saccharomyces_cerevisiae/1-401

**Fig. 30. Δ*npf*, Δ*sds3* and Δ*pho23* strains display a slower linear growth rate relative to a wild-type strain.**

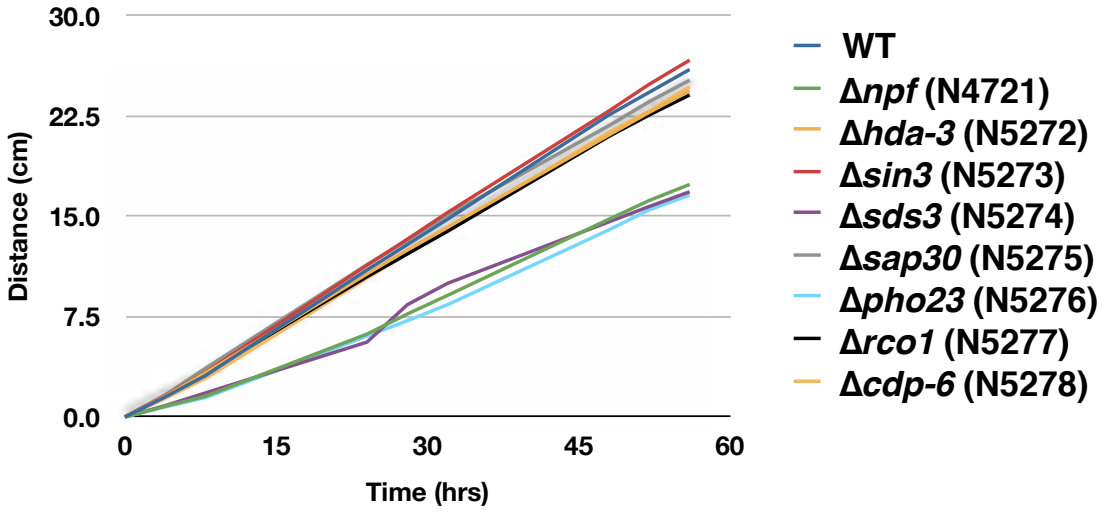

**Fig. 31. The interaction of HDA-3S subunits.** We confirmed the interactions between HDA-3 and the remaining members of the HDA-3S complex, with the exception of RcoI, which did not show strong expression.

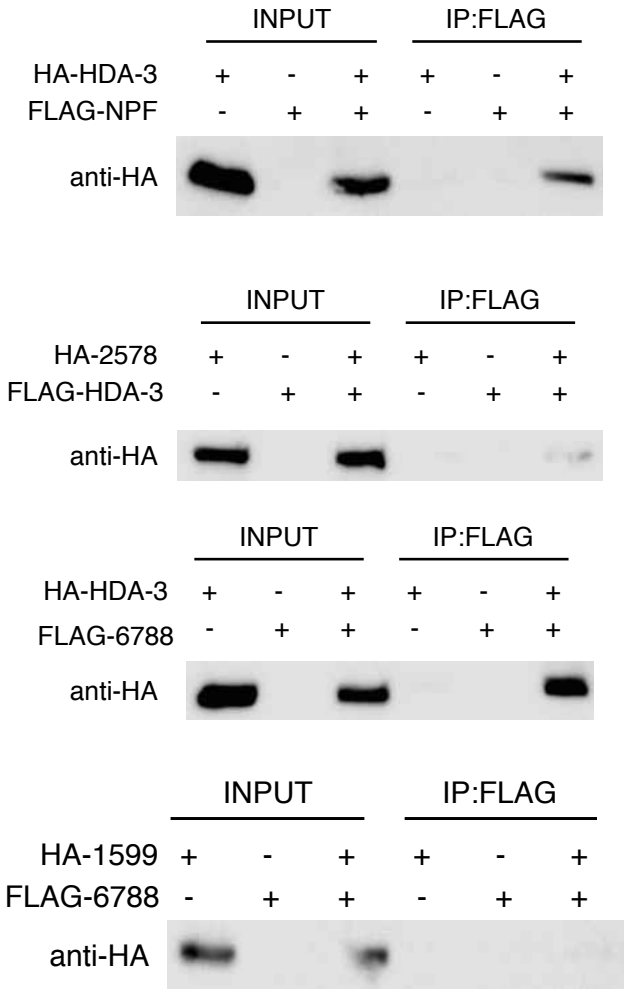

**Fig. 32. Absence of histone hyperacetylation in strains containing deletions of HDA-3S/L subunits.** Western blots of nuclear proteins were probed with the antibodies labeled to the left of each blot. H3K4me2 was used as a loading control.

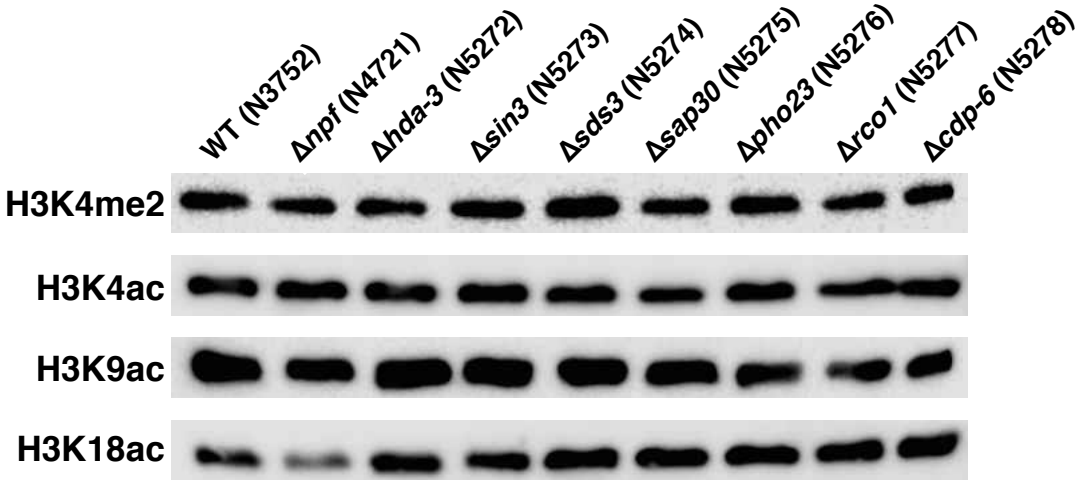

## APPENDIX B

## DATA TABLES

**Table 1. H3K27me3 domain analysis summary in *N. crassa***

| | H3K27me3 domains | Avg. Domain Size (kb) | Largest Domain (kb) | Total Genome Coverage (MB) | Genome Coverage (%) |
|---|---|---|---|---|---|
| WT (Bird's) | 223 | 12.5 | 107.0* | 2.8 | 6.8 |
| WT (Vogel's) | 232 | 12.1 | 107.5* | 2.8 | 6.8 |
| Δ*npf* (Vogel's) | 187 | 8.4 | 79.5* | 1.6 | 3.9 |

*The same domain on LG III. RSEG analysis carried out using a bin-size = 500 bp

**Table 2. H3K27me3 domain analysis in *Neurospora* species**

| Species | H3K27me3 domains | Avg. Domain Size (kb) | Largest Domain (kb) | Total Genome Coverage (MB) | Genome Coverage (%) | H3K27me3-marked Genes |
|---|---|---|---|---|---|---|
| *N. crassa* | 223 | 12.5 | 107.0 | 2.8 | 6.8 | 774 |
| *N. tetrasperma* | 167 | 10.8 | 101.5 | 1.8 | 4.6 | 536 |
| *N. discreta* | 186 | 14.1 | 94.5 | 2.6 | 7.1 | 822 |

RSEG analysis carried out using a bin-size = 500 bp

**Table 3. H3K27me3 status of *N. crassa* orthologs in *N. discreta* and *N. tetrasperma***

| *N. crassa* | *N. discreta* | *N. tetrasperma* | Gene Count |
|---|---|---|---|
| U | - | - | 242 |
| U | - | U | 413 |
| U | - | M | 5 |
| U | U | - | 123 |
| U | U | U | 7927 |
| U | U | M | 11 |
| U | M | - | 8 |
| U | M | U | 186 |
| U | M | M | 21 |
| M | - | - | 66 |
| M | - | U | 32 |
| M | - | M | 78 |
| M | U | - | 8 |
| M | U | U | 85 |
| M | U | M | 44 |
| M | M | - | 25 |
| M | M | U | 136 |
| M | M | M | 258 |

**Table 4. Purification of EED.** An *N. crassa* strain bearing 3xFLAG tagged EED at the amino-terminus and expressed under the *qa-2* promoter was used to purify the PRC2 complex. Associated proteins were identified by mass-spectrometry and the percent coverage of PRC2 members is indicated.

| | Molecular Weight (kDa) | Coverage (%) |
|---|---|---|
| SET-7 NCU07496 | 175.78 | 9 |
| EED NCU05300 | 67.23 | 66.4 |
| SUZ12 NCU05460 | 93.33 | 17.6 |
| NPF NCU06679 | 50.41 | 74 |

**Table 5. Purifications of HDA-3 and NPF.** Separate strains containing 3xFLAG-HDA-3 and 3xFLAG-NPF at the amino-terminus and expressed under the *qa-2* promoter were used to purify HDA-3S and HDA-3L. Associated proteins were identified by mass-spectrometry and the number of peptides and percent coverage for each protein is indicated.

| | Name of Subunit (*S. cerevisiae*) | NCU # (*N. crassa*) | Found in NPF purification # peptides, % coverage | Found in HDA-3 purification # peptides, % coverage |
|---|---|---|---|---|
| Shared core of proteins (both HDA-3S and HDA-3L) | Rpd3 | NCU00824 (HDA-3) | 82, 59 | 197, 66 |
| | Ume1 | NCU06679 (NPF) | 192, 74 | 94, 69 |
| | Sin3 | NCU02578 | 291, 51 | 301, 55 |
| Specific to HDA-3S | Rco1 | NCU00423 | 39, 25 | 85, 30 |
| | Eaf3 | NCU06788 (CDP-6) | 8, 31 | 21, 40 |
| Specific to HDA-3L | Sds3 | NCU01599 | 107, 64 | 58, 59 |
| | Sap30 | NCU05240 | 9, 23 | 10, 27 |
| | Pho23 | NCU03461 | 69, 42 | 55, 37 |
| | Rxt2 | NCU05979 | 36, 43 | 28, 31 |
| | Rxt3 | NCU08417 | 104, 30 | 87, 27 |
| | Cti6 | NCU02121 | 19, 19 | 18, 23 |
| | Dep1 | NCU09130 | 50, 28 | 37, 24 |

## APPENDIX C

## STRAIN TABLES

### Chapter II

All strains are *N. crassa*, except where noted.

| Strain | Genotype | Reference |
|---|---|---|
| N3752 | *mat A* | (82) |
| N3753 | *mat a* | (82) |
| N4718 | *mat a*; Δ*set-7::hph*$^+$ | (82) |
| N4719 | *mat A*; Δ*eed::hph*$^+$ | (82) |
| N4720 | *mat a*; Δ*su(z)12::hph*$^+$ | (82) |
| N4721 | *mat a*; Δ*npf::hph*$^+$ | (82) |
| N4879 | *mat a; loxp::*$P_{trpC}$*::hph*$^+$*::*$P_{qa}$*::loxp::3xFLAG-eed* | (82) |
| N5012 | *mat A; N. tetrasperma* | (82) |
| N5014 | *mat A;N. discreta* | (82) |
| N5103 | *mat A* | (82) |
| N5104 | *mat A*; Δ*set-7::hph*$^+$ | (82) |
| N5105 | *mat A* | (82) |
| N5106 | *mat a*; Δ*eed::hph*$^+$ | (82) |
| N5107 | *mat a* | (82) |
| N5108 | *mat a*; Δ*su(z)12::hph*$^+$ | (82) |
| N5109 | *mat a* | (82) |
| N5110 | *mat A*; Δ*npf::hph*$^+$ | (82) |
| N5145 | *mat A* | (82) |
| N5146 | *mat a* | (82) |
| N5147 | *mat A* | (82) |

| | | |
|---|---|---|
| N5148 | *mat A* | (82) |
| N5149 | *mat A*; Δ*npf::hph*$^{+}$ | (82) |
| N5150 | *mat A*; Δ*npf::hph*$^{+}$ | (82) |
| N5151 | *mat a*; Δ*npf::hph*$^{+}$ | (82) |
| N5152 | *mat a*; Δ*npf::hph*$^{+}$ | (82) |

## Chapter III

| Strain | Genotype | Reference |
|---|---|---|
| N1850 | *mat a;* Δ*dim-2::hph*$^{+}$ | (77) |
| N1851 | *mat A;* Δ*dim-2::hph*$^{+}$ | (77) |
| N2556 | *mat a his-3; hpo*$^{RIP2}$ | (104) |
| N2930 | *mat A his-3;* Δ*mus-52::bar*$^{+}$ | (52) |
| N2931 | *mat a;* Δ*mus-52::bar*$^{+}$ | Chapter III |
| N3064 | *mat A his-3;* Δ*dmm-1::hph*$^{+}$ | (79) |
| N3081 | *mat A; am*$^{132}$ *inl; [(am/hph/am)*$^{ec42pJI2}$*]*$^{RIP}$*(hH3*$^{K4L}$*)*$^{ec}$ | (49) |
| N3135 | *mat a;* Δ*cdp-2::hph*$^{+}$ | (78) |
| N3169 | *mat a;* Δ*cul4::hph*$^{+}$ | (76) |
| N3351 | *mat a;* Δ*set-1::hph*$^{+}$ | Chapter III |
| N3403 | *mat a;* Δ*dim-8::hph*$^{+}$ | (76) |
| N3411 | *mat a;* Δ*dim-9::hph*$^{+}$ | (76) |
| N3435 | *mat A his-3;* Δ*hda-1::hph*$^{+}$ | Chapter III |
| N3474 | *mat a; sad-1 his-3*$^{+}$*::hH3*$^{S10A}$*; hH3*$^{RIP1}$ | (49) |
| N3537 | *mat A; rid*$^{RIP4}$ *his-3*$^{+}$*::hH3*$^{A7M}$*; hH3*$^{RIP1}$*; pan-2*$^{+}$*::hpo*$^{+}$*-sgfp*$^{+}$ | (49) |
| N3553 | *mat A; rid*$^{RIP4}$ *his-3*$^{+}$*::hH3*$^{A15M}$*; hH3*$^{RIP1}$*; pan-2*$^{+}$*::hpo*$^{+}$*-sgfp*$^{+}$ | (49) |
| N3556 | *mat A; rid*$^{RIP4}$ *his-3*$^{+}$*::hH3*$^{P16A}$*; hH3*$^{RIP1}$*; pan-2*$^{+}$*::hpo*$^{+}$*-sgfp*$^{+}$ | (49) |
| N3560 | *mat A; rid*$^{RIP4}$ *his-3*$^{+}$*::hH3*$^{R17L}$*; hH3*$^{RIP1}$*; pan-2*$^{+}$*::hpo*$^{+}$*-sgfp*$^{+}$ | (49) |
| N3520 | *mat A; rid*$^{RIP4}$ *his-3*$^{+}$*::hH3*$^{R2L}$*; hH3*$^{RIP1}$*; pan-2*$^{+}$*::hpo*$^{+}$*-sgfp*$^{+}$ | (49) |

| | | |
|---|---|---|
| N3542 | *mat A; rid$^{RIP4}$ his-3$^{+}$::hH3$^{R8A}$; hH3$^{RIP1}$; pan-2$^{+}$::hpo$^{+}$-sgfp$^{+}$* | (49) |
| N3565 | *mat A; rid$^{RIP4}$ his-3$^{+}$::hH3$^{K18R}$; hH3$^{RIP1}$; pan-2$^{+}$::hpo$^{+}$-sgfp$^{+}$* | (49) |
| N3568 | *mat A; rid$^{RIP4}$ his-3$^{+}$::hH3$^{K23R}$; hH3$^{RIP1}$; pan-2$^{+}$::hpo$^{+}$-sgfp$^{+}$* | (49) |
| N3610 | *mat a; Δhda-1::hph$^{+}$* | (78) |
| N3612 | *mat a; Δchap::hph$^{+}$* | (78) |
| N3752 | *mat A* | (82) |
| N3753 | *mat a* | (82) |
| N3856 | *mat a; Δdim-7::hph$^{+}$* | (113) |
| N3944 | *mat A; Δdim-5::bar$^{+}$* | (76) |
| N4434 | *mat A; his-3; Δset-1::inl$^{+}$* | Chapter III |
| N4705 | *mat A; Δnst-3::hph$^{+}$* | Chapter III |
| N4718 | *mat a*; *Δset-7::hph$^{+}$* | (82) |
| N4719 | *mat A*; *Δeed::hph$^{+}$* | (82) |
| N4722 | *mat a*; Δ16.8 kb::*hph$^{+}$* | Chapter III |
| N4723 | *mat A*; Δ12.5 kb::*hph$^{+}$* | Chapter III |
| N4724 | *mat a*; Δ1.8 kb::*hph$^{+}$* | Chapter III |
| N4725 | *mat a*; Δ11.7 kb::*hph$^{+}$* | Chapter III |
| N4726 | *mat A*; Δ11.3 kb::*hph$^{+}$* | Chapter III |
| N4727 | *mat a*; *hph$^{+}$* | Chapter III |
| N4728 | *mat a*; Δ1.7 kb::*hph$^{+}$* | Chapter III |
| N4873 | *mat A; his-3; set-3$^{Y833F}$loxP::hph::loxP* | Chapter III |
| N4922 | *mat a*; *Δhpo::hph$^{+}$* | Chapter III |
| N4923 | *mat A*; Δ3.9 kb::*hph$^{+}$* | Chapter III |
| N4924 | *mat a*; Δ7.2 kb::*hph$^{+}$* | Chapter III |
| N4933 | *mat a*; Δ47.4 kb::*hph$^{+}$* | Chapter III |
| N4935 | *mat A*; Δ1.2 kb::*hph$^{+}$* | Chapter III |
| N4936 | *mat a*; Δ5.1 kb::*hph$^{+}$* | Chapter III |
| N5095 | *mat A*; Δ1.0 kb::*hph$^{+}$* | Chapter III |
| N5096 | *mat A*; Δ0.9 kb::*hph$^{+}$* | Chapter III |
| N5097 | *mat ?*; Δ5.3 kb::*hph$^{+}$* | Chapter III |

| | | |
|---|---|---|
| N5100 | *mat a;* Translocation In(IL->IR)AR16 | Chapter III |
| N5102 | *mat A;* Translocation T(VI->VIII)OY329 | Chapter III |
| N5267 | *mat a; eed-dam* | Chapter III |
| N5268 | *mat a; suz12-dam* | Chapter III |
| N5269 | *mat a; npf-dam* | Chapter III |
| N5462 | *mat a*; bar$^{ec}$; 9$^{ec}$ (one copy) | Chapter III |
| N5463 | *mat a*; bar$^{ec}$; 9$^{ec}$ (3-5 copies) | Chapter III |
| N5464 | *mat a*; bar$^{ec}$; 10$^{ec}$ (one copy) | Chapter III |
| N5465 | *mat a*; bar$^{ec}$; 1$^{ec}$ (one copy) | Chapter III |
| N5466 | *mat a*; bar$^{ec}$; 2$^{ec}$(one copy) | Chapter III |
| N5467 | *mat a*; bar$^{ec}$; 2$^{ec}$ (two copies) | Chapter III |
| N5468 | *mat a*; bar$^{ec}$; 3$^{ec}$ (likely three copies) | Chapter III |
| N5469 | *mat a*; bar$^{ec}$; 3$^{ec}$ (likely three copies) | Chapter III |
| N5547 | *mat a;* Δ*mus-52::bar*$^{+}$*;* Δ47.4 kb*::hph*$^{+}$ | Chapter III |
| N5776 | *mat a;* Δ*set-2::hph*$^{+}$ | Chapter III |
| N5777 | *mat A;* Δ*dot-1::hph*$^{+}$ | Chapter III |
| N5683 | *mat A his-3*$^{+}$*::1;* Δ47.4 kb*::hph*$^{+}$ | Chapter III |
| N5684 | *mat A his-3*$^{+}$*::2;* Δ47.4 kb*::hph*$^{+}$ | Chapter III |
| N5685 | *mat A his-3*$^{+}$*::3;* Δ47.4 kb*::hph*$^{+}$ | Chapter III |
| N5686 | *mat A his-3*$^{+}$*::4;* Δ47.4 kb*::hph*$^{+}$ | Chapter III |
| N5687 | *mat A his-3*$^{+}$*::5;* Δ47.4 kb*::hph*$^{+}$ | Chapter III |
| N5688 | *mat A his-3*$^{+}$*::6;* Δ47.4 kb*::hph*$^{+}$ | Chapter III |
| N5689 | *mat A his-3*$^{+}$*::7;* Δ47.4 kb*::hph*$^{+}$ | Chapter III |
| N5690 | *mat A his-3*$^{+}$*::8;* Δ47.4 kb*::hph*$^{+}$ | Chapter III |
| N5695 | *mat a csr-1::1;* Δ47.4 kb*::hph*$^{+}$ | Chapter III |
| N5696 | *mat a csr-1::2;* Δ47.4 kb*::hph*$^{+}$ | Chapter III |
| N5697 | *mat a csr-1::3;* Δ47.4 kb*::hph*$^{+}$ | Chapter III |
| N5698 | *mat A csr-1::4;* Δ47.4 kb*::hph*$^{+}$ | Chapter III |
| N5699 | *mat A csr-1::5;* Δ47.4 kb*::hph*$^{+}$ | Chapter III |
| N5700 | *mat a csr-1::6;* Δ47.4 kb*::hph*$^{+}$ | Chapter III |

| | | |
|---|---|---|
| N5701 | *mat a csr-1::7;* Δ47.4 kb*::hph*$^{+}$ | Chapter III |
| N5702 | *mat A csr-1::8;* Δ47.4 kb*::hph*$^{+}$ | Chapter III |

## Chapter IV

| Strain | Genotype | Reference |
|---|---|---|
| N2930 | *mat A; his-3; Δmus-52::bar*$^{+}$ | (52) |
| N3752 | *mat A* | (82) |
| N3753 | *mat a* | (82) |
| N4721 | *mat a; Δnpf::hph*$^{+}$ | (82) |
| N4880 | *mat a; loxp::*$P_{trpC}$*::hph*$^{+}$*::*$P_{qa}$*::loxp::3xFLAG-npf* | Chapter IV |
| N5263 | *mat A; loxp::*$P_{trpC}$*::hph*$^{+}$*::*$P_{qa}$*::loxp::3xFLAG-hda-3* | Chapter IV |
| N5272 | *mat ?;* Δ*hda-3::hph*$^{+}$ | Chapter IV |
| N5273 | *mat a;* Δ*sin3::hph*$^{+}$ | Chapter IV |
| N5274 | *mat A;* Δ*sds3::hph*$^{+}$ | Chapter IV |
| N5275 | *mat a;* Δ*sap30::hph*$^{+}$ | Chapter IV |
| N5276 | *mat a;* Δ*pho23::hph*$^{+}$ | Chapter IV |
| N5277 | *mat a;* Δ*rco1::hph*$^{+}$ | Chapter IV |
| N5278 | *mat a;* Δ*cdp-6::hph*$^{+}$ | Chapter IV |
| N5401 | *mat A; loxp::*$P_{trpC}$*::hph*$^{+}$*::*$P_{qa}$*::loxp::3xFLAG-npf* | Chapter IV |
| N5404 | *mat a; loxp::*$P_{trpC}$*::hph*$^{+}$*::*$P_{qa}$*::loxp::3xHA-hda-3* | Chapter IV |
| N5453 | *mat a; loxp::*$P_{trpC}$*::hph*$^{+}$*::*$P_{qa}$*::loxp::3xHA-sin3* | Chapter IV |
| N5454 | *mat A; loxp::*$P_{trpC}$*::hph*$^{+}$*::*$P_{qa}$*::loxp::3xFLAG-rco1* | Chapter IV |
| N5455 | *mat A; his-3; loxp::*$P_{trpC}$*::hph*$^{+}$*::*$P_{qa}$*::loxp::3xFLAG-cdp-6* | Chapter IV |
| N5457 | *mat a; his-3; loxp::*$P_{trpC}$*::hph*$^{+}$*::*$P_{qa}$*::loxp::3xHA-sds3* | Chapter IV |
| N5539 | *mat a; loxp::*$P_{trpC}$*::hph*$^{+}$*::*$P_{qa}$*::loxp::3xHA-hda-3; loxp::*$P_{trpC}$*::hph*$^{+}$*::*$P_{qa}$*::loxp::3xFLAG-npf* | Chapter IV |
| N5714 | *mat a; loxp::*$P_{trpC}$*::hph*$^{+}$*::*$P_{qa}$*::loxp::3xHA-hda-3;* | Chapter IV |

| | | |
|---|---|---|
| | *loxp::$P_{trpC}$::hph$^{+}$::$P_{qa}$::loxp::3xFLAG-rco1* | |
| N5715 | *mat a*; *loxp::$P_{trpC}$::hph$^{+}$::$P_{qa}$::loxp::3xHA-hda-3*; *loxp::$P_{trpC}$::hph$^{+}$::$P_{qa}$::loxp::3xFLAG-cdp-6* | Chapter IV |
| N5716 | *mat A; his-3; loxp::$P_{trpC}$::hph$^{+}$::$P_{qa}$::loxp::3xHA-sds3; loxp::$P_{trpC}$::hph$^{+}$::$P_{qa}$::loxp::3xFLAG-cdp-6* | Chapter IV |
| N5717 | *mat a*; *his-3; loxp::$P_{trpC}$::hph$^{+}$::$P_{qa}$::loxp::3xHA-sin3*; *loxp::$P_{trpC}$::hph$^{+}$::$P_{qa}$::loxp::3xFLAG-hda-3* | Chapter IV |

## APPENDIX D

## PRIMER TABLES

### Chapter II

| Primer | Description | Sequence (5' to 3') | Reference |
|---|---|---|---|
| 2972 | Gene 1 NCU06955 FP | GTCTTCGGGCATGGGTATAA | (82) |
| 3004 | Gene 1 NCU06955 RP | GATCAATCCTCTCGACTGGG | (82) |
| 2977 | Gene 2 NCU09590 FP | AGCATCCTCCACTGAGCACT | (82) |
| 3006 | Gene 2 NCU09590 RP | TCGAGTTTGGTAAGTGCTGTT | (82) |
| 3565 | Tel 1L NCU10129 FP | AGCGTTCAAATGCCGTGACCTGT | (82) |
| 3566 | Tel 1L NCU10129 RP | AGTCCAATGGTGCTAACGGCGA | (82) |
| 3908 | Tel 1R NCU10130 FP | GACGGACCTCTTCCGCTCGC | (82) |
| 3909 | Tel 1R NCU10130 RP | CCCTGCACGAGACGGTTCGA | (82) |
| 3998 | *hH4* NCU01634 FP | CATCAAGGGGTCATTCAC | (82) |
| 3999 | *hH4* NCU01634 RP | TTTGGAATCACCCTCCAG | (82) |
| 3931 | Construction of *3xFLAG-eed* (N4879) | GATGCGCCCAAGGAGGGTGC | (82) |
| 3932 | | CATTATACGAAGTTATGCGGCCCGTATGGTG TTCCTTCGAATTTTGACTCC | (82) |
| 3933 | | GCGGCGGAGGCGGCGGAGGCGGCGGAGGCC CCACCAATAAAGCCCCGACCTCGAACG | (82) |
| 3934 | | GCCGTGGCCTACGAGGGTCTGTT | (82) |

| | | | |
|---|---|---|---|
| N.A. | NCU08907 FP | CTCACCACCCTCCTCGCCCTCGCC | (82) |
| N.A. | NCU08907 RP | CCTCAAGCAGCACACAAATCCAAC | (82) |
| N.A. | NCU05897 FP | CTATGGCCTCGGCGCCCTTCTCGCG | (82) |
| N.A. | NCU05897 RP | GCCATTACAGGCCCTTCTCGCCGAC | (82) |
| N.A. | NCU08541 FP | GCAATCAAAATGTCCGTCAACCGC | (82) |
| N.A. | NCU08541 RP | GACTTGCAATGAGCCCTCAAGCC | (82) |
| N.A. | NCU09663 FP | GTCGAGGCCGCCGCCTCCGTCTCC | (82) |
| N.A. | NCU09663 RP | CTAGAAGAGACCAAGACCCATACC | (82) |
| N.A. | NCU11292 FP | CGCTAGCAATATGGCAGGCAAACCG | (82) |
| N.A. | NCU11292 RP | CCATCAACCTAAGCTTTCGATTCCC | (82) |
| N.A. | Paired end top adapter | 5'ACACTCTTTCCCTACACGACGCTCTTCCGA TC-barcode-T-3' | (82) |
| N.A. | Paired end bottom adapter | 5'P-barcode-GATCGGAAGAGCGGTTCAGCAGGAATGCCG AG-3' | (82) |
| N.A. | Paired end barcode #1 | TAACCC (top adapter) / GGGTTA (bottom adapter) | (82) |
| N.A. | Paired end barcode #2 | TAAGGG (top adapter) / CCCTTA (bottom adapter) | (82) |
| N.A. | Paired end barcode #3 | TCAGTC (top adapter) / GACTGA (bottom adapter) | (82) |
| N.A. | Paired end barcode #4 | TCGCGC (top adapter) / GCGCGA (bottom adapter) | (82) |
| N.A. | Paired end barcode #5 | TCTTTCC (top adapter) / GGAAGA (bottom adapter) | (82) |
| N.A. | Paired end barcode #6 | TGCCGG (top adapter) / CCGGCA (bottom adapter) | (82) |
| N.A. | Paired end barcode #7 | TGTGTG (top adapter) / CACACA (bottom adapter) | (82) |
| N.A. | Paired end barcode #8 | TCCTTG (top adapter) / CAAGGA (bottom | (82) |

| | | | |
|---|---|---|---|
| | | adapter) | |
| N.A. | Paired end barcode #9 | TCACAG (top adapter) / CTGTGA (bottom adapter) | (82) |
| N.A. | Paired end barcode #10 | TGGTTC (top adapter) / GAACCA (bottom adapter) | (82) |

## Chapter III

Primers that contain built-in restriction sites are indicated in parentheses after the sequence.

| Primer | Description | Sequence (5' to 3') | Reference |
|---|---|---|---|
| 3249 | Construction of *hph*$^+$(N4727) | GTAACGCCAGGGTTTTCCCAGTCACGACGAC CGGACCCGAGATGCTGCT | Chapter III |
| 3250 | | ACCGGGATCCACTTAACGTTACTGAAATCGA TGGTTTTCTTGGTCATTG | Chapter III |
| 3251 | | GCTCCTTCAATATCATCTTCTGTCGACGGCT CGTCACTGGTGCCACCGG | Chapter III |
| 3252 | | GCGGATAACAATTTCACACAGGAAACAGCT GAATCCAAGATGCCTCAAGCTCCA | Chapter III |
| 3943 | Construction of Δ47.4 kb::*hph*$^+$(N4933) | GTAACGCCAGGGTTTTCCCAGTCACGACGTG TGGCTTGCAGGCACGCAA | Chapter III |
| 3944 | | ACCGGGATCCACTTAACGTTACTGAAATCAG TCCGAGTGGGCCTGCCTC | Chapter III |
| 3945 | | GCTCCTTCAATATCATCTTCTGTCGACGGAC CACCACCCAGCGTGGAAAG | Chapter III |
| 3946 | | GCGGATAACAATTTCACACAGGAAACAGCT TGCCGCCGGCTGAGAAACC | Chapter III |
| 3191 | Construction of Δ16.8 kb::*hph*$^+$(N4722) | GTAACGCCAGGGTTTTCCCAGTCACGACGAC CCATGTCTGACCTAACGC | Chapter III |

| | | | |
|---|---|---|---|
| 3192 | | ACCGGGATCCACTTAACGTTACTGAAATCCC ACCTGGATGAGCAAGAAT | Chapter III |
| 3205 | | GCTCCTTCAATATCATCTTCTGTCGACGGCA CAATCCTTAGCTCCCCAA | Chapter III |
| 3206 | | GCGGATAACAATTTCACACAGGAAACAGCG AGGACATGATGGACTGGCT | Chapter III |
| 3193 | Construction of Δ12.5 kb::*hph*$^{+}$(N4723) | GTAACGCCAGGGTTTTCCCAGTCACGACGGT GCTTGCATCAAGGAGACA | Chapter III |
| 3194 | | ACCGGGATCCACTTAACGTTACTGAAATCCT GCCTTCTTCTTCACGTCC | Chapter III |
| 3203 | | GCTCCTTCAATATCATCTTCTGTCGACGGGA AAGATCCATCGAGGTCCA | Chapter III |
| 3204 | | GCGGATAACAATTTCACACAGGAAACAGCC GTTCTCTTCCACAGCCTTC | Chapter III |
| 3191 | Construction of Δ11.7 kb::*hph*$^{+}$(N4725) | GTAACGCCAGGGTTTTCCCAGTCACGACGAC CCATGTCTGACCTAACGC | Chapter III |
| 3192 | | ACCGGGATCCACTTAACGTTACTGAAATCCC ACCTGGATGAGCAAGAAT | Chapter III |
| 3201 | | GCTCCTTCAATATCATCTTCTGTCGACGGTTC CACCAGACTTCGCTCTT | Chapter III |
| 3202 | | GCGGATAACAATTTCACACAGGAAACAGCC AGCGTTGAGTATGAAGGCA | Chapter III |
| 3197 | Construction of Δ11.3 kb::*hph*$^{+}$(N4726) | GTAACGCCAGGGTTTTCCCAGTCACGACGCT CTGAAACGCGGAGAAAAC | Chapter III |
| 3198 | | ACCGGGATCCACTTAACGTTACTGAAATCTT TTCATGCGTGAATGTGGT | Chapter III |
| 3207 | | GCTCCTTCAATATCATCTTCTGTCGACGGAC AATGGCTCTTACAACCCG | Chapter III |
| 3208 | | GCGGATAACAATTTCACACAGGAAACAGCA CTGAAATACCAACGGCAGG | Chapter III |

| | | | |
|---|---|---|---|
| 3191 | Construction of Δ5.1 kb::*hph*$^+$(N4936) | GTAACGCCAGGGTTTTCCCAGTCACGACGAC CCATGTCTGACCTAACGC | Chapter III |
| 3192 | | ACCGGGATCCACTTAACGTTACTGAAATCCC ACCTGGATGAGCAAGAAT | Chapter III |
| 3972 | | GCTCCTTCAATATCATCTTCTGTCGACGGGC CGACGGCTAAAATGGCCAC | Chapter III |
| 3973 | | GCGGATAACAATTTCACACAGGAAACAGCT GAACTCCCGCCGTCACCTGT | Chapter III |
| 3968 | Construction of Δ1.2 kb::*hph*$^+$(N4935) | GTAACGCCAGGGTTTTCCCAGTCACGACGTT CAACAATGTCACCGTCGT | Chapter III |
| 3969 | | ACCGGGATCCACTTAACGTTACTGAAATCTG GATGATTTGGATTTGGGT | Chapter III |
| 3201 | | GCTCCTTCAATATCATCTTCTGTCGACGGTTC CACCAGACTTCGCTCTT | Chapter III |
| 3202 | | GCGGATAACAATTTCACACAGGAAACAGCC AGCGTTGAGTATGAAGGCA | Chapter III |
| 3522 | Construction of Δ1.7 kb::*hph*$^+$(N4728) | GTAACGCCAGGGTTTTCCCAGTCACGACGGC CGACGGCTAAAATGGCCAC | Chapter III |
| 3523 | | ACCGGGATCCACTTAACGTTACTGAAATCTG AACTCCCGCCGTCACCTGT | Chapter III |
| 3524 | | GCTCCTTCAATATCATCTTCTGTCGACGGTG ATGTGTCACAGGCATTCAAAGAAGG | Chapter III |
| 3525 | | GCGGATAACAATTTCACACAGGAAACAGCG ATCCAGGCTGCTTGCCGCA | Chapter III |
| 3197 | Construction of Δ1.8 kb::*hph*$^+$(N4724) | GTAACGCCAGGGTTTTCCCAGTCACGACGCT CTGAAACGCGGAGAAAAC | Chapter III |
| 3198 | | ACCGGGATCCACTTAACGTTACTGAAATCTT TTCATGCGTGAATGTGGT | Chapter III |
| 3199 | | GCTCCTTCAATATCATCTTCTGTCGACGGTTC AACAATGTCACCGTCGT | Chapter III |

| | | | |
|---|---|---|---|
| 3200 | | GCGGATAACAATTTCACACAGGAAACAGCT GGATGATTTGGATTTGGGT | Chapter III |
| 3197 | Construction of Δ5.1 kb::*hph*$^+$(N4936) | GTAACGCCAGGGTTTTCCCAGTCACGACGCT CTGAAACGCGGAGAAAAC | Chapter III |
| 3198 | | ACCGGGATCCACTTAACGTTACTGAAATCTT TTCATGCGTGAATGTGGT | Chapter III |
| 3518 | | GCTCCTTCAATATCATCTTCTGTCGACGGCA GCTCTGTGGAGCGCGGTG | Chapter III |
| 3519 | | GCGGATAACAATTTCACACAGGAAACAGCG TAGGGGCTCAGGGGGTGCT | Chapter III |
| 3197 | Construction of Δ12.5 kb::*hph*$^+$(N4723) | GTAACGCCAGGGTTTTCCCAGTCACGACGCT CTGAAACGCGGAGAAAAC | Chapter III |
| 3198 | | ACCGGGATCCACTTAACGTTACTGAAATCTT TTCATGCGTGAATGTGGT | Chapter III |
| 3201 | | GCTCCTTCAATATCATCTTCTGTCGACGGTTC CACCAGACTTCGCTCTT | Chapter III |
| 3202 | | GCGGATAACAATTTCACACAGGAAACAGCC AGCGTTGAGTATGAAGGCA | Chapter III |
| 3197 | Construction of Δ7.2 kb::*hph*$^+$(N4924) | GTAACGCCAGGGTTTTCCCAGTCACGACGCT CTGAAACGCGGAGAAAAC | Chapter III |
| 3198 | | ACCGGGATCCACTTAACGTTACTGAAATCTT TTCATGCGTGAATGTGGT | Chapter III |
| 3203 | | GCTCCTTCAATATCATCTTCTGTCGACGGGA AAGATCCATCGAGGTCCA | Chapter III |
| 3204 | | GCGGATAACAATTTCACACAGGAAACAGCC GTTCTCTTCCACAGCCTTC | Chapter III |
| 4012 | Construction of Δ1.0 kb::*hph*$^+$(N5095) | GTAACGCCAGGGTTTTCCCAGTCACGACGCC GCCTGGGCCAGCTATTCT | Chapter III |
| 4013 | | ACCGGGATCCACTTAACGTTACTGAAATCAG TTTGGTAGTACATGGTACCAGTAG | Chapter III |

| | | | |
|---|---|---|---|
| 4014 | | GCTCCTTCAATATCATCTTCTGTCGACGGGT GACAGTCACTGATGAGTGCCGC | Chapter III |
| 4015 | | GCGGATAACAATTTCACACAGGAAACAGCA CCGCCAATATGGCATCGCCC | Chapter III |
| 4016 | Construction of Δ0.9 kb::*hph*$^{+}$(N5096) | GTAACGCCAGGGTTTTCCCAGTCACGACGTA AGAGGCACCGGAAGGAGCA | Chapter III |
| 4017 | | ACCGGGATCCACTTAACGTTACTGAAATCGC CTAGAGGCAGGGGAATGATC | Chapter III |
| 4018 | | GCTCCTTCAATATCATCTTCTGTCGACGGGA ACCGCCAAAATGAAGTTCACAATCC | Chapter III |
| 4019 | | GCGGATAACAATTTCACACAGGAAACAGCT CGACGTCACAAGCCGGCAC | Chapter III |
| 4012 | Construction of Δ5.3 kb::*hph*$^{+}$(N5097) | GTAACGCCAGGGTTTTCCCAGTCACGACGCC GCCTGGGCCAGCTATTCT | Chapter III |
| 4013 | | ACCGGGATCCACTTAACGTTACTGAAATCAG TTTGGTAGTACATGGTACCAGTAG | Chapter III |
| 4018 | | GCTCCTTCAATATCATCTTCTGTCGACGGGA ACCGCCAAAATGAAGTTCACAATCC | Chapter III |
| 4019 | | GCGGATAACAATTTCACACAGGAAACAGCT CGACGTCACAAGCCGGCAC | Chapter III |
| 2894 | *hph* | CCGTCGACAGAAGATGATATTGAAGGAGC | Chapters II, III and IV |
| 2895 | *hph* | AGCTGACATCGACACCAACG | Chapters II, III and IV |
| 2954 | Internal *hph* primer | AAAAAGCCTGAACTCACCGCGACG | Chapter III and IV |
| 2955 | Internal *hph* primer | TCGCCTCGCTCCAGTCAATGACC | Chapter III and IV |
| 1652 | *bar* | CCGTCGACAGAAGATGATATTGAAGGAGC | Chapter III |

| | | | |
|---|---|---|---|
| 1653 | *bar* | AATTAACCCTCACTAAAGGGAACAAAAGC | Chapter III |
| 3998 | qChIP *hH4* NCU01634 | CATCAAGGGGTCATTCAC | (82) |
| 3999 | qChIP *hH4* NCU01634 | TTTGGAATCACCCTCCAG | (82) |
| 3565 | qChIP Tel 1L NCU10129 | AGCGTTCAAATGCCGTGACCTGT | (82) |
| 3566 | qChIP Tel 1L NCU10129 | AGTCCAATGGTGCTAACGGCGA | (82) |
| 3321 | qChIP and deletion analysis | TGAACAGGTGACGGCGGGAGT | Chapter III |
| 3564 | qChIP and deletion analysis | CGGGTCCGGAGTCCATCACCA | Chapter III |
| 3954 | qChIP deletion analysis | GTAGCTAGCGGGTGCTGCCG | Chapter III |
| 3955 | qChIP deletion analysis | AGGCGCCAGGAAGAGTATAGCCC | Chapter III |
| 4784 | qChIP *his-3* & *csr-1* targeting P1Fwd | AATGCAAGGTCCCGAACACT | Chapter III |
| 4785 | qChIP *his-3* & *csr-1* targeting P1Rev | TGGCTGTCGCAATTACCAGT | Chapter III |
| 4786 | qChIP *his-3* & *csr-1* targeting P2Fwd | GACCAAGCATGCGTTAGCTG | Chapter III |
| 4787 | qChIP *his-3* & *csr-1* targeting P2Rev | ACCCAAGGTGGGTGTGTTTT | Chapter III |
| 4788 | qChIP *his-3* & *csr-1* targeting P3Fwd | CCGTTTGAGCTGGTCTTCCT | Chapter III |
| 4789 | qChIP *his-3* & *csr-1* targeting P3Rev | TGACGGATGCTCTTTGTCCC | Chapter III |
| 4790 | qChIP *his-3* & *csr-1* | CAACCAGCTTGACGGCTTTC | Chapter III |

| | | | |
|---|---|---|---|
| | targeting P4Fwd | | |
| 4791 | qChIP *his-3* & *csr-1* targeting P4Rev | TACCGTAGGTGCCCTGTGTA | Chapter III |
| 3317 | qChIP *his-3* & *csr-1* targeting P5Fwd and deletion analysis | CCCCTTCCTGCCGTGGGAGA | Chapter III |
| 3562 | qChIP *his-3* & *csr-1* targeting P5Rev and deletion analysis | TCAGCAGGCATAGTCAAGACTGGT | Chapter III |
| 4782 | qChIP *his-3* & *csr-1* targeting P6Fwd | CCCGCTTCAGCAACCAAGTT | Chapter III |
| 4783 | qChIP *his-3* & *csr-1* targeting P6Rev | AACTTTAGCCCGCGTTACGG | Chapter III |
| 3319 | qChIP *his-3* & *csr-1* targeting P7Fwd and deletion analysis | TGGGTCGATGGAGTACCTTCCCC | Chapter III |
| 3563 | qChIP *his-3* & *csr-1* targeting P7Rev and deletion analysis | TGCACTATCCTTTTCAGGGGCTTGT | Chapter III |
| 3902 | qChIP *his-3* & *csr-1* targeting P8Fwd | GACCTACACGGCCCGGGGAA | Chapter III |
| 3903 | qChIP *his-3* & *csr-1* targeting P8Rev | ACCGACGAGACTTGACTGCCCA | Chapter III |
| 3986 | qChIP *his-3* & *csr-1* targeting P9Fwd | GTGGCGGCGTGAACGGTCAT | Chapter III |
| 3987 | qChIP *his-3* & *csr-1* targeting P9Rev | AGTCAAGCCTCGCGATCGTGA | Chapter III |
| 3321 | qChIP *his-3* & *csr-1* targeting P10Fwd | TGAACAGGTGACGGCGGGAGT | Chapter III |
| 3564 | qChIP *his-3* & *csr-1* | CGGGTCCGGAGTCCATCACCA | Chapter III |

| | | | |
|---|---|---|---|
| | targeting P10Rev | | |
| 3976 | qChIP *his-3* & *csr-1* targeting P11Fwd | AGTGGTCCAGAGTGGGATCGGT | Chapter III |
| 3977 | qChIP *his-3* & *csr-1* targeting P11Rev | ACCGCCAATATGGCATCGCCC | Chapter III |
| 3974 | qChIP *his-3* & *csr-1* targeting P12Fwd | TGACGGCGCGCAGATTGGAG | Chapter III |
| 3975 | qChIP *his-3* & *csr-1* targeting P12Rev | TCGCTTCCCTTCTCCCACCATCC | Chapter III |
| 3978 | qChIP *his-3* & *csr-1* targeting P13Fwd | TTGACGGCGCGCAGATTGGAG | Chapter III |
| 3979 | qChIP *his-3* & *csr-1* targeting P13Rev | CCACCATCCTTCCCTCTGCCACA | Chapter III |
| 3992 | qChIP *his-3* & *csr-1* targeting P14Fwd | CATCGCAGCTCAACCGCAGA | Chapter III |
| 3993 | qChIP *his-3* & *csr-1* targeting P14Rev | GCCAGCCGGTGTCAAGACAGA | Chapter III |
| 3904 | qChIP *his-3* & *csr-1* targeting P15Fwd | AACAAAGACGCTCTTCTGGTGGCC | Chapter III |
| 3905 | qChIP *his-3* & *csr-1* targeting P15Rev | ACTACCAAACTGCCGACGGCT | Chapter III |
| 4108 | Construction of *dam-set-7* (no strain number available) | GCCAACTTCCAGCCTTTCAC | Chapter III |
| 4109 | | CCTCCGCCTCCGCCTCCGCCGCCTCCGCCCT CCTCCTCGTTCCGATATC | Chapter III |
| 4110 | | TGCTATACGAAGTTATGGATCCGAGCTCGGT ATTTGACTCGTGATTCTAGATATC | Chapter III |
| 4111 | | GCATCACCCACTACACGACA | Chapter III |
| 4112 | Construction of *dam-eed (*N5267) | GTCATCCACTACCCGCACTT | Chapter III |
| 4113 | | CCTCCGCCTCCGCCTCCGCCGCCTCCGCCCT TCCCCCACCGCTGAAA | Chapter III |

| | | | |
|---|---|---|---|
| 4114 | | TGCTATACGAAGTTATGGATCCGAGCTCGAG AGTAAATAGGGTGGGAGGGC | Chapter III |
| 4115 | | GAAGAAGACGAACGGCAAAG | Chapter III |
| 4116 | Construction of *dam-suz12* (N5268) | AGAAGGGCATGTACCTGGTG | Chapter III |
| 4117 | | CCTCCGCCTCCGCCTCCGCCGCCTCCGCCAT GGCCCACTGCTTCGCACT | Chapter III |
| 4118 | | TGCTATACGAAGTTATGGATCCGAGCTCGAA GTGGCAGCAGCCCAAAGT | Chapter III |
| 4119 | | GTCCGAGCTGTCTCGTTTTC | Chapter III |
| 4120 | Construction of *dam-npf* (N5269) | GCCTACCCTCACGACACAAT | Chapter III |
| 4121 | | CCTCCGCCTCCGCCTCCGCCGCCTCCGCCGT GACTAGATTGCTTCGGTTT | Chapter III |
| 4122 | | TGCTATACGAAGTTATGGATCCGAGCTCGGA TGAGGAAACTTCGGCCTT | Chapter III |
| 4122 | | CAAAGGGTTCGAGACAGCTC | Chapter III |
| 3325 | Construction of *his-3$^{+}$::1* (N5683) | CGGGATCCCCGGATCGAACGGCGGATGG (BamHI) | Chapter III |
| 3326 | | GCTCTAGATGAGCTCCTTCCCCCACGGT (XbaI) | Chapter III |
| 3327 | Construction of *his-3$^{+}$::2* (N5684) | CGGGATCCCGTGGGTTCCAGTGCGTCCC (BamHI) | Chapter III |
| 3328 | | GCTCTAGATGGCAAGCGCCGACATGTGA (XbaI) | Chapter III |
| 3329 | Construction of *his-3$^{+}$::3* (N5685) | GGGCCCAGGGAACAGGCGCAGTGCAG (ApaI) | Chapter III |
| 3330 | | GACTAGTTGGCGCGCTTGACCAGCAAA (SpeI) | Chapter III |
| 3331 | Construction of *his-3$^{+}$::4* (N5686) | GACTAGTTCCCGGAACGGCCACTCCAT (SpeI) | Chapter III |
| 3332 | | GCTCTAGAGTGCTGCCAAGGCCCGACAT (XbaI) | Chapter III |
| 3297 | Construction of *his-* | GGAATTCCAAAGGATCGCGCCCGGAGG | Chapter III |

| | | | |
|---|---|---|---|
| | *3$^{+}$::5* (N5687) | (EcoRI) | |
| 3333 | | CGGGATCCACGACGGGAAGACGAGGGGT (BamHI) | Chapter III |
| 3334 | Construction of *his-3$^{+}$::6* (N5688) | GGGCCCGGGAGTGTGGCGCTGTGGAC (ApaI) | Chapter III |
| 3335 | | GACTAGTAGCAGCATCTCGGGTCCGGT (SpeI) | Chapter III |
| 3301 | Construction of *his-3$^{+}$::7* (N5689) | GGAATTCGGCATGCCCAGGGATTGGGG (EcoRI) | Chapter III |
| 3336 | | GCTCTAGAGACGGAACGGTGACAGGCGG (XbaI) | Chapter III |
| 3303 | Construction of *his-3$^{+}$::8* (N5690) | GGAATTCTGGTTCGCGGACGAGGGCTA (EcoRI) | Chapter III |
| 3337 | | CGGGATCCGGCTATTGCTGCCAGCCGGT (BamHI) | Chapter III |
| 4004 | Construction of *his-3$^{+}$::*9 | GACTAGTCCGGATCGAACGGCGGATGG (SpeI) | Chapter III |
| 4005 | | ATAAGAATGCGGCCGCACGACGGGAAGACG AGGGGT (NotI) | Chapter III |
| 4006 | Construction of *his-3$^{+}$::*10 | GCTCTAGAGGCATGCCCAGGGATTGGGG (XbaI) | Chapter III |
| 4007 | | ATAAGAATGCGGCCGCTTCGCCTCCGCAGA AAGCCT (NotI) | Chapter III |
| N4654 | 3' *csr-1* RP | AACACCTCCGTCGCCATAAACTCC | Chapter III |
| N4655 | 5' *csr-1* FP | GGCCCCTGGTTTACTGAGGGC | Chapter III |
| 4721 | 5' *csr-1* RP | TGCAGCCATTGACGACATTGC | Chapter III |
| 4722 | 3' *csr-1* FP | TGGATTTCCTGCGCTGCACAC | Chapter III |
| 4723 | Construction of *csr-1::1* (N5695) | GCAATGTCGTCAATGGCTGCACCGGATCGA ACGGCGGATGG | Chapter III |
| 4724 | | GTGTGCAGCGCAGGAAATCCATGAGCTCCTT CCCCCACGGT | Chapter III |
| 4725 | Construction of *csr-* | GCAATGTCGTCAATGGCTGCACGTGGGTTCC | Chapter III |

| | | | |
|---|---|---|---|
| | *1::2* (N5696) | AGTGCGTCCC | |
| 4726 | | GTGTGCAGCGCAGGAAATCCATGGCAAGCG CCGACATGTGA | Chapter III |
| 4727 | Construction of *csr-1::3* (N5697) | GCAATGTCGTCAATGGCTGCAAGGGAACAG GCGCAGTGCAG | Chapter III |
| 4728 | | GTGTGCAGCGCAGGAAATCCATGGCGCGCT TGACCAGCAAA | Chapter III |
| 4729 | Construction of *csr-1::4* (N5698) | GCAATGTCGTCAATGGCTGCATCCCGGAACG GCCACTCCAT | Chapter III |
| 4730 | | GTGTGCAGCGCAGGAAATCCAGTGCTGCCA AGGCCCGACAT | Chapter III |
| 4731 | Construction of *csr-1::5* (N5699) | GCAATGTCGTCAATGGCTGCACAAAGGATC GCGCCCGGAGG | Chapter III |
| 4732 | | GTGTGCAGCGCAGGAAATCCAACGACGGGA AGACGAGGGGT | Chapter III |
| 4733 | Construction of *csr-1::6* (N5700) | GCAATGTCGTCAATGGCTGCAGGGAGTGTG GCGCTGTGGAC | Chapter III |
| 4734 | | GTGTGCAGCGCAGGAAATCCAAGCAGCATC TCGGGTCCGGT | Chapter III |
| 4735 | Construction of *csr-1::7* (N5701) | GCAATGTCGTCAATGGCTGCAGGCATGCCCA GGGATTGGGG | Chapter III |
| 4736 | | GTGTGCAGCGCAGGAAATCCAGACGGAACG GTGACAGGCGG | Chapter III |
| 4737 | Construction of *csr-1::8* (N5702) | GCAATGTCGTCAATGGCTGCATGGTTCGCGG ACGAGGGCTA | Chapter III |
| 4738 | | GTGTGCAGCGCAGGAAATCCAGGCTATTGCT GCCAGCCGGT | Chapter III |
| 3960 | qChIP in *hph* (H3K27me3 spreading) | GCTGCAGAACAGCGGGCAGT | Chapter III |

| | | | |
|---|---|---|---|
| 3961 | qChIP in *hph* (H3K27me3 spreading) | TTGCATCTCCCGCCGTGCAC | Chapter III |
| 3962 | qChIP in *hph* (H3K27me3 spreading) | CACGAGGTGCCGGACTTCGG | Chapter III |
| 3963 | qChIP in *hph* (H3K27me3 spreading) | CGACACCGTCAGTGCGTCCG | Chapter III |
| 3966 | qChIP in *hph* (H3K27me3 spreading) | TCGTGCACCAAGCAGCAGATGA | Chapter III |
| 3967 | qChIP in *hph* (H3K27me3 spreading) | GCGGCGCTCGAAGTGTGACT | Chapter III |

**Chapter IV**

| Primer | Description | Sequence (5' to 3') | Reference |
|---|---|---|---|
| 2894 | *hph* | CCGTCGACAGAAGATGATATTGAAGGAGC | Chapters II, III and IV |
| 2895 | *hph* | AGCTGACATCGACACCAACG | Chapters II, III and IV |
| 2954 | Internal *hph* | AAAAAGCCTGAACTCACCGCGACG | Chapters III and IV |
| 2955 | Internal *hph* | TCGCCTCGCTCCAGTCAATGACC | Chapters III and IV |

| | | | |
|---|---|---|---|
| 4077 | Construction of 3xFLAG- and 3xHA-*hda-3* (N5263 and N5404) | ACACCACTAGCCACGAACCCGT | Chapter IV |
| 4065 | | CATTATACGAAGTTATGCGGCCGGTGGGCA GATGTTGCCGGG | Chapter IV |
| 4066 | | GCGGCGGAGGCGGCGGAGGCGGCGGAGGCC CTTCCACATTCACCGATCCCGCC | Chapter IV |
| 4067 | | TGCGACGTTGCGCATGGTGT | Chapter IV |
| 3939 | Construction of 3xFLAG-*npf* (N4880) | CGGGTTAGCCGTCCAAACGT | Chapter IV |
| 3940 | | CATTATACGAAGTTATGCGGCCCTTGAGTGC GTAGATTCAGTAAAGC | Chapter IV |
| 3941 | | GCGGCGGAGGCGGCGGAGGCGGCGGAGGC GCGCGCGACGAGATTGTCGACGATGTTG | Chapter IV |
| 3942 | | GGCGGACGCAGTCGCAATGATGG | Chapter IV |
| 4228 | Construction of 3xHA-*sin3* (N5453) | ACCATCAACGGGTGGGAAGT | Chapter IV |
| 4229 | | CATTATACGAAGTTATGCGGCCCGTGGTTGG ACTGTTCGAAGGC | Chapter IV |
| 4230 | | GCGGCGGAGGCGGCGGAGGCGGCGGAGGC AACTCCCAGCCCCAGCCTCTGC | Chapter IV |
| 4231 | | GGCCAACATACGTTTGGCTCTTGA | Chapter IV |
| 4240 | Construction of 3xFLAG-*rco1* (N5454) | ACCCTACTAACTCCACAGCA | Chapter IV |
| 4241 | | CATTATACGAAGTTATGCGGCCGTGGTATGG CCAGAAAGAC | Chapter IV |
| 4242 | | GCGGCGGAGGCGGCGGAGGCGGCGGAGGC GTGTCACCAAGTACGAGAAGC | Chapter IV |
| 4243 | | GGCTGTTCAGGCTGTTTTGG | Chapter IV |
| 4244 | Construction of 3xFLAG-*cdp-6* (N5455) | ATTAGCAAAGCGGCCGTAGC | Chapter IV |
| 4245 | | CATTATACGAAGTTATGCGGCCTTTGAGAGA CTGGGGTGGCCG | Chapter IV |
| 4246 | | GCGGCGGAGGCGGCGGAGGCGGCGGAGGC GCCCCGTCCAAAACGCCCC | Chapter IV |
| 4247 | | AACGCCGCCACTTACTGTTT | Chapter IV |

| | | | |
|---|---|---|---|
| 4224 | Construction of 3xHA-*sds3* (N5457) | TGAGAGGCAGCGACGAGAAG | Chapter IV |
| 4225 | | CATTATACGAAGTTATGCGGCCGGCGAAAG GGGGGTCCTCG | Chapter IV |
| 4226 | | GCGGCGGAGGCGGCGGAGGCGGCGGAGGC GCTTCTACCGACGTTACCATGGCCG | Chapter IV |
| 4227 | | CGCTGGGCACTCTCTTTCGT | Chapter IV |
| 4281 | Construction of 3xFLAG-*sap30* (N5459) | ATGATGCCGCTGTCAGAACA | Chapter IV |
| 4282 | | CATTATACGAAGTTATGCGGCCAAAAGAGA CTCCCGCAGTGG | Chapter IV |
| 4238 | | GCGGCGGAGGCGGCGGAGGCGGCGGAGGC GCACCACCAAGGAAGAACC | Chapter IV |
| 4239 | | GTTTGTAGGCGGTAGGCTCG | Chapter IV |
| 4272 | Construction of 3xFLAG-*cti6* (N5458) | CAACCTGAACCAGACCCGAC | Chapter IV |
| 4273 | | CATTATACGAAGTTATGCGGCCGTCGTCAGT CGACTGGAGAG | Chapter IV |
| 4274 | | GCGGCGGAGGCGGCGGAGGCGGCGGAGGC ATTCACAGACAACGCTATTCGCACTACC | Chapter IV |
| 4275 | | CGGAGTGGACTGTGAGGCAG | Chapter IV |
| 4276 | Construction of 3xFLAG-*dep1* (N5460) | TTCGCTGGACCAACCTACAC | Chapter IV |
| 4277 | | CATTATACGAAGTTATGCGGCCCGCGGATCA TAGAATCCGACG | Chapter IV |
| 4278 | | GCGGCGGAGGCGGCGGAGGCGGCGGAGGC GCTACCGGTGACACCGCGCTG | Chapter IV |
| 4283 | | GACTCACCGCTCCCGGAAACTGC | Chapter IV |

## APPENDIX E

## SOUTHERN BLOT PROBES AND RESTRICTION DIGESTS

### Chapter II

| Strain | [redacted] | Primers used to make probe | Restriction Digest 1 | Restriction Digest 2 |
|---|---|---|---|---|
| N4718 | | 2894, 2895 | EcoRI | EcoRV and HindIII |
| N4719 | | 2894, 2895 | EcoRI | EcoRV and HindIII |
| N4720 | | 2894, 2895 | EcoRI | EcoRV and HindIII |
| N4721 | | 2894, 2895 | EcoRI | EcoRV and HindIII |
| N4879 | | 3931, 3932 | BamHI and FspI | XhoI |

### Chapter III

| Strain | Primers used to make probe | Restriction Digest 1 | Restriction Digest 2 |
|---|---|---|---|
| N4933 | 3943, 3944 | MluI and XhoI | XmaI |
| N4727 | 3249, 3250 | EcoRI | FspI and SpeI |
| N4722 | 3191, 3192 | EcoRI and NdeI | HindIII and NdeI |
| N4723 | 3193, 3194 | EcoRI | HindIII and XhoI |
| N4725 | 3191, 3192 | HindIII | EcoRV and NdeI |
| N4726 | 3522, 3523 | EcoRV | XhoI |
| N4936 | 3191, 3192 | NheI and SpeI | EcoRV and NdeI |
| N4935 | 3968, 3969 | BamHI | EcoRI |
| N4728 | 3968, 3969 | SmaI | EcoRI |
| N4724 | 3197, 3198 | HindIII and XhoI | EcoRI |
| N4937 | 3968, 3969 | EcoRI | FspI and XhoI |
| N4923 | 3201, 3202 | EcoRI | FspI |
| N4924 | 3203, 3204 | EcoRI | EcoRV |

| | | | |
|---|---|---|---|
| N5095 | 4012, 4013 | EcoRI and EcoRV | ApaI and HindIII |
| N5096 | 4016, 4017 | XmaI | XhoI |
| N5097 | 4012, 4013 | ApaI and XmaI | BamHI |
| N5267 | 4112, 4113 | EcoRI | NdeI |
| N5268 | 4116, 4117 | EcoRI and FspI | ApaI and EcoRV |
| N5269 | 4120, 4121 | HindIII | ApaI and SmaI |
| N5462 | 4004, 4005 | EcoRV | HindIII |
| N5463 | 4004, 4005 | EcoRV | HindIII |
| N5464 | 4006, 4007 | EcoRV | SmaI |
| N5465 | 3325, 3326 | EcoRV | EcoRI and MluI |
| N5466 | 3327, 3328 | EcoRI and FspI | HindIII |
| N5467 | 3327, 3328 | EcoRI and FspI | HindIII |
| N5468 | 3329, 3330 | EcoRI | NheI and XbaI |
| N5469 | 3128 and 5' delta *his-3* (S.H.) | MluI and SpeI | HindIII and SpeI |
| N5684 | 3128 and 5' delta *his-3* (S.H.) | MluI and EcoRI | HindIII and NheI |
| N5685 | 3128 and 5' delta *his-3* (S.H.) | MluI and EcoRI | NheI and XbaI |
| N5686 | 3128 and 5' delta *his-3* (S.H.) | MluI and SpeI | HindIII and NdeI |
| N5687 | 3128 and 5' delta *his-3* (S.H.) | NdeI and XbaI | ApaI and NdeI |
| N5688 | 3128 and 5' delta *his-3* (S.H.) | MluI and EcoRI | NheI and XbaI |
| N5689 | 3128 and 5' delta *his-3* (S.H.) | MluI and SpeI | HindIII and NdeI |
| N5690 | 3128 and 5' delta *his-3* (S.H.) | HindIII and NdeI | ApaI and NdeI |
| N5695 | 4655, 4721 | BamHI and EcoRV | FspI and NdeI |
| N5696 | 4655, 4721 | FspI | BamHI and NdeI |
| N5697 | 4655, 4721 | BamHI and NdeI | EcoRI |
| N5698 | 4655, 4721 | FspI and NdeI | EcoRI |
| N5699 | 4655, 4721 | BamHI and EcoRV | EcoRI and MluI |
| N5700 | 4655, 4721 | EcoRI | BamHI |
| N5701 | 4655, 4721 | EcoRI and NdeI | BamHI |
| N5702 | 4655, 4721 | EcoRI and NdeI | BamHI |

**Chapter IV**

| Strain | Primers to make probe | Restriction Digest 1 | Restriction Digest 2 |
|---|---|---|---|
| N4721 | 2894, 2895 | EcoRI | EcoRV and HindIII |
| N4880 | 3939, 3940 | EcoRI | XbaI |
| N5263 | 4065, 4077 | XbaI | NheI and SpeI |
| N5272 | 2894, 2895 | HindII | XbaI |
| N5273 | 2894, 2895 | BamHI | EcoRV |
| N5274 | 2894, 2895 | BamHI | XhoI |
| N5275 | 2894, 2895 | HindIII | XbaI |
| N5276 | 2894, 2895 | EcoRV | XbaI |
| N5277 | 2894, 2895 | HindIII | XbaI |
| N5278 | 2894, 2895 | EcoRV | XbaI |
| N5401 | 3939, 3940 | EcoRI | XbaI |
| N5404 | 4065, 4077 | XbaI | NheI and SpeI |
| N5453 | 4228, 4229 | HindIII | FspI |
| N5454 | 4240, 4241 | NheI | XhoI |
| N5455 | 4244, 4245 | EcoRV | HindIII |
| N5457 | 4224, 4225 | FspI | XhoI |
| N5539 | 2894, 2895 | XbaI | EcoRV |
| N5714 | 2894, 2895 | XbaI | -- |
| N5715 | 2894, 2895 | EcoRV | -- |
| N5716 | 2894, 2895 | HindIII | -- |
| N5717 | 2894, 2895 | EcoRV | -- |

## REFERENCES CITED


1. Ferrari KJ et al. (2013) Polycomb-Dependent H3K27me1 and H3K27me2 Regulate Active Transcription and Enhancer Fidelity. *Molecular Cell*.

2. Davis RH, Perkins DD (2002) Timeline: Neurospora: a model of model microbes. *Nature Reviews Genetics* 3:397–403.

3. Aramayo R, Selker EU (2013) Neurospora crassa, a Model System for Epigenetics Research. *Cold Spring Harbor Perspectives in Biology* 5:a017921–a017921.

4. O'Carroll D et al. (2001) The polycomb-group gene Ezh2 is required for early mouse development. *Molecular and Cellular Biology* 21:4330–4336.

5. Deng X, Berletch JB, Nguyen DK, Disteche CM (2014) X chromosome regulation: diverse patterns in development, tissues and disease. *Nature Reviews Genetics* 15:367–378.

6. Pinter SF et al. (2012) Spreading of X chromosome inactivation via a hierarchy of defined Polycomb stations. *Genome Research* 22:1864–1876.

7. Simon JA, Lange CA (2008) Roles of the EZH2 histone methyltransferase in cancer epigenetics. *Mutat Res* 647:21–29.

8. Yu J et al. (2007) A polycomb repression signature in metastatic prostate cancer predicts cancer outcome. *Cancer Res* 67:10657–10663.

9. Wu G et al. (2012) Somatic histone H3 alterations in pediatric diffuse intrinsic pontine gliomas and non-brainstem glioblastomas. *Nature Publishing Group* 44:251–253.

10. Sturm D et al. (2012) Hotspot mutations in H3F3A and IDH1 define distinct epigenetic and biological subgroups of glioblastoma. *Cancer Cell* 22:425–437.

11. Schwartzentruber J et al. (2012) Driver mutations in histone H3.3 and chromatin remodelling genes in paediatric glioblastoma. *Nature* 482:226–231.

12. Simon JA, Kingston RE (2013) Occupying chromatin: polycomb mechanisms for getting to genomic targets, stopping transcriptional traffic, and staying put. *Molecular Cell* 49:808–824.

13. Tie F, Prasad-Sinha J, Birve A, Rasmuson-Lestander A, Harte PJ (2003) A 1-megadalton ESC/E (Z) complex from Drosophila that contains polycomblike and RPD3. *Molecular and Cellular Biology* 23:3352–3362.

14. Tie F, Furuyama T, Harte PJ (1998) The Drosophila Polycomb Group proteins

ESC and E(Z) bind directly to each other and co-localize at multiple chromosomal sites. *Development* 125:3483–3496.

15. van der Vlag J, Otte AP (1999) Transcriptional repression mediated by the human polycomb-group protein EED involves histone deacetylation. *Nat Genet* 23:474–478.

16. Müller J et al. (2002) Histone methyltransferase activity of a *Drosophila* Polycomb group repressor complex. *Cell* 111:197–208.

17. Schwartz YB, Pirrotta V (2007) Polycomb silencing mechanisms and the management of genomic programmes. *Nature Reviews Genetics* 8:9–22.

18. Qian C, Zhou MM (2006) SET domain protein lysine methyltransferases: Structure, specificity and catalysis. *Cell Mol Life Sci* 63:2755–2763.

19. Nekrasov M, Wild B, Müller J (2005) Nucleosome binding and histone methyltransferase activity of *Drosophila* PRC2. *EMBO reports* 6:348–353.

20. Margueron R et al. (2009) Role of the polycomb protein EED in the propagation of repressive histone marks. *Nature* 461:762–767.

21. Margueron R, Reinberg D (2011) The Polycomb complex PRC2 and its mark in life. *Nature* 469:343–349.

22. Shaver S, Casas-Mollano JA, Cerny RL, Cerutti H (2010) Origin of the polycomb repressive complex 2 and gene silencing by an E(z) homolog in the unicellular alga Chlamydomonas. *Epigenetics* 5:301–312.

23. Li B, Carey M, Workman JL (2007) The Role of Chromatin during Transcription. *Cell* 128:707–719.

24. Bouyer D et al. (2011) Polycomb Repressive Complex 2 Controls the Embryo-to-Seedling Phase Transition. *PLoS Genet* 7:e1002014.

25. Boyer LA et al. (2006) Polycomb complexes repress developmental regulators in murine embryonic stem cells. *Nature* 441:349–353.

26. Bracken AP, Dietrich N, Pasini D, Hansen KH, Helin K (2006) Genome-wide mapping of Polycomb target genes unravels their roles in cell fate transitions. *Genes & Development* 20:1123–1136.

27. Lee TI et al. (2006) Control of developmental regulators by Polycomb in human embryonic stem cells. *Cell* 125:301–313.

28. Leeb M et al. (2010) Polycomb complexes act redundantly to repress genomic repeats and genes. *Genes & Development* 24:265–276.

29. Weinhofer I, Hehenberger E, Roszak P, Hennig L, Köhler C (2010) H3K27me3 profiling of the endosperm implies exclusion of polycomb group protein targeting by DNA methylation. *PLoS Genet* 6.

30. Kirmizis A et al. (2004) Silencing of human polycomb target genes is associated with methylation of histone H3 Lys 27. *Genes & Development*.

31. Beisel C, Paro R (2011) Silencing chromatin: comparing modes and mechanisms. *Nature Reviews Genetics* 12:123–135.

32. Simon JA, Kingston RE (2009) Mechanisms of polycomb gene silencing: knowns and unknowns. *Nature Reviews Molecular Cell Biology* 10:697–708.

33. Pauler FM et al. (2009) H3K27me3 forms BLOCs over silent genes and intergenic regions and specifies a histone banding pattern on a mouse autosomal chromosome. *Genome Research* 19:221–233.

34. Schwartz YB et al. (2006) Genome-wide analysis of Polycomb targets in *Drosophila melanogaster*. *Nat Genet* 38:700–705.

35. Zhang X et al. (2007) Whole-genome analysis of histone H3 lysine 27 trimethylation in *Arabidopsis*. *Plos Biol* 5:e129.

36. Lachner M, Sengupta R, Schotta G, Jenuwein T (2004) Trilogies of histone lysine methylation as epigenetic landmarks of the eukaryotic genome. *Cold Spring Harb Symp Quant Biol* 69:209–218.

37. Tamaru H et al. (2003) Trimethylated lysine 9 of histone H3 is a mark for DNA methylation in Neurospora crassa. *Nat Genet* 34:75–79.

38. Lewis ZA et al. (2009) Relics of repeat-induced point mutation direct heterochromatin formation in *Neurospora crassa*. *Genome Research* 19:427–437.

39. Smith KM et al. (2008) The fungus *Neurospora crassa* displays telomeric silencing mediated by multiple sirtuins and by methylation of histone H3 lysine 9. *Epigenetics & Chromatin* 1:5.

40. Charron J-BF, He H, Elling AA, Deng XW (2009) Dynamic landscapes of four histone modifications during deetiolation in *Arabidopsis*. *Plant Cell* 21:3732–3748.

41. Ernst J et al. (2011) Mapping and analysis of chromatin state dynamics in nine human cell types. *Nature* 473:43–49.

42. Kharchenko PV et al. (2011) Comprehensive analysis of the chromatin landscape in *Drosophila melanogaster*. *Nature* 471:480–485.

43. Squazzo SL et al. (2006) Suz12 binds to silenced regions of the genome in a cell-type-specific manner. *Genome Research* 16:890–900.

44. Davis RH, De Serres FJ (1970) Genetic and microbiological research techniques for *Neurospora crassa*. *Meth Enzymol* 17A:47–143.

45. Metzenberg RL (2004) Bird medium: an alternative to Vogel medium. *Fungal Genet Newsl* 51:19–20.

46. Borkovich KA et al. (2004) Lessons from the genome sequence of Neurospora crassa: tracing the path from genomic blueprint to multicellular organism. *Microbiol Mol Biol Rev* 68:1–108.

47. Colot HV et al. (2006) A high-throughput gene knockout procedure for *Neurospora* reveals functions for multiple transcription factors. *Proc Natl Acad Sci USA* 103:10352–10357.

48. Polo SE, Almouzni G (2006) Chromatin assembly: a basic recipe with various flavours. *Current Opinion in Genetics & Development* 16:104–111.

49. Adhvaryu KK, Berge E, Tamaru H, Freitag M, Selker EU (2011) Substitutions in the amino-terminal tail of Neurospora histone H3 have varied effects on DNA methylation. *PLoS Genet* 7:e1002423.

50. Nègre N et al. (2011) A cis-regulatory map of the *Drosophila* genome. *Nature* 471:527–531.

51. Kuzmichev A, Nishioka K, Erdjument-Bromage H, Tempst P, Reinberg D (2002) Histone methyltransferase activity associated with a human multiprotein complex containing the Enhancer of Zeste protein. *Genes & Development* 16:2893–2905.

52. Honda S, Selker EU (2008) Direct interaction between DNA methyltransferase DIM-2 and HP1 is required for DNA methylation in *Neurospora crassa*. *Molecular and Cellular Biology* 28:6044–6055.

53. Roudier F et al. (2011) Integrative epigenomic mapping defines four main chromatin states in Arabidopsis. *The EMBO Journal* 30:1928–1938.

54. Shi J, Dawe RK (2006) Partitioning of the maize epigenome by the number of methyl groups on histone H3 lysines 9 and 27. *Genetics* 173:1571–1583.

55. Turck F et al. (2007) Arabidopsis TFL2/LHP1 Specifically Associates with Genes Marked by Trimethylation of Histone H3 Lysine 27. *PLoS Genet* 3:e86.

56. Murzina NV et al. (2008) Structural basis for the recognition of histone H4 by the histone-chaperone RbAp46. *Structure* 16:1077–1085.

57. Song JJ, Garlick JD, Kingston RE (2008) Structural basis of histone H4 recognition by p55. *Genes & Development* 22:1313–1318.

58. Bouveret R, Schönrock N, Gruissem W, Hennig L (2006) Regulation of flowering time by *Arabidopsis* MSI1. *Development* 133:1693–1702.

59. Azuara V et al. (2006) Chromatin signatures of pluripotent cell lines. *Nat Cell Biol* 8:532–538.

60. Lafos M et al. (2011) Dynamic regulation of H3K27 trimethylation during *Arabidopsis* differentiation. *PLoS Genet* 7:e1002040.

61. Schwartz YB et al. (2010) Alternative epigenetic chromatin states of polycomb target genes. *PLoS Genet* 6:e1000805.

62. Davis RH (2000) *Neurospora: Contributions of a Model Organism* (Oxford University Press, Inc., New York, New York).

63. Rountree MR, Selker EU (1997) DNA methylation inhibits elongation but not initiation of transcription in *Neurospora crassa*. *Genes & Development* 11:2383–2395.

64. Galagan JE et al. (2003) The genome sequence of the filamentous fungus Neurospora crassa. *Nature* 422:859–868.

65. Ellison CE et al. (2011) Massive changes in genome architecture accompany the transition to self-fertility in the filamentous fungus Neurospora tetrasperma. *Genetics* 189:55–69.

66. Dewey CN (2007) Aligning multiple whole genomes with Mercator and MAVID. *Methods Mol Biol* 395:221–236.

67. Li L, Stoeckert CJ, Roos DS (2003) OrthoMCL: identification of ortholog groups for eukaryotic genomes. *Genome Research* 13:2178–2189.

68. Enright AJ, Van Dongen S, Ouzounis CA (2002) An efficient algorithm for large-scale detection of protein families. *Nucleic Acids Research* 30:1575–1584.

69. Stajich JE et al. (2002) The Bioperl toolkit: Perl modules for the life sciences. *Genome Research* 12:1611–1618.

70. Langmead B (2010) Aligning short sequencing reads with Bowtie. *Curr Protoc Bioinformatics* Chapter 11:Unit 11.7.

71. Li H et al. (2009) The Sequence Alignment/Map format and SAMtools. *Bioinformatics* 25:2078–2079.

72. Trapnell C et al. (2010) Transcript assembly and quantification by RNA-Seq

reveals unannotated transcripts and isoform switching during cell differentiation. *Nat Biotechnol* 28:511–515.

73. Robinson JT et al. (2011) Integrative genomics viewer. *Nat Biotechnol* 29:24–26.

74. Craig JM (2005) Heterochromatin--many flavours, common themes. *Bioessays* 27:17–28.

75. Oberdoerffer P, Sinclair DA (2007) The role of nuclear architecture in genomic instability and ageing. *Nature Reviews Molecular Cell Biology* 8:692–702.

76. Lewis ZA et al. (2010) DNA Methylation and Normal Chromosome Behavior in Neurospora Depend on Five Components of a Histone Methyltransferase Complex, DCDC. *PLoS Genet* 6:e1001196.

77. Kouzminova E, Selker EU (2001) dim-2 encodes a DNA methyltransferase responsible for all known cytosine methylation in Neurospora. *The EMBO Journal* 20:4309–4323.

78. Honda S et al. (2012) Heterochromatin protein 1 forms distinct complexes to direct histone deacetylation and DNA methylation. *Nature Structural & Molecular Biology*.

79. Honda S et al. (2010) The DMM complex prevents spreading of DNA methylation from transposons to nearby genes in Neurospora crassa. *Genes & Development* 24:443–454.

80. Denslow SA, Wade PA (2007) The human Mi-2/NuRD complex and gene regulation. *Oncogene* 26:5433–5438.

81. Trojer P, Reinberg D (2007) Facultative heterochromatin: is there a distinctive molecular signature? *Molecular Cell* 28:1–13.

82. Jamieson K, Rountree MR, Lewis ZA, Stajich JE, Selker EU (2013) Regional control of histone H3 lysine 27 methylation in Neurospora. *Proceedings of the National Academy of Sciences* 110:6027–6032.

83. Connolly LR, Smith KM, Freitag M (2013) The Fusarium graminearum Histone H3 K27 Methyltransferase KMT6 Regulates Development and Expression of Secondary Metabolite Gene Clusters. *PLoS Genet* 9:e1003916.

84. Bartke T et al. (2010) Nucleosome-Interacting Proteins Regulated by DNA and Histone Methylation. *Cell* 143:470–484.

85. Brinkman AB et al. (2012) Sequential ChIP-bisulfite sequencing enables direct genome-scale investigation of chromatin and DNA methylation cross-talk. *Genome Research*.

86. Wang Z et al. (2008) Combinatorial patterns of histone acetylations and methylations in the human genome. *Nature Publishing Group* 40:897–903.

87. McGarvey KM et al. (2006) Silenced tumor suppressor genes reactivated by DNA demethylation do not return to a fully euchromatic chromatin state. *Cancer Res* 66:3541–3549.

88. Schlesinger Y et al. (2007) Polycomb-mediated methylation on Lys27 of histone H3 pre-marks genes for de novo methylation in cancer. *Nat Genet* 39:232–236.

89. Law JA, Jacobsen SE (2010) Establishing, maintaining and modifying DNA methylation patterns in plants and animals. *Nature Reviews Genetics*:1–18.

90. Deleris A et al. (2012) Loss of the DNA Methyltransferase MET1 Induces H3K9 Hypermethylation at PcG Target Genes and Redistribution of H3K27 Trimethylation to Transposons in Arabidopsis thaliana. *PLoS Genet* 8:e1003062.

91. Reddington JP et al. (2013) Redistribution of H3K27me3 upon DNAhypomethylation results in de-repression ofPolycomb target genes. *Genome Biol* 14:R25.

92. Hagarman JA, Motley MP, Kristjansdottir K, Soloway PD (2013) Coordinate regulation of DNA methylation and H3K27me3 in mouse embryonic stem cells. *PLoS ONE* 8:e53880.

93. Ringrose L, Paro R (2007) Polycomb/Trithorax response elements and epigenetic memory of cell identity. *Development* 134:223–232.

94. Zeng J, Kirk BD, Gou Y, Wang Q, Ma J (2012) Genome-wide polycomb target gene prediction in Drosophila melanogaster. *Nucleic Acids Research*.

95. Liu Y, Shao Z, Yuan G-C (2010) Prediction of Polycomb target genes in mouse embryonic stem cells. *Genomics* 96:17–26.

96. Ringrose L, Rehmsmeier M, Dura J-M, Paro R (2003) Genome-wide prediction of Polycomb/Trithorax response elements in Drosophila melanogaster. *Developmental Cell* 5:759–771.

97. Buzas DM, Tamada Y, Kurata T (2011) FLC: A Hidden Polycomb Response Element Shows Up in Silence. *Plant Cell Physiol*.

98. Woo CJ, Kharchenko PV, Daheron L, Park PJ, Kingston RE (2010) A Region of the Human HOXD Cluster that Confers Polycomb-Group Responsiveness. *Cell* 140:99–110.

99. Sing A et al. (2009) A Vertebrate Polycomb Response Element Governs Segmentation of the Posterior Hindbrain. *Cell* 138:885–897.

100. Jermann P, Hoerner L, Burger L, Schübeler D (2014) Short sequences can efficiently recruit histone H3 lysine 27 trimethylation in the absence of enhancer activity and DNA methylation. *Proceedings of the National Academy of Sciences*.

101. Lynch MD et al. (2011) An interspecies analysis reveals a key role for unmethylated CpG dinucleotides in vertebrate Polycomb complex recruitment. *The EMBO Journal*.

102. Mendenhall EM et al. (2010) GC-rich sequence elements recruit PRC2 in mammalian ES cells. *PLoS Genet* 6:e1001244.

103. Meissner A et al. (2008) Genome-scale DNA methylation maps of pluripotent and differentiated cells. *Nature* 454:766–770.

104. Freitag M, Hickey PC, Khlafallah TK, Read ND, Selker EU (2004) HP1 is essential for DNA methylation in neurospora. *Molecular Cell* 13:427–434.

105. Adhvaryu KK, Selker EU (2008) Protein phosphatase PP1 is required for normal DNA methylation in Neurospora. *Genes & Development* 22:3391–3396.

106. Zhang X et al. (2003) Structural Basis for the Product Specificity of Histone Lysine Methyltransferases. *Molecular Cell* 12:177–185.

107. Beadle GW, Tatum EL (1945) JSTOR: American Journal of Botany, Vol. 32, No. 10 (Dec., 1945), pp. 678-686. *American Journal of Botany*.

108. Perkins DD (1996) Chromosome rearrangements in Neurospora and other filamentous fungi. *Adv Genet* 36:239–398.

109. Smith KM et al. (2010) H2B- and H3-specific histone deacetylases are required for DNA methylation in Neurospora crassa. *Genetics* 186:1207–1216.

110. Herz HM, Shilatifard A (2010) The JARID2-PRC2 duality. *Genes & Development* 24:857–861.

111. Klose RJ, Kallin EM, Zhang Y (2006) JmjC-domain-containing proteins and histone demethylation. *Nature Reviews Genetics* 7:715–727.

112. Voigt P et al. (2012) Asymmetrically modified nucleosomes. *Cell* 151:181–193.

113. Lewis ZA, Adhvaryu KK, Honda S, Shiver AL, Selker EU (2010) Identification of DIM-7, a protein required to target the DIM-5 H3 methyltransferase to chromatin. *Proceedings of the National Academy of Sciences* 107:8310–8315.

114. Cruz CC et al. (2007) The Polycomb Group Protein SUZ12 regulates histone H3 lysine 9 methylation and HP1α distribution. *Chromosome Res*.

115. Rathert P, Zhang X, Freund C, Cheng X, Jeltsch A (2008) Analysis of the substrate specificity of the Dim-5 histone lysine methyltransferase using peptide arrays. *Chem Biol* 15:5–11.

116. Jacobs SA, Khorasanizadeh S (2002) Structure of HP1 chromodomain bound to a lysine 9-methylated histone H3 tail. *Science* 295:2080–2083.

117. Miao VP, Freitag M, Selker EU (2000) Short TpA-rich segments of the zeta-eta region induce DNA methylation in Neurospora crassa. *J Mol Biol* 300:249–273.

118. Tamaru H, Selker EU (2003) Synthesis of signals for de novo DNA methylation in Neurospora crassa. *Molecular and Cellular Biology* 23:2379–2394.

119. Mikkelsen TS et al. (2007) Genome-wide maps of chromatin state in pluripotent and lineage-committed cells. *Nature* 448:553–560.

120. Ku M et al. (2008) Genomewide analysis of PRC1 and PRC2 occupancy identifies two classes of bivalent domains. *PLoS Genet* 4:e1000242.

121. Margolin BS, Freitag M, Selker EU (1997) Improved plasmids for gene targeting at the his-3 locus of Neurospora crassa by electroporation. *Fungal Genetics Newsletter*.

122. Workman JL, Kingston RE (1998) Alteration of nucleosome structure as a mechanism of transcriptional regulation. *Annu Rev Biochem* 67:545–579.

123. Lee KK, Workman JL (2007) Histone acetyltransferase complexes: one size doesn't fit all. *Nature Reviews Molecular Cell Biology* 8:284–295.

124. Grunstein M (1997) Histone acetylation in chromatin structure and transcription. *Nature* 389:349–352.

125. Yang X-J, Seto E (2008) The Rpd3/Hda1 family of lysine deacetylases: from bacteria and yeast to mice and men. *Nature Reviews Molecular Cell Biology* 9:206–218.

126. Suka N, Suka Y, Carmen AA, Wu J, Grunstein M (2001), pp 473–479.

127. Carrozza MJ et al. (2005) Histone H3 methylation by Set2 directs deacetylation of coding regions by Rpd3S to suppress spurious intragenic transcription. *Cell* 123:581–592.

128. Lee J-S, Shilatifard A (2007) A site to remember: H3K36 methylation a mark for histone deacetylation. *Mutat Res* 618:130–134.

129. Li B et al. (2007) Combined action of PHD and chromo domains directs the Rpd3S HDAC to transcribed chromatin. *Science* 316:1050–1054.

130. Wang Z et al. (2009) Genome-wide mapping of HATs and HDACs reveals distinct functions in active and inactive genes. *Cell* 138:1019–1031.

131. van Oevelen C et al. (2008) A role for mammalian Sin3 in permanent gene silencing. *Molecular Cell* 32:359–370.

132. Tompa R, Madhani HD (2007) Histone H3 lysine 36 methylation antagonizes silencing in Saccharomyces cerevisiae independently of the Rpd3S histone deacetylase complex. *Genetics* 175:585–593.

133. Biswas D, Takahata S, Stillman DJ (2008) Different genetic functions for the Rpd3(L) and Rpd3(S) complexes suggest competition between NuA4 and Rpd3(S). *Molecular and Cellular Biology* 28:4445–4458.

134. Furuyama T, Tie F, Harte PJ (2003) Polycomb group proteins ESC and E(Z) are present in multiple distinct complexes that undergo dynamic changes during development. *Genesis* 35:114–124.

135. Leitner A et al. (2012) The molecular architecture of the eukaryotic chaperonin TRiC/CCT. *Structure* 20:814–825.

136. Loyola A, Almouzni G (2004) Histone chaperones, a supporting role in the limelight. *Biochim Biophys Acta* 1677:3–11.

137. Selker EU (1998) Trichostatin A causes selective loss of DNA methylation in Neurospora. *Proc Natl Acad Sci USA* 95:9430–9435.

138. Czermin B et al. (2001) Physical and functional association of SU(VAR)3-9 and HDAC1 in Drosophila. *EMBO reports* 2:915–919.

139. Tie F et al. (2009) CBP-mediated acetylation of histone H3 lysine 27 antagonizes Drosophila Polycomb silencing. *Development* 136:3131–3141.

140. Ausin I, Alonso-Blanco C, Jarillo JA, Ruiz-García L, Martínez-Zapater JM (2004) Regulation of flowering time by FVE, a retinoblastoma-associated protein. *Nat Genet* 36:162–166.

141. Smith KM et al. (2010) H2B- and H3-Specific Histone Deacetylases Are Required for DNA Methylation in Neurospora crassa. *Genetics* 186:1207–1216.

142. Honda S, Selker EU (2009) Tools for fungal proteomics: multifunctional neurospora vectors for gene replacement, protein expression and protein purification. *Genetics* 182:11–23.

143. Pomraning KR, Smith KM, Freitag M (2009) Genome-wide high throughput analysis of DNA methylation in eukaryotes. *Methods* 47:142–150.